

SANDIA REPORT

SAND89-3039 • UC-212
Unlimited Release
Printed October 1989

RS-8232-2/ 70067



8232-2/070067

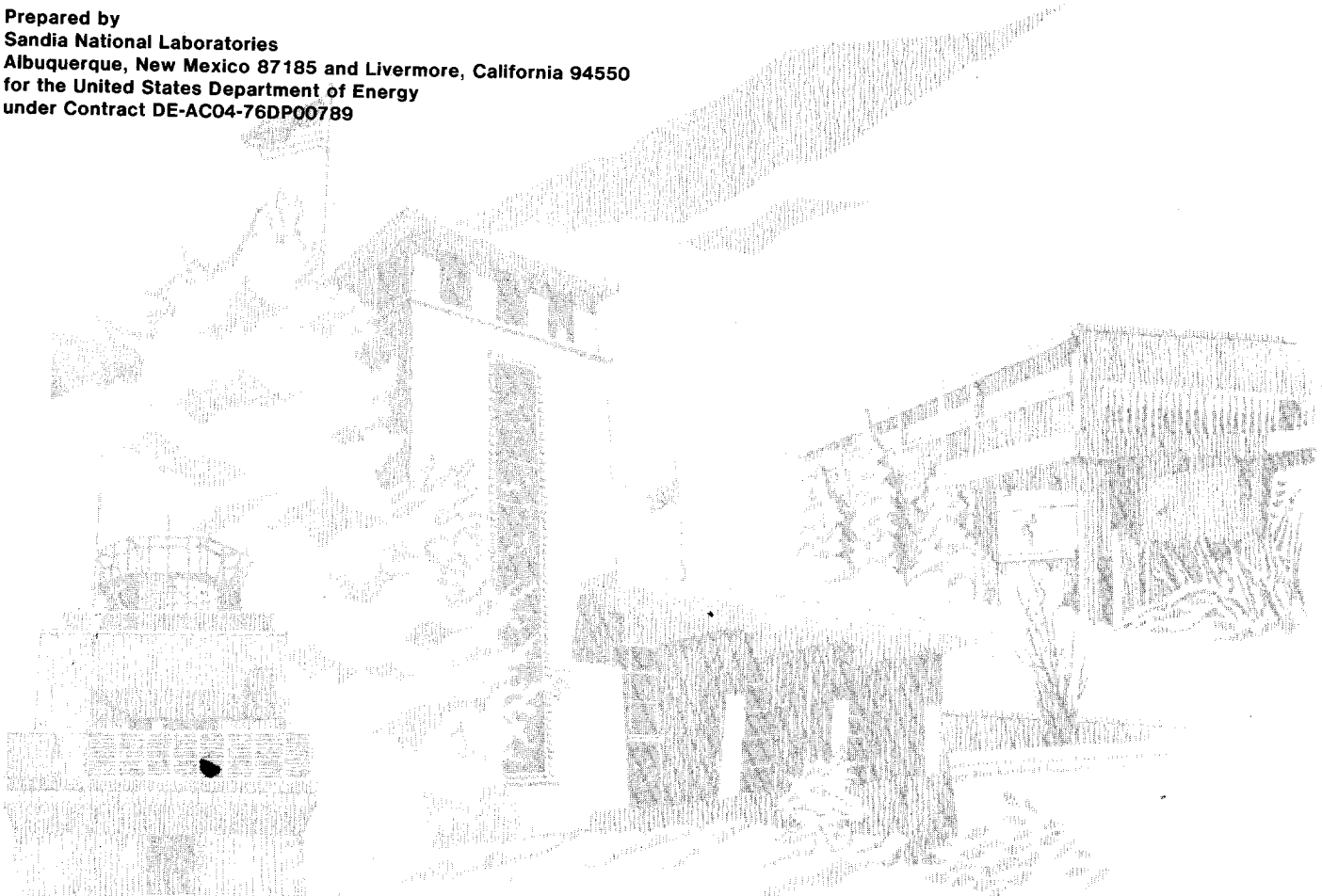


00000001 -

Exploratory Battery Technology Development and Testing Report for 1988

Nicholas J. Magnani, Ronald B. Diegle, Jeffrey W. Braithwaite,
Donald M. Bush, Paul C. Butler, James M. Freese,
Kenneth R. Grothaus, Kevin D. Murphy

Prepared by
Sandia National Laboratories
Albuquerque, New Mexico 87185 and Livermore, California 94550
for the United States Department of Energy
under Contract DE-AC04-76DP00789



Issued by Sandia National Laboratories, operated for the United States Department of Energy by Sandia Corporation.

NOTICE: This report was prepared as an account of work sponsored by an agency of the United States Government. Neither the United States Government nor any agency thereof, nor any of their employees, nor any of their contractors, subcontractors, or their employees, makes any warranty, express or implied, or assumes any legal liability or responsibility for the accuracy, completeness, or usefulness of any information, apparatus, product, or process disclosed, or represents that its use would not infringe privately owned rights. Reference herein to any specific commercial product, process, or service by trade name, trademark, manufacturer, or otherwise, does not necessarily constitute or imply its endorsement, recommendation, or favoring by the United States Government, any agency thereof or any of their contractors or subcontractors. The views and opinions expressed herein do not necessarily state or reflect those of the United States Government, any agency thereof or any of their contractors.

Printed in the United States of America. This report has been reproduced directly from the best available copy.

Available to DOE and DOE contractors from
Office of Scientific and Technical Information
PO Box 62
Oak Ridge, TN 37831

Prices available from (615) 576-8401, FTS 626-8401

Available to the public from
National Technical Information Service
US Department of Commerce
5285 Port Royal Rd
Springfield, VA 22161

NTIS price codes
Printed copy: A06
Microfiche copy: A01

SAND89-3039
Unlimited Release
Printed in October 1989

Distribution
Category UC - 212

Exploratory Battery Technology Development and Testing Report for 1988

Nicholas J. Magnani
Power Sources Department
Ronald B. Diegle, Jeffrey W. Braithwaite,
Donald M. Bush, Paul C. Butler, James M. Freese,
Kenneth R. Grothaus, and Kevin D. Murphy
Storage Batteries Division

Sandia National Laboratories
Albuquerque, NM 87185

Abstract

Sandia National Laboratories, Albuquerque, has been designated as Lead Center for the Exploratory Battery Technology Development and Testing Project, which is sponsored by the U.S. Department of Energy's Office of Energy Storage and Distribution. In this capacity, Sandia is responsible for the engineering development of advanced rechargeable batteries for both mobile and stationary energy storage applications. This report details the technical achievements realized in pursuit of the Lead Center's goals during calendar year 1988.

Contents

Acronyms and Abbreviations	xi
Chapter 1. Executive Summary	1
Introduction	1
Sodium/Sulfur Technology	1
Technology Development	1
CSPL Technology Development	2
Posttest Analysis at ANL	2
Technology Evaluation	3
SNL Evaluations	3
ANL Evaluations	3
Technology Improvement	3
Component Stress During F/T Cycling	3
Development of Improved Chromium Plating Techniques	3
Zinc/Bromine Technology	4
Technology Development	4
ERC Technology Development	4
JCI Technology Development	4
Technology Evaluation	5
Technology Improvement	5
Advanced Membrane Development for Zinc/Bromine Batteries	5
Durability of Zinc/Bromine Materials	5
Nickel/Hydrogen Technology	5
Technology Development	5
Technology Evaluation	6
Aluminum/Air Technology	6
Technology Development	6
Technology Evaluation	6
Chapter 2. Aqueous Battery Development	7
Introduction	7
Zinc/Bromine Battery Development - ERC	7
Hardware Development	8
Stack Clamping Assembly	8
1,500-cm ² Flow Frame Design	8
1,500-cm ² Stack Test Results	10
872-cm ² Battery Design and Testing	11
Hardware Development Status	12

Material Stability Studies	13
Plastic Stability Studies	13
Separator Stability	13
Electrochemical Stability	14
Material Stability Status	14
Future Work	14
Development of a Zinc/Bromine Load Management Battery - JCI	15
Materials and Electrochemical Research	15
Electrode	15
Electrolyte	15
V-Design Flow Frames	16
Z-20LL	17
Nickel/Hydrogen Battery Development - JCI	18
Background	18
Technical Effort for 1988	18
Summary	21
Aluminum/Air Battery Development - Eltech	21
Introduction	21
Research Engineering in 1988	22
Eltech Characterization of Fluid Flow Rates in the B-300 Cell	23
Eltech Electrolyte Composition	23
Case Western Mathematical Model of the B-300 Cell	23
Case Western Analysis of Shunt Currents	24
Characterization of the Solids Separator by Helipump	24
Mathematical Model of the Helipump by Case Western	25
Eltech Heat Exchange in the Battery System	25
Summary	26
Chapter 3. Nonaqueous Battery Development	27
Introduction	27
Background	27
Core Technology Research and Development	28
Overview	28
Electrolyte Research and Development	29
Materials Development and Qualification	29
Alpha-Alumina to Beta"-Alumina Glass Seals	29
Metal to Alpha-Alumina Seals	30
Sodium Electrode	31
Sulfur Electrode	32
Containment	32

Cell Development	33
PB Cell Development	33
Reliability	33
Electrical Performance	35
Battery Performance	36
XPB Cell Development	38
XPB Safety Testing	38
Cell Test and Posttest Analysis	39
Module Testing	40
PB Module	40
XPB Module	40
Battery Engineering and Testing	43
Sodium/Sulfur Battery Development - SAIC	44
Battery Design Support	46
X-Radiography Analysis	46
Development of Cell-Failure Device	47
Battery-Performance Model Development	48
Posttest Analysis of CSPL Sodium/Sulfur Cells	49
Positive-Electrode	49
Sulfur Container	50
Electrolyte	51
Glass Seals	51
Chapter 4. Battery Technology Evaluation	53
Introduction	53
Battery Evaluations at ANL	53
Battery Evaluations at SNL	56
Flowing Electrolyte Battery Testing	56
Flow Battery Evaluation Procedures	56
ERC Zinc/Bromine 5-Cell Battery (SNL ID 456)	57
ERC Zinc/Bromine 30-Cell Battery (SNL ID 459)	60
Eltech Aluminum/Air Cell (SNL ID 468)	63
Sodium/Sulfur Technology	64
CSPL Technology	65
MkIIa Cells	67
MkIII Cells and Cell Strings	67
FACC Technology	68
Powerplex Technology	69
Ceramatec Technology	70

Nickel/Hydrogen Testing at SNL	71
Cycle Tests	71
Solar Tests	73
Chapter 5. Battery Technology Improvement	77
Advanced Membrane Development for Zinc/Bromine Batteries	77
Membrane Preparation	77
Membrane Characterization	78
Results and Discussion	78
Durability of Zinc/Bromine Materials	80
Generic Structure of PVC Additives	80
Surface Degradation of PVC Flow Frames	81
Comparative Stability Tests	82
Stress-Rupture Studies of PVC Materials	82
Failure Analysis of the Beta"-Alumina Electrolyte	83
Component Stress During F/T Cycling of Sodium/Sulfur Cells	83
Physical Properties of Positive-Electrode Materials	84
Cell Behavior	85
Modeling of Cell Behavior	86
Improved Chromium Plating of Sodium/Sulfur Cell Containers	88
Program Plan	90
Crack-Free	90
Pulse-Plating	91
Highly Cracked	91
Evaluation	91
Results	91
Crack-Free	91
Highly Cracked	91
Pulse-Plating	91
Appendix: Presentations and Publications, 1988	A-1

Figures

1-1.	1988 ETD Project Organization	2
2-1.	Comparison of 872-cm ² and 1,500-cm ² Frame Designs	9
2-2.	5-Cell Stack 1500-5-1	10
2-3.	1,500-cm ² 5-Cell Stack 1500-5-2	10
2-4.	Cycle Performance (5-Cell Stack SNL-5-3)	11
2-5.	Cycle Performance (5-Cell Stack SNL-5-4)	11
2-6.	30-Cell Stack SNL-30-2	12
2-7.	Cycle Performance (30-Cell Stack SNL-30-2)	12
2-8.	General Configuration for 36-kWh Zn/Br ₂ Battery System	15
2-9.	Zn/Br ₂ Concentration (M)	16
2-10.	MEP Concentration (M)	16
2-11.	Zinc/Bromine Battery - Load Management Cycle Efficiencies	18
2-12.	Standard 150-Ah Cell	19
2-13.	Preliminary Design of Stainless Steel Liner for Filament-Wound Hydrogen Pressure Vessel	20
2-14.	Battery Current and SOC vs Time (No Load Shedding)	21
2-15.	PV Array/Battery Performance, January 1988	21
2-16.	Aluminum/Air Battery Process Diagram	22
2-17.	B-300 Aluminum/Air Cell	22
2-18.	Schematic of the Aluminum/Air Battery	24
2-19.	Mechanism of Fluidization	25
3-1.	Peak Power at Depth of Discharge, Cell 469	31
3-2.	Temperature Exotherms Resulting from Safety Testing of MkIII PB Cells Containing Safety Features	31
3-3.	24-Cell PB Module (upper) and One String (lower) After Safety Testing	32
3-4.	PB Cell After Side-Impact Testing	32
3-5.	Number of PB Cells Exceeding 500 Cycles	33
3-6.	Status of MkIIa - MkIII Reliability Trial	34
3-7.	Comparison of PB Cell Discharge with and without Safety Features	37
3-8.	Resistance and Capacity of MkIII Cell with Safety Features	37
3-9.	Capacity History of DOE/SNL EV Intermediate Deliverable Battery	37
3-10.	Temperature Profiles of XPB Cells After Safety Testing	39
3-11.	Statistical Analysis of XPB Safety Test Data	39
3-12.	Typical 120-PB Test Bank	40
3-13.	Typical Performance Characteristic of 120-Cell Bank	41
3-14.	Resistance and Capacity of 120-Cell Bank B87	41
3-15.	Thermal Management System - XPB Cell Module	42
3-16.	Cell Temperature Distribution - XPB Cell Module	42
3-17.	Temperature Distribution of Cell 2 - XPB Module	42
3-18.	Temperature Distribution of Cell 8 - XPB Module	43
3-19.	Temperature Distribution of Cell 11 - XPB Module	43
3-20.	Artist's Sketch of the 100-MWh Utility Load Leveling Battery Developed in Phase P of EPRI Contract No. 2123-4	44
3-21.	Artist's Sketch of Four-Module Thermal Management System for 100-MWh Utility Battery	44
3-22.	General Arrangement of 200-XPB Cell Array	45
3-23.	Comparison of Battery Capacity Degradation Curves for Alpha = 1,300	46

3-24.	Four-Cell Strings - Weibull Lifetime vs Cycles to 80% of Capacity	48
3-25.	Four-Cell Strings - Number of Active Strings vs Percent of Failed Cells	48
3-26.	Overview of BATSIM Program	48
3-27.	Corrosion Penetration for the Chromized Cell Cases	51
4-1.	Peak Power of Four Advanced Battery Technologies as a Function of DOD Derived from Driving Profile Discharges	54
4-2.	Effect of Discharge Specific Power on the Available Energy of Four Advanced Battery Technologies Evaluated at the ANL/ADL	54
4-3.	Internal Resistance of a 24-cell Sodium/Sulfur Module as a Function of DOD Level During a Driving Profile Discharge (J227aD/IETV-1)	56
4-4.	Efficiency Performance of ERC Zinc/Bromine Battery 456 at SNL	58
4-5.	Bromine End Electrode of ERC Zinc/Bromine Battery 456.	59
4-6.	Efficiency Performance of ERC Zinc/Bromine Battery 459	60
4-7.	Voltage vs Time for ERC Zinc/Bromine Battery 459, Cycles 5, 65, and 66.	61
4-8.	Picture of the Eltech Aluminum/Air Single Cell (SNL ID 468 on Test at SNL)	62
4-9.	Cell and Reference Electrode Voltages for Aluminum/Air Cell (October - December 1988)	64
4-10.	CSPL Average Capacity vs Charge Rate and Temperature—Cell 469	68
4-11.	CSPL Average Capacity vs Discharge Rate and Temperature—Cells 469, 470, 471, and 472	68
4-12.	Powerplex Average Capacity vs Charge Rate and Cell Temperature—Cell 462	70
4-13.	Average Capacity vs Discharge Rate—Powerplex Cells 462 and 463	70
4-14.	Predicted Capacity of Ceramatec Sodium/Sulfur Cell 454 vs Temperature and Charge Rate (8-A Discharge Rate)	70
4-15.	Ceramatec Average Capacity vs Charge Rate—Cell 454	71
4-16.	Ceramatec Average Capacity vs Discharge Rate—Cells 454 and 455	71
4-17.	Ragone Plot for Ceramatec Cell 454	71
4-18a.	Voltage vs Time, 7-kWh Battery (Cycle 251)	74
4-18b.	Current vs Time, 7-kWh Battery (Cycle 251)	74
4-19a.	State-of-Charge vs Time, 7-kWh Battery (September 2 - 15, 1988)	75
4-19b.	State-of-Charge vs Time, 7-kWh Battery (September 17 - October 2, 1988)	75
4-20a.	State-of-Charge vs Time, 7-kWh Battery (October 26 - 30, 1988)	75
4-20b.	Array and Load Current vs Time, 7-kWh Battery (October 26 - 30, 1988)	75
4-21a.	State-of-Charge vs Time, 7-kWh Battery (December 15 - 22, 1988)	76
4-21b.	Load Current vs Time, 7-kWh Battery (December 15 - 22, 1988)	76
5-1.	Sulfur Content as a Function of Depth Across the Thickness Dimension of Two Membranes	79
5-2.	Voltaic, Coulombic, and Energy Efficiencies Calculated with a Cell Performance Model	80
5-2a.	Daramic Separator	80
5-2b.	Daramic Separator Vacuum Immersed in 20% SPS Solution at 90°C	80
5-3.	¹³ C NMR Spectra of (a) Unaged and (b) Aged PVC-1 (solid). Aging Conditions: 60°C for 18 Weeks in a Bromine-Containing Electrolyte.	81
5-4.	Tensile Modulus as a Function of Location on Surface of PVC-1 Flow Frame Used in an Operational Battery for About 1 Year	82
5-5.	Effect of Aging on the Shear Modulus of Various Thermoplastics	82
5-6.	Effect of Temperature on the Strain Observed in Ceramatec Beta"-Alumina for Numerous Samples Taken in Various Orientations from Actual SNL Cell Electrolytes	85
5-7.	Average Mechanical Strain Measured During the Freezing of a Discharged SNL Cell. Cell 1, Freeze Cycle 16	85
5-8.	Average Mechanical Strain Measured During the Freezing of a Discharged SNL Cell. Cell 2, Freeze Cycle 4	86
5-9.	Average Mechanical Strain Measured During the Freezing of a Discharged SNL Cell. Cell 2, Freeze Cycle 6	86

5-10.	Calculated Coefficient of Thermal Expansion for Sodium Tetrasulfide/Graphite Composite as Function of Temperature.	87
5-11.	Schematic Diagrams of a CSPL-PB Cell Used in the Mathematical Analyses of the Effect of Voids in the Positive Electrode on Electrolyte Stress	88
5-11a.	General Shapes of Observed Voids	88
5-11b.	Finite-Element Mesh of an Axisymmetric Cell Section	88
5-12.	Stress Contours Calculated for the CSPL-PB Cell That Result from a Freeze Cycle to 25°C	89
5-12a.	Cell without Void in Positive Electrode	89
5-12b.	Cell with Void	89
5-13.	Stress Contours Calculated for Two Seal Designs in CSPL-PB Cells due to a Freeze Cycle to 25°C. Region Shown Is Indicated by Circle in Figure 5-11a.	90
5-13a.	Flexible Seal	90
5-13b.	Rigid Seal	90
5-14.	Optical Micrograph (Upper), and X-Ray Dispersive Chemical Analysis (Lower) of Chromium Deposit Produced with the M&T Unichrome CF-500 Electrolyte Modified with the Addition of 10 g/l of Vanadium Pentoxide.	92

Tables

2-1.	V-Design Flow Frame Parameters	17
2-2.	Electrolyte Comparison Studies	17
3-1.	CSPL Electrolyte Output and Yield	29
3-2.	Cycle Status - High Zirconia TD Cells	30
3-3.	Freeze/Thaw of MkIII PB Cell	31
3-4.	High Recharge Current Testing of PB Cells	33
3-5.	PB Cell Reliability Trial	34
3-6.	Weibull Statistics for MkIIa Cells in MkIIa - MkIII Repeatability Trial	35
3-7.	Failure of Cells in MkIIa - MkIII Reliability Trial	35
3-8.	Comparison of Standard Production and Reliability Groups	36
3-9.	Life Data on MkIII PB Cells (No Safety Features)	36
3-10.	Life Data on MkIII PB Cells (with Safety Features)	36
3-11.	Projected Ranges for Simulated Driving Profiles	38
3-12.	Summary of XPB Single-Cell Test Data for Cycle 55	38
3-13.	Battery Capacity Modeling Results	46
3-14.	Characteristics of PB Cells Analyzed with X-Radiography	47
3-15.	Summary of Posttest Findings for CSPL Sodium/Sulfur Cells	49
3-16.	Gases Found Within the Sulfur Electrode Compartments	50
4-1.	Performance Data for EV Modules Tested at the ADL from January 1 Through December 31, 1988	54
4-2.	Projected Ranges for Simulated Driving Profiles	55
4-3.	Flowing Electrolyte Cell and Batteries Tested at SNL in 1988	56
4-4.	Flowing Electrolyte Cell and Battery Data Summary, December 1988	57
4-5.	Eltech Aluminum/Air Cell Tests at SNL, December 31, 1988	63
4-6.	Sodium/Sulfur Cells and Cell Strings Tested at SNL in 1988	65
4-7.	Summary of Sodium/Sulfur Testing at SNL	66
4-7.	Summary of Sodium/Sulfur Testing at SNL (Continued)	67
4-8.	Configuration and Test Conditions	72

4-9.	Summary of Cycle Test Results (December 23, 1988)	72
4-10.	Initial Cycle Test Results for Battery 212	73
4-11.	Array Output for Battery 212	74
5-1.	Status of Membrane Development Task	78
5-2.	Performance Parameters of Various Zinc/Bromine Battery Separators	78
5-3.	Program Status of PVC Durability Task	81

Acronyms and Abbreviations

ABS	Advanced Battery Systems
ADL	Analysis and Diagnostic Laboratory
ANL	Argonne National Laboratory
AOC	alloy-on-carbon
BBC	Brown, Boveri, and Cie
BEST	Battery Energy Storage Test Facility
BET	Brunauer, Emmett, and Teller (method for determining particle surface area)
BSI	British Standards Institute
COMSAT	Communications Satellite Corporation
CPVC	chlorinated polyvinyl chloride
CSPL	Chloride Silent Power, Ltd.
CTE	coefficient of thermal expansion
DCOV	discharge cut-off voltage
DMA	dynamic mechanical analysis
DMF	dimethylformamide
DOD	depth-of-discharge
DOE	Department of Energy
DSEP	Dual Shaft Electric Propulsion Program
EHP	Electric and Hybrid Propulsion (a branch of DOE/OTS)
EMS	energy management system
EPD	electrophoretic deposition
EPI	Eagle-Picher Industries
EPRI	Electric Power Research Institute
ERC	Energy Research Corporation
ETD	Exploratory Battery Technology Development and Testing Project
ETX	Electric Transaxle Experimental Test Vehicle Project
EV	electric vehicle
FACC	Ford Aerospace and Communications Corporation
FRP	fiber-reinforced epoxy
F/T	freeze/thaw
FTIR	Fourier transform infrared analysis

GPC	gel permeation chromatography
HNEI	Hawaii Natural Energy Institute
IDSEP	improved DSEP
IEC	ion exchange capacity
IR	internal resistance; infrared analysis
JCI	Johnson Controls, Inc.
LL	load leveling
LVDT	linear variable differential transformer
M	molar
NBTL	National Battery Test Laboratory
NMR	nuclear magnetic resonance
OCV	open-circuit voltage
OESD	DOE Office of Energy Storage and Distribution
OTS	DOE Office of Transportation Systems
PAA	polyacrylic acid
PASTF	Photovoltaic Advanced Systems Test Facility
PB	designation for the standard CSPL sodium/sulfur cell
PTA	posttest analysis
PV	photovoltaic
PVC	polyvinyl chloride
PVDC	polyvinylidene chloride
PVDF	polyvinylidene fluoride, also known as Kynar
SES	Stationary Energy Storage
SFS	sulfonated polysulfone
SFUDS	Simplified Federal Urban Driving Schedule
SNL	Sandia National Laboratories
SOC	state-of-charge
TD	Technology Demonstration
XPB	designation for an expanded-size CSPL sodium/sulfur cell

Chapter 1. Executive Summary

Introduction

This report documents the activities of the Exploratory Battery Technology Development and Testing (ETD) Lead Center for calendar year 1988, ETD's eighth program year. (See SAND88-2154, *Exploratory Technology Development and Testing Report for 1987*, for a description of the previous year's activities.) The ETD Project, directed by Sandia National Laboratories (SNL), is supported by the U.S. Department of Energy, Office of Energy Systems Research, Energy Storage and Distribution Division (DOE/OESD). This project is operated in conjunction with the Technology Base Research (TBR) Project, which is under the direction of Lawrence Berkeley Laboratory. Together these two projects seek to establish the scientific feasibility of advanced electrochemical energy storage systems and to conduct the initial engineering development on systems suitable for mobile and stationary commercial applications.

The ETD Project assumes responsibility for the engineering development of electrochemical couples whose feasibility has been demonstrated by either the TBR Project or other technically sound investigations. These systems will be incorporated into batteries for use in electric and hybrid vehicles, utility and commercial load leveling, and photovoltaic and wind-based electricity-generating systems. Battery development is accomplished through cost-sharing contracts with industrial partners. SNL is responsible for the technical direction of the development contracts and lead-center project management. Additionally, SNL conducts various applied research activities (advanced membrane development, solid electrolyte fracture analysis, material durability studies, and container-plating development). Testing and analysis of the resulting batteries or components are performed either at SNL or, with SNL's guidance, at Argonne National Laboratory (ANL). SNL also undertakes a variety of battery cost-and-performance studies and analyses in connection with the ETD Project.

The ETD Lead Center is directed by Dr. Nicholas J. Magnani, manager of SNL's Power Sources Department. Lead Center operations are managed by Dr. Ronald B. Diegle, supervisor of SNL's Storage Batteries Division.

The organization of the ETD project for 1988 is illustrated in Figure 1-1. Its technical work is divided into three elements:

- Battery Technology Development
- Battery Technology Evaluation
- Battery Technology Improvement

Supporting elements include Budget and Project Analysis and Planning. Each element is supported by one or more staff members who are responsible for activities within that element.

In 1988, the ETD project continued research in four advanced secondary battery technologies:

- sodium/sulfur
- zinc/bromine
- nickel/hydrogen
- aluminum/air

A summary of the progress of the ETD Project in 1988, organized by battery technology, follows. More detailed information is contained in Chapters 2 through 5 of this report.

Sodium/Sulfur Technology

Technology Development

The primary developer of the sodium/sulfur technology for the ETD Project during 1988 was Chloride Silent Power, Ltd. (CSPL). They recently completed the third year of a four-year contract to continue the research and development of the core aspects of the sodium/sulfur technology for both stationary and electric vehicle applications. In support of the CSPL activities, Science Applications International Corporation (SAIC), a major subcontractor to CSPL, performed modeling analyses and cell-performance studies, and ANL completed detailed posttest analyses of several CSPL cells.

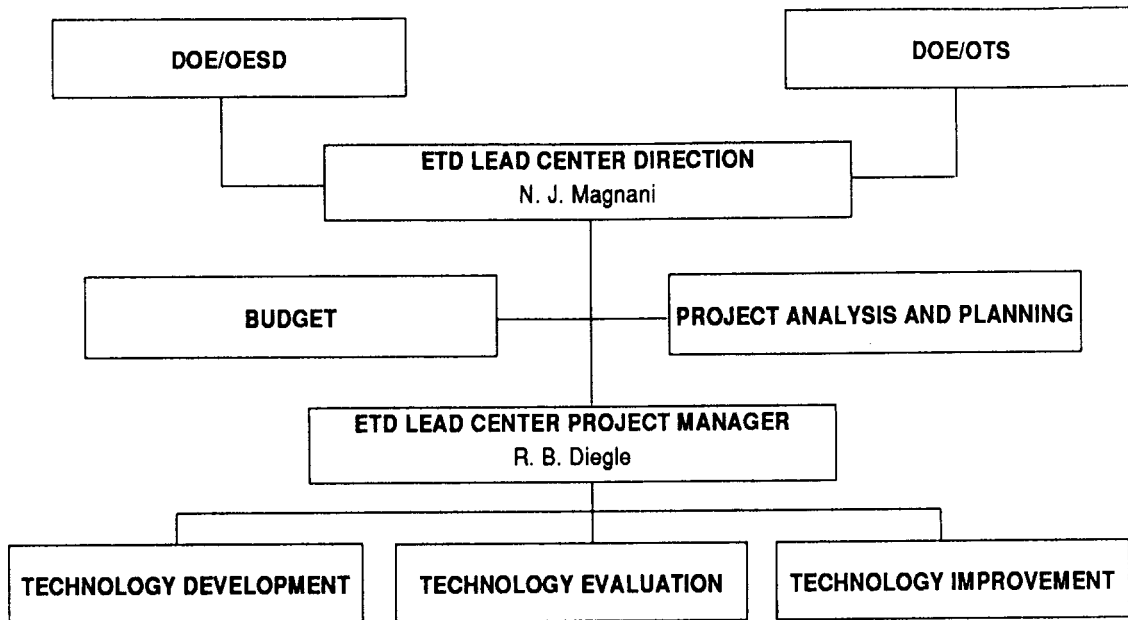


Figure 1-1. 1988 ETD Project Organization

CSPL Technology Development

During 1988, several cell component improvements were made. The yield during production of beta"-alumina electrolyte exceeded the goal of 50% at a rate of 500 cells per week. Cells containing zirconia-toughened electrolytes have now completed 4,000 cycles with low incidence of failure. The MkIII metal-to-ceramic seal that was developed to reduce the corrosion problems with the previous seal became the standard seal design. The freeze/thaw (F/T) resistance of this seal was shown to be excellent; a high probability exists that over 100 F/T cycles can be achieved without failure. The safety performance of the cell was dramatically improved with the addition of a sodium container within the beta"-alumina electrolyte.

Regarding PB-cell development, the improved safety performance of MkIII cells was accompanied by improved electrical performance; also PB cells were fabricated with the lowest resistance ever tested. The decrease in reliability observed in 1987 recovered with improved process control and detailed design changes. Almost 1,500 MkIII have been warmed up with no failures and, thus, infant mortality rates are practically zero. The 120-cell bank has become the standard test configuration for cell qualification. Nineteen modules have been tested with over 950 cells accumulating 210,000 cell cycles.

Because the results from the 1987-1988 XPB-cell reliability experiments were inadequate, the cell was redesigned and 50 new cells were fabricated. Single-cell tests produced the lowest average resistance and

most consistent XPB cells to date. A 16-cell module was given a successful and deliberate F/T cycle. Two XPB cells have successfully been subjected to eight F/T cycles each. The safety tests on the new cells have shown greatly improved performance.

A preliminary design for the final contract deliverable, a stationary-energy-storage (SES) module, was completed. Based on this design, the size of the modules was increased to 200 cells to better approximate a SES tray.

At SAIC, computer modeling of an XPB sub-battery design and two EV batteries was performed to predict capacity degradation as a function of time and the failure characteristics of the cells. This analysis showed, for example, that the capacity of an SES battery constructed with cells having a characteristic life of 2,000 charge/discharge cycles and a Weibull shape parameter of 2 would decline to 80% of its initial value after 470 cycles. Additionally, SAIC studied the performance characteristics of five CSPL-PB cells with real-time x-radiographic techniques. These analyses were performed to provide information about the processes occurring during cell break-in and the causes for high discharge resistance and recharge polarization periodically observed in specific cells.

Posttest Analysis at ANL

The major findings from the detailed posttest analysis of CSPL cells performed at ANL include the following:

- Three PB cells were examined. For a cell with 20 cycles, thermal cycling induced a partial fracture through the glass seal and shallow cracks existed on the sodium side of the electrolyte. Extended periods in the discharged state accelerated corrosion of the container. For a cell with 699 cycles, the glass seal contained spall-type fractures on the sodium side, a calcium layer was present on the inner electrolyte surface, and corrosion penetrated 90% of the chromized layer at the base of the container. The major constituents of the gas over the sulfur electrode were H₂S, COS, CO₂, and N₂.
- For two XPB cells at 424 cycles, the glass seals on the sodium side again showed spall-type fractures, minor quantities of FeS₂ were deposited on the outer surface of the electrolyte, and reduced levels of calcium (compared to PB cells) were present on the inner electrolyte surface.

Technology Evaluation

SNL Evaluations

During 1988, SNL tested 10 sodium/sulfur cells and two 4-cell strings from CSPL, two cells from Ford Aerospace and Communications Company (FACC), six cells from Powerplex, and two cells from Ceramatec. Test regimes included capacity, charge rate, discharge rate, constant power, peak power, Simplified Federal Urban Driving Schedule (SFUDS), and parametric. The CSPL PB cell 437 (with MkIIa seal) has now completed 1,564 cycles. SNL evaluations of MkIII cells and 4-cell strings showed that these cells must be charged at lower rates than previous CSPL cells to attain full capacity. Cell capacity diminished with increasing charge rate, especially at lower temperatures. At 375°C, there was 18% loss in capacity when charge current varied from 1.0 A to 3.0 A with the greatest capacity losses occurring at charge rates above 2.5 A.

ANL Evaluations

The Argonne Analysis and Diagnostics Laboratory (ADL) completed life tests on eight cells and initiated the evaluation of two 24-cell modules. The eight cells had an average cell life of 892 cycles (from 388 to 1,221 cycles). The first 60-Ah, 480-Wh CSPL sodium/sulfur module, which contained 24 PB-cells of the MkII design, was operated for only 14 cycles before being returned to CSPL. Over 100 cycles have been accrued

in an ongoing evaluation of a second CSPL sodium/sulfur module.

Technology Improvement

Component Stress During F/T Cycling

Further container strain measurements were completed on the SNL cell to show that the observed strain variability from F/T cycle to cycle is real (i.e., not representative of an instrumentation problem) and is caused by changes in the behavior of the positive electrode materials. The volumetric change associated with different phases probably produced the differences in strain behavior. Two consequences of this variability are that effects on strain due to time, electrical cycling, and rate of heat-up/cool-down cannot be statistically identified and that a failure during a freeze or thaw is not probable.

To aid in the mathematical analysis of F/T effects, an analytical (nonnumerical) solution to the governing stress and strain equations was developed. A numerical simulation was then performed using experimental strain data that showed the calculated coefficients of thermal expansion for the positive electrode to be in reasonable agreement with those obtained separately by Brown, Boveri, and Cie (BBC) and in this task. These results demonstrate that the model has been refined such that accurate correlations are now possible.

The progress during this task has yielded sufficient confidence in the status of the model that, at a minimum, semi-quantitative analyses of actual cell performance can be made. Two F/T simulations relative to CSPL-PB cells were completed that involved analyzing the potential effect of a gap in the positive electrode on electrolyte stress and of a seal design change.

Development of Improved Chromium Plating Techniques

The initial screening of potential plating techniques was completed. In this activity, the effect of four different electrolyte compositions on deposit quality and performance was studied. Encouraging results were obtained with M&T Unichrome CF-500, a proprietary, chemical self-regulating electrolyte. Also, this electrolyte was used with an addition of vanadium pentoxide V₂O₅. By adding 10 g/l of V₂O₅ to the electrolyte, the plating rate can be increased from 25 mm/h to 100 mm/h. Analysis of the plating quality showed no cracking, no co-deposition of vanadium, and the stress in the deposit reduced to 300 psi compressive, compared with

a 23,000 psi tensile stress produced when the vanadium is not present.

Zinc/Bromine Technology

Technology Development

The largest ETD-supported developmental program for the zinc/bromine battery was at Energy Research Corporation (ERC). The objective of this 4-year contract that concludes in 1989 is to demonstrate a proof-of-concept 36-kWh stationary battery by continuing development of ERC's zinc/bromine core technology acquired from Gould in 1982. In addition, Johnson Controls, Inc. (JCI), was contracted in February 1987 to fabricate and qualify a 20-kWh proof-of-concept zinc/bromine load management battery. This unit had completed 182 cycles by the end of 1988, substantially exceeding its 100-cycle anticipated life.

ERC Technology Development

ERC continued development of the zinc/bromine battery system for stationary energy storage applications. Progress in 1988 included the following:

- Problems in the end electrode design and in the seal between the flow frame stacks and the end assembly were resolved with additional improvements in the stack clamping procedure. Newly designed flow-frame hardware increases the electrode active area from 872 cm² to 1,500 cm² and significantly changes the design approach. The new frame takes into account piece-to-piece variations in injection molding, avoiding interference of raised sections on the frame that could cause cracking as the parts are stacked. It also addresses the problem of electrolyte leakage observed in some 872-cm² stack tests.
- Based on the performance observed during cycle testing of two 5-cell stacks and one 30-cell stack using the 872-cm² flow frame hardware, the hardware development effort has apparently addressed the earlier end-assembly problems. Resolution of this issue was important to the successful operation of the 1,500-cm² hardware. After a delay in acquiring the 1,500-cm² frame injection mold, testing began on the first stacks with the new hardware. Coulombic, voltaic, and energy efficiencies of 87.5%, 76.8%, and 67.2%, respectively were obtained. Testing will continue on the

150-mAh/cm² zinc loading regime to establish a performance baseline.

- An expanded stability test program was initiated for candidate battery materials. Plastic stability tests in 1988 validated the PVC selection made based on earlier screening test results. Three injection-molding grades of PVC (designated PVC-1, PVC-4, and PVC-6) are on test. PVC-6 exhibited improved stability in the screening tests compared to the baseline PVC-1 and had the additional advantage of containing no tin. PVC-6 was selected for use in the 1,500-cm² frame.
- The cell and stack components currently used in the ERC zinc/bromine battery system have been screened using immersion and electrochemical stability tests to evaluate bromine electrode and separator design options. Using the same test matrix as the PVC studies, immersion tests on separator materials including Daramic (25-mm and 35-mm thick), AmerSil™ PVC separator (from Amerace Corporation), silicone-filled Daramic, and Daramic filled with fluoropolymer sealant are underway. After 16 weeks, both 25-mm and 35-mm Daramic separators showed some decrease in tensile strength but are well within battery requirements. The latter exhibited about a 10% dimensional and weight change in polybromide at 45°C. All other properties showed no significant change within test error limits. A material stability concern is the Daramic separator material which has exhibited surface roughening and loss of the silicone gasket filler. Work needs to be done to identify a more stable alternative to the silicone gasket filler. The bipolar electrode and felt components remained stable over 3,000 charge/discharge cycles.

Evaluation of the new frame hardware will continue in larger battery systems. The last build is planned to consist of two 52-cell stacks plumbed into a common flow system, for a total energy rating of 36-kWh.

JCI Technology Development

Qualification of the JCI load-management 20-kWh battery continued. A new type of reinforced high-density polyethylene electrode material, comparable in cost to the current material (≈\$4.00/kWh for 0.025-in polyethylene), with glass loadings up to 50% was developed. Polyvinylidene fluoride (PVDF), also known as Kynar, has also been tested for use as the base

polymer for an electrode. An optimization study was performed on a 1-kWh laboratory battery to evaluate three electrolyte components for use in the anticipated load-leveling electrolyte with the V-design system. The JCI computer model has been used to optimize battery component thicknesses for the V-design flow frame for load-leveling batteries.

The Z-20LL 20-kWh load management battery, consisting of two stacks of 78 cells each with an adhesive and bolt assembly, is on test at the JCI Keefe Avenue Facility. After completing 159 cycles, with the battery performing at 60% energy efficiency, the electrolyte was changed to reflect advances in electrolyte composition, and nine additional cycles were run with some decline in coulombic and energy efficiencies. After repairs, continued testing of the new electrolyte showed a 2.4% increase in energy efficiency over the original electrolyte. During cycle 182, a short circuit caused the battery to fail. This performance, however, exceeded the, originally anticipated 100 life cycles.

Technology Evaluation

During 1988, one 5-cell ERC zinc/bromine battery was evaluated at SNL, and it operated for 100 cycles. Testing was terminated after the rapid drop in efficiencies was observed at cycle 98. The battery will be torn down to determine the cause of the efficiency drop. A 30-cell ERC zinc/bromine battery was still on test at the end of 1988 with 66 cycles completed. Initial performance was comparable to the expected levels, but the efficiencies became inconsistent late in 1988 and began to decrease.

Technology Improvement

Advanced Membrane Development for Zinc/Bromine Batteries

This effort involves improving separator performance by impregnating and/or coating microporous materials with small quantities of cationic polyelectrolytes. Progress included the following: uniform impregnation of microporous separators, an extensive range of separator performance, and development of a mathematical model of cell performance that will be used to guide future activities. Currently, the actual performance of these hybrid materials is being evaluated in single-cell tests.

Durability of Zinc/Bromine Materials

Studies have been made of the durability of several PVC formulations under consideration by ERC as flow frame materials. The results showed that the concentration of both aliphatic and aromatic additives in the PVC was reduced by about 90% after exposure to electrolyte at 60°C for 18 weeks. Surface degradation in the flow channels and adjacent regions was observed in an ERC flow frame that had been in use for one year. Pure PVC is more stable to bromine-containing electrolytes than commercial PVC formulations. Pure PVC is too brittle, however, to consider for use in the flow frame. Because of a potential long-term durability problem, Tefzel was identified as a possible alternate.

Nickel/Hydrogen Technology

Technology Development

JCI, the sole developer of nickel/hydrogen technology for the ETD Project, continued development of a terrestrial nickel/hydrogen battery that seems ideally suited for remote solar applications. Previous studies indicated that a competitive life-cycle cost is achievable and, therefore the 1988 effort centered on reducing costs of the negative catalyst, the hydrophobic backing on the negative electrode, the asbestos separator, the nickel sinter, and the pressure vessel.

- Negative electrodes with reduced quantities of 10% platinum-on-carbon catalyst have performed well to date. Above-average performance was achieved in the polarization tests by using a lower cost alloy-on-carbon (AOC) catalyst.
- Full-size negative electrodes were prepared using three times the normal quantity of fluoroplastic binder instead of fluoroplastic films. In another approach, purchased fluoroplastic films were replaced with less expensive JCI-prepared films. Both electrodes are performing well and result in ≈\$50/kWh reduction in cost.
- Because of environmental concerns about the use of fuel-cell grade asbestos separator material and its uncertain availability, candidate non-asbestos materials were screen-tested throughout the year.

- Developing a thicker positive electrode, and consequently using fewer cell components, would reduce cost and improve energy density. Also, less costly substitutes for the sintered nickel plaque such as fiber and foam materials are being sought.
- A new fiber/epoxy reinforced metal-shell pressure vessel was designed and drawings submitted to vendors. Two other configurations, an all-fiber-reinforced-epoxy vessel and an all-metal vessel, remain viable pressure vessel candidates.

A photovoltaic test system, consisting of a solar array, a battery, and a load, was set up in Milwaukee. A simple energy management system, which sheds four individual loads at different states of charge, was connected to the system.

Technology Evaluation

Six nickel/hydrogen cells and three batteries were subjected to cycle and solar tests at SNL during 1988. A 7-kWh battery is being evaluated using a flat plate photovoltaic array and an electrical load. No controller was used between the three elements since the gases generated on battery overcharge are recombined internally.

Aluminum/Air Technology

Technology Development

Eltech Research Corporation continued ETD-sponsored research and development of aluminum/air batteries for electric vehicle (EV) applications. The present program addresses design and optimization of the aluminum/air cell and of the auxiliary systems (including heat exchanger, solids separation, control of carbon dioxide, and the disposal of hydrogen gas). Progress in 1988 included the following:

- Extensive single-cell evaluations validated the B-300 design as a laboratory test unit and focused on the key technical challenges facing this technology. A mathematical model of the B-300 cell, developed by Dr. Robert Savinell at Case Western Reserve University, correlated the results obtained from a study of the

electrolyte flow rates and has been used to identify operating conditions and cell-design features that affect performance. According to the analysis over the ranges of values selected for the matrix, the cell performance was insensitive to fluid flow rates. The shunt currents in a B-300 battery were estimated, and the power losses were shown to be less than 0.3%.

- An electrolyte-water-air system was selected as a heat exchange unit for the aluminum/air battery and, based upon the results obtained from a simulated 12-V battery system, a plate and frame exchanger design was recommended.
- The Helipump fluidizer impeller, a device potentially capable of efficiently separating fine particles of hydrargillite from the electrolyte, was characterized. In all cases, the efficiencies of separating fine particles (sizes less than 10 microns) were low, ranging from 55% to 65%. A mathematical model of the device was developed by Dr. Robert Adler, at Case Western Reserve University, and the model clearly indicated this limitation.
- An alloy development task was defined to identify a high performance aluminum anode. Also, studies were begun to investigate design improvements for air electrode performance and longevity.
- A 10-cell battery was designed and fabrication began in late 1988. The evaluation of this unit next year will be a critical test of progress in the technology.

Technology Evaluation

An Eltech aluminum/air single cell was installed at SNL during the week of June 20, 1988. When fully charged with aluminum (≈ 350 g), the cell had a theoretical capacity of $\approx 1,040$ Ah. During 1988, the cell was run a total of 48 times using 24 anodes for an elapsed run-time of 232 hours. The aluminum electrode efficiency varied from 70-90%, while the corrosion rate ranged from 20-80 mA/cm². Aluminum energy output was consistent at about 2.6 Wh/g. Anode utilization was limited to a maximum of about 57%. The air cathode was replaced seven times during these tests. Eltech has redesigned the B-300 cell to resolve most of the mechanical problems identified.

Chapter 2. Aqueous Battery Development

Introduction

During 1988, the Exploratory Battery Technology Development and Testing Project continued to support the zinc/bromine and nickel/hydrogen advanced secondary battery systems. In addition, ETD continued development support of a mechanically rechargeable aluminum/air system. In all cases, these developmental activities were implemented by industrial organizations through cost-shared contracts.

The following developmental programs were supported in 1988:

- Zinc/bromine battery by Energy Research Corporation (ERC) (Danbury, Connecticut)
- Zinc/bromine load management battery at Johnson Controls, Inc. (JCI) (Milwaukee, Wisconsin)
- Nickel/hydrogen battery at JCI (Milwaukee, Wisconsin)
- Aluminum/air battery at Eltech Systems Corporation (Fairport Harbor, Ohio).

The largest program in this series is the zinc/bromine battery development with ERC. This \$5.1M program began in September 1985. The objective is to demonstrate a proof-of-concept 36-kWh stationary battery during the final contract year (1989) by continuing the development of ERC's zinc/bromine core technology acquired from Gould in 1982. The 1988 activities represented 75% of this 4-year contract.

In February 1987, JCI was contracted to fabricate and qualify a 20-kWh proof-of-concept zinc/bromine load management battery. The battery stacks were fabricated from residual Exxon piece parts, and the battery system was evaluated at the JCI Keefe Avenue Facility. The unit had completed 182 cycles by the end of 1988, and it substantially exceeded its anticipated life of 100 cycles.

The development of a nickel/hydrogen battery for terrestrial applications continued at JCI. The overriding mission is to reduce component cost without compromising performance. Previous studies indicated that a competitive life-cycle cost is achievable, and they pointed to the nickel sinter, the negative catalyst, the hydrophobic backing on the negative electrode, the

asbestos separator, and the pressure vessel as having the most impact on cost. Thus, the effort in 1988 centered on reducing these costs.

In 1988, the development of aluminum/air batteries for electric vehicle applications continued at Eltech Research Corporation. Extensive single-cell evaluations at Eltech characterized the B-300 cell performance. These tests validated the B-300 design as a laboratory test unit, and they focused the development project on the key technical challenges facing this technology. The aluminum anode required further research, and an alloy development task was defined to address this need. Air electrode performance and longevity were other key challenges, and studies were begun to investigate design improvements. Modeling and experimentation with the Helipump solids separator indicated that it would not satisfy the requirements, but other experiments with single cells demonstrated that gravity separation techniques may be feasible. An electrochemical model of the B-300 cell quantified the possible operating ranges of several key variables, such as electrolyte and air flow rates. Finally, a 10-cell battery was designed, and fabrication began in late 1988. The unit will be evaluated next year, and this will be a critical test of the technology.

Zinc/Bromine Battery Development - ERC

ERC is developing the zinc/bromine battery system for stationary energy storage applications. Two projects are under way in the program. Technology development work is supported by the U.S. DOE through SNL. A smaller project supported by the Electric Power Research Institute (EPRI) examines design and commercialization issues specific to the utility load leveling application. This report describes the work conducted in the SNL-supported technology development project.

The SNL project, which began in September 1985 and runs through December 1989, has focused on hardware testing and the development of a new generation of stack hardware. Earlier work involved material and component development. The final year (1989) will involve fabricating and testing a 36-kWh proof-of-concept battery system.

Specifically, progress in 1988 was made in the following tasks:

- **Hardware Development.** Additional improvements were made in the stack clamping procedure, resolving problems in the end electrode design and in the seal between the flow frame stacks and the end assembly. The first 1,500 cm² flow frames were tested.
- **Battery Testing.** Cycle testing continued with two 5-cell stacks and one 30-cell stack, using the 872-cm² flow frame hardware.
- **Material Stability Studies.** An expanded stability test program was initiated for candidate battery materials.
- **Component and Subsystem Development.** Bromine electrode and separator design options were evaluated in small-cell electrochemical tests.

In addition to hardware improvements in the stack clamping system, the most significant area of hardware development was in the testing of the first 1,500-cm² flow frames. The new hardware was evaluated in dye-injection flow tests, single-cell zinc deposition tests, and 5-cell stack tests.

Battery tests in 1988 included the continued cycle testing of two 5-cell stacks and one 30-cell stack, using the 872-cm² flow frame hardware. Testing also began on the first 1,500-cm² 5-cell stacks. In addition to demonstrating system performance and life capabilities, the stack tests have been used to evaluate iterations of hardware designs and system instrumentation and control.

Material stability studies continued in 1988 with the initiation of an expanded stability test program for candidate battery materials. These studies followed a series of screening studies that evaluated several different plastics. The new tests focused on the more promising materials in the screening tests, addressing fewer materials in more detail. The plastics currently on test are all PVC injection molding resins. A similar test is being conducted on separator and gasket materials.

Small-cell electrochemical stability testing also continued, with 20-cm² cells logging up to 3,000 short cycles (1-h charge input). These tests evaluated bromine electrode and separator design options.

The following sections describe the hardware testing and hardware development activities as well as the results of the material stability studies.

Hardware Development

Stack Clamping Assembly

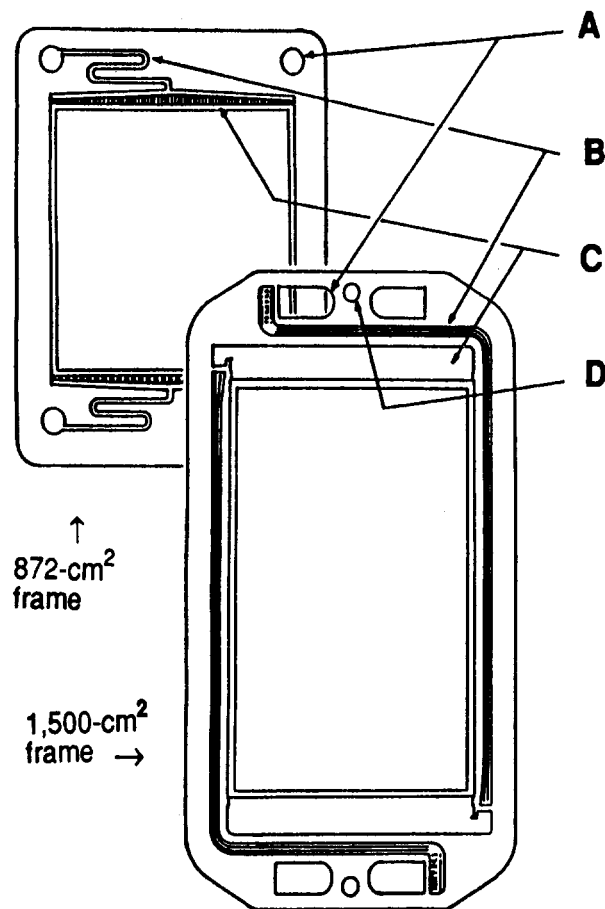
The zinc/bromine battery stack consists of a bipolar configuration of electrode/flow frame assemblies. The stack of frames is held together by tie bolts, whose tension is distributed over the flow frame area by clamping hardware at each end of the stack. The load is distributed by a 1.3-cm-thick steel strongback, with stiffening ribs to ensure even clamping. A PVC end plate is used at each end of the stack, between the steel strongback and the stack of flow frames. The end plate contains the end electrode current collector and provides for the flow connections to the stack. The end electrode is a 0.6-cm-thick titanium plate with a centrally located current collecting post. Contact with the first working carbon-plastic bipolar electrode is via carbon felt between the bipolar plate and the end electrode for uniform electrical contact between electrodes that compensates for any slight misalignment of the plates.

During operation of 5-cell stacks with the new hardware, a problem was found with the end electrode connections. In the initial design, the support in this felt contact area was insufficient. The hydraulic pressure of the electrolyte on the working side of the end bipolar electrode caused the end flow frames in the stack to crack. The end contact system was improved by increasing the compression of the carbon felt contact distributor.

After extended testing with this end design, the elastomer gasket that sealed the end assembly to the stack of flow frames swelled and clogged the flow channels. The end assembly was redesigned to eliminate the gasket. The seal between the end assembly and the flow frames is now made with a solvent bond by machining off the sealing ridges on the nonworking (dry) side of the flow frame to create a flat sealing surface. The bonded subassembly consists of the PVC end plate (either the end electrode and flow connections) on one side and the first working flow frame on the opposite side. This end assembly design is currently on test in two 5-cell stacks (one 872-cm² stack and one 1,500-cm² stack) and one 872-cm² 30-cell stack.

1,500-cm² Flow Frame Design

The hardware development focused on the design of a new generation of stack flow-frame hardware, which increases the electrode active area from 872 cm² to 1,500 cm² and significantly changes the design approach. The two flow frames are compared in Figure 2-1. The most apparent design change in the new



- A. Flow Manifolds** are oversized in new frame to eliminate pressure drop in stack manifold. This promotes good cell-to-cell flow uniformity in multi-cell stacks.
- B. Flow Channels** are deeper in new frame to lower pumping power requirements and reduce likelihood of clogging.
- C. Flow Distributor Plenum** is larger in new frame to provide more uniform flow over cell area.
- D. Line-Up Mandril Holes** to ensure good stack line-up.

Figure 2-1. Comparison of 872-cm² and 1,500-cm² Frame Designs

frame is the narrow, high-cell geometry for zinc deposition considerations. The narrow cell geometry achieves the flow velocity for good deposit quality at a

lower volumetric flow rate than a wider cell has which reduces pumping losses in the long flow channels and in the ancillary piping.

Other differences between the two frame designs relate to problems with the 872-cm² flow frames such as flow channel clogging, frame cracking, electrolyte leaking, high pumping-pressure requirements, and poor cell-to-cell flow uniformity in multicell stacks.

Flow channel clogging occurred in the 872-cm² frames from three causes. As described above, swelling of the end assembly gasket clogged end cell flow channels. This was addressed by eliminating the gasket. Debris clogging was observed in some 872-cm² stack tests. In addition to using basket strainers in the flow lines, the debris clogging problem was addressed in the new frame design by increasing the number of flow channels and making those channels deeper. The third source of flow blockage, separator bowing, was addressed by the deeper flow channels (0.32 cm vs 0.13 cm in the 872-cm² frame) as well. As the stack of frames is compressed, the separator (in the filled gasket area) bows into the flow channels, reducing the channel area by up to 80%. The variability in the degree of bowing results in cell-to-cell flow nonuniformity, precluding operation of multicell stacks at higher capacity densities. The deeper flow channels in the 1,500-cm² frame should eliminate the separator clogging problem as well as reduce pumping-pressure requirements significantly.

Another problem with the 872-cm² frame was frame cracking under stack compressive loading. This problem stemmed from switching the frame material from polypropylene to PVC after component bonding problems with polypropylene and after it was demonstrated that polypropylene would not be stable enough for the 10-year utility load-leveling mission. The frame design called for tight tolerances in sealing ridge line-up and included several high-stress, right-angle corners. Polypropylene can creep enough to absorb the stresses of overlapping sealing ridges and misaligned frames, while PVC cannot. Frame cracking in the 872-cm² frames has been addressed by annealing the parts before use and by reducing the level of stack compression. The sealing ridge alignment remains a problem because ridges on opposite sides of the frame are close enough to overlap, given normal piece-to-piece variation of injection-molded PVC components.

The new frame takes into account piece-to-piece variations in injection molding, avoiding interference of raised sections on the frame that could cause cracking as the parts are stacked. Additional structural support has

been built into areas where cracks occurred in the 872-cm² frames, and rounded corners have replaced sharp corner areas where stress concentration could occur.

The new frame design also addresses the problem of electrolyte leakage observed in some 872-cm² stack tests. The sealing technique in both frame designs uses ridges outside the channel areas that are impressed into the separator gasket material, creating the required seals. The 1,500-cm² frame uses multiple sealing ridges where the 872-cm² frame has only single ridges. The larger frame has also been designed to run at lower electrolyte leakage.

To improve cell-to-cell flow uniformity, the manifold holes at the top and bottom of the frame have been made much larger. This ensures that the pressure in the manifold is very low so that all cells in the stack have the same inlet and outlet pressures. In theory the large manifolds also increase shunt currents; however, the contribution of the manifolds to shunt resistance is minimal compared to the cell flow channels.

1,500-cm² Stack Test Results

The first 1,500-cm² multicell stack tested was a 5-cell stack designated 1500-5-1, built with machined flow-frame prototypes before molded frames were available. Most cycle testing was done on a 150-mAh/cm² regime, which used a 5-h, 35-mA/cm² charge followed by a discharge at 37.5-mA/cm² to a 6-V cutoff. This is the regime proposed for testing the 36-kWh module to be built at the end of the program. Although it is anticipated that stacks built with the new frames can be cycled at 200 mAh/cm², the rating of the modules is based on 150 mAh/cm² since limited cycle testing has been done on stacks at the higher loading level.

Figure 2-2 shows the efficiency for 1500-5-1 over the 85-cycle test. Initially, the voltage of the stack was more sensitive to electrolyte pressure differential than were the 872-cm² stacks. For example, if the anolyte flow pressure was raised to 5 to 7 psi higher than the catholyte pressure, stack resistance immediately decreased. The larger bipolar plates and separators flexed more than the 872-cm² components, compressing the carbon felt electrodes and lowering the felt-to-plate contact resistance. While it would be desirable to operate continuously with the lower resistance, the high pressure differential caused excessive electrolyte crossover.

During cycles 32 through 39, a second layer of carbon felt was installed in each of the five cells to compress the cathodes mechanically, achieving the lower resistance without the hydraulic pressure differential and its resulting crossover. Voltaic efficiency

was raised by about 5% to 80%, but coulombic efficiency fell as low as 60%. The second felt pieces were removed after cycle 39, and regular cycle testing resumed. With continued cycling at 150 mAh/cm², coulombic efficiency recovered and remained stable at about 85%, while energy efficiency averaged slightly less than 60%.

Testing recently began on the first stack built with injection-molded 1,500-cm² flow frames. The first cycle was short, with only 1-h charge input and 93% coulombic efficiency. Figure 2-3 shows voltage performance for the stack on the second charge/discharge cycle, which was run on the full 150-mAh/cm² regime. Coulombic, voltaic, and energy efficiencies of 87.5%, 76.8%, and 67.2% were obtained. Testing will continue on the 150-mAh/cm² regime to establish a performance

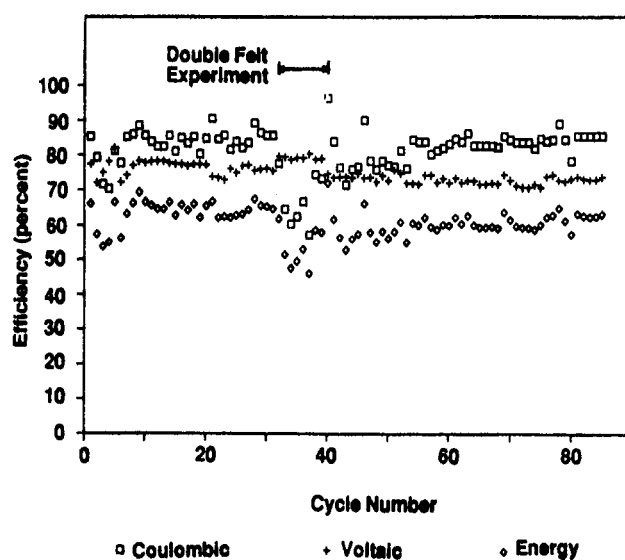


Figure 2-2. 5-Cell Stack 1500-5-1

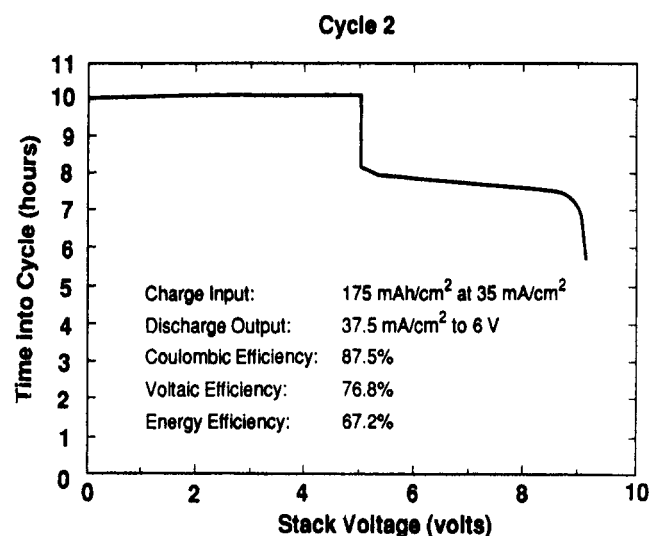


Figure 2-3. 1,500-cm² 5-Cell Stack 1500-5-2

baseline. Additional testing will include cycling on a regime with 200-mAh/cm² discharge capacity density, as well as characterization testing such as polarization and stand-loss tests.

872-cm² Battery Design and Testing

System and component designs were evaluated in continuing 5-cell and 30-cell battery tests using the 872-cm² flow frame hardware. The standard cycle test consists of a 5-h charge at 30-A (172-mAh/cm² charge) followed by a 30-A discharge to a voltage cutoff (1.2 V/cell). Typical discharge capacity on the baseline regime is 150 mAh/cm². After each discharge, a brief low-rate discharge is usually conducted, followed by an open-circuit stand period to remove residual zinc.

The 5-cell stack SNL-5-3 was originally built using the three-loop flow system. In this system, the polybromide was recirculated in a separate flow loop and mixed with the catholyte in a static mixer in the flow line. As described in the *ETD Annual Report for 1987* (page 30), a new system was designed in which the mixing and separation of the polybromide and catholyte fluids occurs in the catholyte tank.

Efficiency data for the SNL-5-3 cycle tests are shown in Figure 2-4. An electrolyte cleaning was required to achieve acceptable performance after 11 cycles. Although performance improved, coulombic efficiency was erratic in subsequent tests and, after 40 cycles, the stack was taken apart for inspection. The end frame was found to have cracked because of

insufficient support in the contact area. The stack was rebuilt with the new end plate design described above; however, an elastomer gasket still sealed the end assembly to the flow frame stack.

Two other design changes were made when the stack was rebuilt. The flow system was replaced with the two-loop system design and the 0.025-in-thick Daramic separators were replaced with 0.035-in-thick separators. Testing resumed and performance remained stable until cycle 160, when voltaic efficiency began to decline. The decline of voltaic efficiency is believed to have been caused by the swelling of the elastomer gasket, which clogged end-cell flow channels.

Stack SNL-5-4 was built and put on test at the same time as SNL-5-3, and it also contained 0.025-in-thick Daramic separators. This battery was the first to incorporate the two-loop flow system design and variable frequency pump motors. The system also included the first electrolyte level sensor, and the battery has been used to evaluate automatic pump speed control techniques. Figure 2-5 shows efficiency data for the stack on the cycle test. On test for more than 280 cycles, SNL-5-4 has gone through two end electrode design revisions.

The first end electrode modification was to increase the level of compression on the dry carbon-felt contact in the end electrode. After 108 cycles had been run on the stack, the end assembly was replaced. No cracked frames were observed; however, performance improved after the end plate was installed because of better end contact.

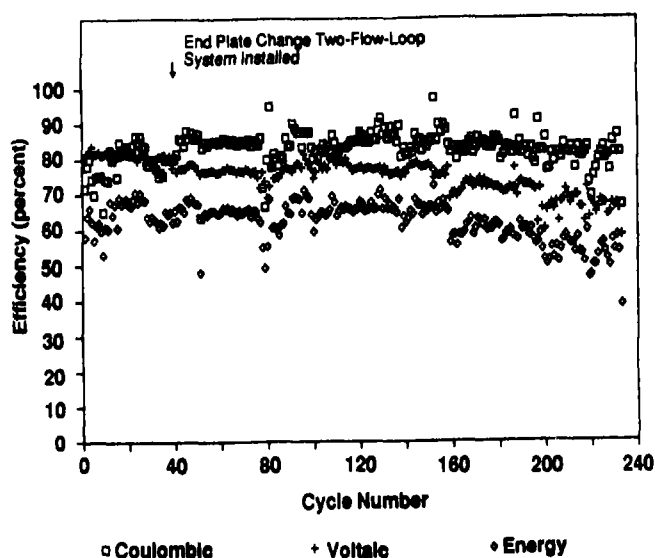


Figure 2-4. Cycle Performance (5-Cell Stack SNL-5-3)

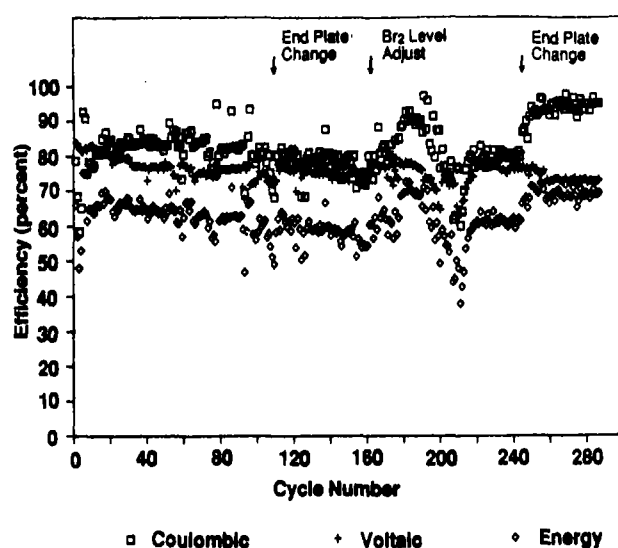


Figure 2-5. Cycle Performance (5-Cell Stack SNL-5-4)

After cycle 160, the catholyte bromine level was adjusted to replace evaporated bromine. Coulombic efficiency increased to above 90%. A subsequent decline in efficiency was observed, which was determined to have been caused by clogged flow channels in the positive end cell because of the swelling end-assembly gasket. The end assembly was designed to eliminate the unstable gasket, as described above. This end design modification was used in SNL-5-4 after cycle 244. In the 40 cycles since the end assembly was installed, coulombic, voltaic, and energy efficiencies have averaged 93.5%, 73.7%, and 68.9%, respectively.

Testing has also continued on 30-cell stack SNL-30-2, which also used the new two-loop flow system. A performance curve for 30-2, which had been on test for more than 300 cycles, is shown in Figure 2-6. The efficiency performance over the cycle test is shown in Figure 2-7. This stack has also gone through two end electrode assembly design revisions. The newest end assembly design (eliminating the elastomer gasket) was installed in the stack after 263 cycles. In installing the new end assembly, the effect of the flow channel clogging could be seen, as salts had built up in the end cell, which had been starved of electrolyte because of the swelling gasket. The salts had built up to a level beyond the cell channel gap thickness, cracking the bipolar electrodes of the two cells adjacent to the positive end cell. The first five flow frame assemblies at the positive end of the stack were replaced, and the stack was rebuilt. Over the history of the test, coulombic, voltaic, and energy efficiencies have averaged 84.9%, 73.5%, and 62.4%, respectively. Since the installation of the new end assemblies, these efficiencies have averaged 86.4%, 76.6%, and 66.1%.

The 30-cell SNL-30-2 system has also been used as the test bed for a variety of system instrumentation and control strategies. The system is equipped with a state-of-charge indicator that monitors anolyte specific gravity to determine charge level. An on-line pH meter is installed in the anolyte flow system. An optical probe system monitors tank electrolyte levels.

Since the new end assembly was installed, the stack has been tested on an automatic cycle regime, logging two baseline cycles per day. After running six to eight cycles, coulombic efficiency declined to about 80% because of the buildup of residual zinc. This decline occurred because the open circuit stand time between cycles was not sufficient to strip residual zinc from the electrodes. In current testing, an extended stripping cycle is done after every five cycles, and coulombic efficiency stays above 85%.

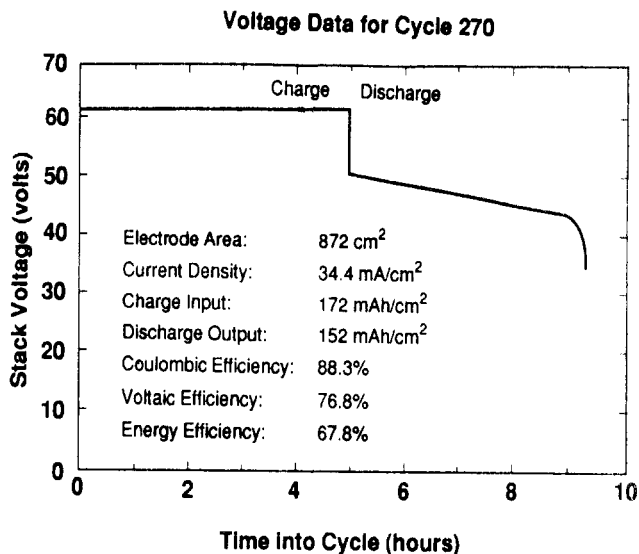


Figure 2-6. 30-Cell Stack SNL-30-2

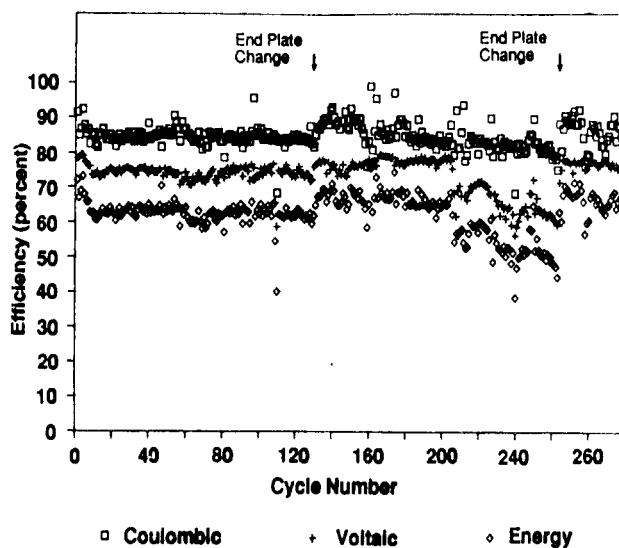


Figure 2-7. Cycle Performance (30-Cell Stack SNL-30-2)

Hardware Development Status

Based on the continuing performance of 872-cm² 5- and 30-cell stacks, the hardware development effort has apparently successfully addressed the earlier end assembly problems. The new solvent-bonded end assembly is performing well in SNL-5-4 and SNL-30-2, with energy efficiencies of 67% to 70%. Resolution of this issue was important to the successful operation of the 1,500-cm² hardware. The first stack built with molded frames is on test and initial test results are promising. A delay in acquiring the 1,500-cm² frame

injection mold has led to delay in testing the first stacks with the new hardware.

Material Stability Studies

Plastic Stability Studies

The plastic stability tests in 1988 followed a series of screening tests earlier in the project. These screening tests examined the stability of a number of plastic materials, including polyolefins, polyvinylchloride, and chlorinated polyvinylchloride (CPVC). The PVC and CPVC materials were most stable in the screening tests, although high levels of tin leached out of the CPVC, which ruled out its use. It was decided to study the most stable materials in an expanded test matrix.

The test matrix included three immersion temperatures: 35, 45, and 55°C. The solutions used were electrolyte with 10 g/l Br₂, and the polybromide complexing agent. In addition, some samples were aged in air at room temperature to separate chemical changes from other aging phenomena.

Three injection molding grades of PVC designated PVC-1, PVC-4, and PVC-6 are on test. PVC-1 is the baseline material in all 872-cm² flow frames. PVC-4 was the most stable material in the screening tests, but one component is a tin-based stabilizer that could affect cell performance if it leached into the electrolyte. PVC-6 also exhibited improved stability in the screening tests compared to the baseline PVC-1, and it had the additional advantage of not containing any tin. PVC-6 was selected in the 1,500-cm² frame mold based on the earlier screening tests.

The test samples are molded tensile test bars immersed in tubes of electrolyte. A small quantity of polybromide is placed at the bottom of each tube, below the sample, to maintain a constant Br₂ level during evaporation and absorption into the sample. All the samples were annealed before immersion. When removed from the tubes, samples are tested for size, weight, and tensile strength changes.

Samples have been removed and analyzed after 4 weeks and 16 weeks of immersion. The greatest weight gain was in PVC-1 after 16 weeks immersion in 55°C electrolyte (20 g/l Br₂), which increased in weight by 17%. Under the same conditions, PVC-4 gained 9% and PVC-6 gained 14%.

The dimensional changes in the samples have been negligible, with the greatest change being a 0.5% increase in length for PVC-1 in 55°C electrolyte (20 g/l Br₂). The strength changes have all been negligible

except for PVC-1, which exhibited a 5% to 20% strength decrease over the temperature range in brominated electrolyte. All the samples exhibited a 3% to 4% strength increase when aged in air at 55°C for 16 weeks, probably from continued annealing.

Future sampling will be at 60 weeks and 120 weeks. The data obtained in the test indicate that the relative stability ranking in the earlier screening tests is valid. The selection of PVC-6 over the baseline PVC-1 appears to have been justified by the improved stability in the expanded tests, particularly by the strength data. As the test proceeds, the additional data should allow estimation of engineering properties for these materials over time, which will be used to estimate lifetimes for flow frame and piping components made from these materials.

Separator Stability

Using the same test matrix as the PVC studies, separator materials immersion tests are also under way. The materials under test include Daramic (25- and 35-mm-thick), Amer-Sil™ PVC separator (from Amerace Corporation), silicone-filled Daramic, and Daramic filled with a fluoropolymer sealant. The fluoropolymer sealant had been investigated as a more stable alternative to the silicone, although sufficient pore filling could not be achieved with it. (This sealant was included in these stability tests to provide data if more uniform pore filling can be achieved.)

The analyses after immersion include dimensional and weight measurements, porosimetry, tensile strength testing, and evaluation of bromine permeability and resistance. After 16 weeks, both 25- and 35-mm Daramic separators showed some decrease in tensile strength, but they are well within battery requirements. The 35-mm material exhibited about a 10% dimensional and weight change in polybromide at 45°C. All other properties showed no significant change within test error limits.

The Amer-Sil separator after 4 weeks had only one significant property change, a 2- to 3-fold decrease in resistivity, which coincided with a lower mean pore size. After 16 weeks, the resistance rose and the pore size returned to the control range. All other properties showed no significant change.

The fluoropolymer-coated Daramic samples were tacky upon removal from media after 16 weeks of immersion, and the samples from the quaternary ammonium bromine complex (QBr) media were covered with hard, nodular blisters. None of the samples showed any loss in tensile strength or resiliency, but some samples increased in porosity.

The silicone-coated samples were also tacky upon removal from solution. Both porosity and pore size increased with immersion time in the test media, indicating loss of impregnated silicone for the immersed samples. Samples at 15 weeks for 10 g/l and QBr media reached 20% porosity. Conductivity remained immeasurably small for all coated samples tested, which is the desired characteristic for the filled gasket material.

As with the PVC tests, additional data points at 60 and 120 weeks will provide a basis for estimating the useful lifetime of the separator and gasket materials. To assess the degree of acceleration caused by the test conditions, separator and gasket samples from the SNL-30-2 rebuild are being evaluated using the same characterization tests that were used in the stability work. This indicated how the immersion tests correlate with cycle history and calendar time.

Electrochemical Stability

Cell component stability is also being studied in 20-cm² cell tests. These tests use a 1-h charge time to log cycles quickly. Cells are tested in groups, and individual cells are removed at scheduled intervals for analysis. The longest scheduled cycle test on any group of cells is 3,000 cycles. As cells are taken off test, components are evaluated visually and microscopically. Porosimetry and surface area tests are conducted on the separator and bipolar plate components as well as tensile strength tests. Cells have been cycled for up to 3,000 cycles with no detectable degradation of the bipolar electrode material. None of the bromine electrodes made with the current baseline felt have exhibited significant degradation. The most significant degradation has been observed in the separator material, which has exhibited surface roughening and loss of the silicone gasket filler. While this has not led to impaired cell performance, it is being studied further in conjunction with the immersion tests described above to assess the impact on long-term battery operation.

The tests have been used to evaluate the stability of a ruthenia catalyst, which improves bromine electrode performance. Another bromine electrode variation, felt carbonized in an oxidizing atmosphere, was also evaluated in the stability test. Both electrodes are stable over the 3,000 cycle test; however, because the materials have not been tested extensively in full-size stacks, the baseline carbon felt electrode has been specified for use in the 36-kWh modules.

Material Stability Status

The cell and stack components currently used in the ERC zinc/bromine battery system have been screened in immersion and electrochemical stability tests. The bipolar electrode and felt components remained stable over 3,000 charge/discharge cycles. The immersion test data on the bipolar electrode material (discussed in the *ETD Annual Report for 1987*, page 37) indicate that the material may be stable enough to last the 10-year load-leveling life requirement. In the small cell test as well as full-size stack tests, no degradation of the carbon felt bromine electrode has yet been observed.

The plastic stability test results are providing data for selecting component specification (e.g., pipe or tank wall thickness), as well as estimating the useful life of the flow frame. The studies have validated the PVC selection made earlier based on screening test results, and they indicate that the currently used material is significantly more stable with respect to tensile strength than the previous baseline.

An area of concern in material stability is the Daramic separator. This material has never been identified as a cause of stack failure, although some degradation was observed in small cell tests. The stability of the silicone gasket filler is also uncertain, and work needs to be done to identify a more stable alternative. Based on stack results to date, these concerns relate more to the long-term 10-year stack life requirement than to short-term testing.

Future Work

Evaluation of the performance of the new frame hardware is just beginning. The remainder of the core technology program will center on evaluating the new hardware in larger battery systems. The 5-cell tests will continue as the first 52-cell system is fabricated. When operated with 150-mAh/cm² capacity density, each frame will store 360 Wh of energy; thus, a 52-cell system operated at this level will store 18 kWh of energy.

The last build in the current core technology program will consist of two 52-cell stacks plumbed into a common flow system, for a total energy rating of 36 kWh. Figure 2-8 shows the general configuration of the 36-kWh system. If extended cycling at 200 mAh/cm² is demonstrated, the system can store up to 50 kWh of energy. While the system is not being configured as a

Materials and Electrochemical Research

Electrode

A new type of reinforced high-density polyethylene electrode material with glass loadings up to 50% was developed. This material has demonstrated a low expansion (0.24% after 24 h in bromine vapor), with only a small penalty in resistivity. This compares to 1.54% expansion for polyethylene with 16% carbon black and 16% glass fiber. It is expected that the resistivity increase can be countered by using higher carbon loadings in this material. No significant change in expansion and resistivity was observed beyond 24 h. The cost of this material is comparable to the cost of the current material ($\approx \$4.00/\text{kWh}$ for 0.025-in polyethylene).

Polyvinylidene fluoride (PVDF), also known as Kynar, has also been tested for use as the base polymer for an electrode. With 16% carbon-black filler and no glass fiber, expansion in bromine vapor was only 0.18% after 24 h. Extended bromine exposure testing (for 1 week) of the Kynar has shown that expansion increases to $\approx 1\%$.

Two areas of concern in using of Kynar are compatibility and cost. For battery use, Kynar electrodes must be capable of having adherent polyethylene frames molded around them. Ordinarily, Kynar would not bond well with polyethylene, but loading the Kynar with glass, graphite, or silica should improve the adhesion. Preliminary calculations show that 0.020-in-thick Kynar electrodes, with 50% filler, would cost about $\$11.50/\text{kWh}$.

Electrolyte

A load-leveling electrolyte component optimization study was performed on a 1-kWh laboratory battery. The study evaluated the three electrolyte components, zinc bromide (ZnBr_2), zinc chloride (ZnCl_2), and N-methyl, N-ethylpyrrolidinium bromide (MEP), for use in the anticipated load-leveling electrolyte with the V-design system. The initial study evaluated zinc bromide concentrations from 2.0 M to 3.0 M (in steps of 0.5 M), zinc chloride concentrations from 0.0 M to 1.0 M (in steps of 0.5 M), and MEP concentrations from 0.6 M to 1.4 M (in steps of 0.2 M). An electrolyte of 2.5-M

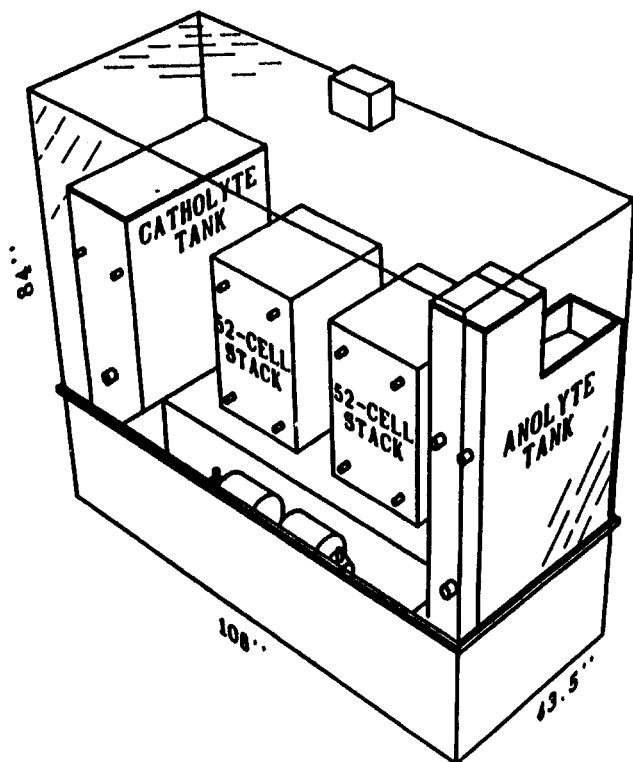


Figure 2-8. General Configuration for 36-kWh Zn/Br₂ Battery System

commercially viable unit, it will demonstrate the technology proposed for large utility load leveling systems.

Development of a Zinc/Bromine Load Management Battery - JCI

In March 1987, the Advanced Battery Business Unit of JCI, began work on a \$25,000 fixed-fee zinc/bromine load management contract. (This work was also partly sponsored by DOE contracts.) The contract scope included the fabrication and 10-cycle qualification of a proof-of-concept 120-V, 20-kWh zinc/bromine load management battery in JCI's Load Management Test Facility. In addition, 97 charge/discharge cycles were completed in 1987.

Installation of the Load Management Test Facility was completed early in 1987. Progress in the JCI load management battery is discussed below.

zinc bromide, 0.5-M zinc chloride, and 0.8-M MEP was used as a baseline for the analysis.

When the effect of zinc-bromide concentration was evaluated, the maximum energy efficiency (69%) was obtained with 2.5-M zinc bromide. The 2.0- and 3.0-M quantity electrolytes both exhibited significantly lower efficiencies (Figure 2-9). More detailed studies at other zinc bromide concentrations will be pursued.

The effect of the quaternary component was even more evident. A 1.0-M quantity of MEP had the highest energy efficiency at 71%. Figure 2-10 exhibits the data from this portion of the study. The lower energy efficiencies at concentrations below 1.0-M MEP can be explained by decreased coulombic efficiencies caused by bromine diffusion across the separator. This occurs because there is not enough quaternary ion in the electrolyte to complex all the bromine generated in charge. Higher concentrations of MEP increased the electrolyte resistivities, thereby also decreasing the energy efficiency.

Zinc-chloride studies did not show as appreciable an effect on energy efficiencies with the base electrolyte as did the zinc-bromide and MEP studies. Questions regarding the effect of zinc-bromide to zinc-chloride ratio will be tested in the near future.

General effects and trends of the component concentrations were evaluated at normal 8-cell operating temperatures (30 to 35°C). Evaluation of temperature effects on these components should be pursued.

V-Design Flow Frames

The JCI model has been used to optimize the battery component thicknesses for the V-design flow frame for load-leveling batteries. The V-design is an EV design developed under the DOE contract No. DE-AC04-88AL54304, also monitored by SNL. Four component parameters are directly related to the flow frame: electrode thickness, separator thickness, anolyte gap

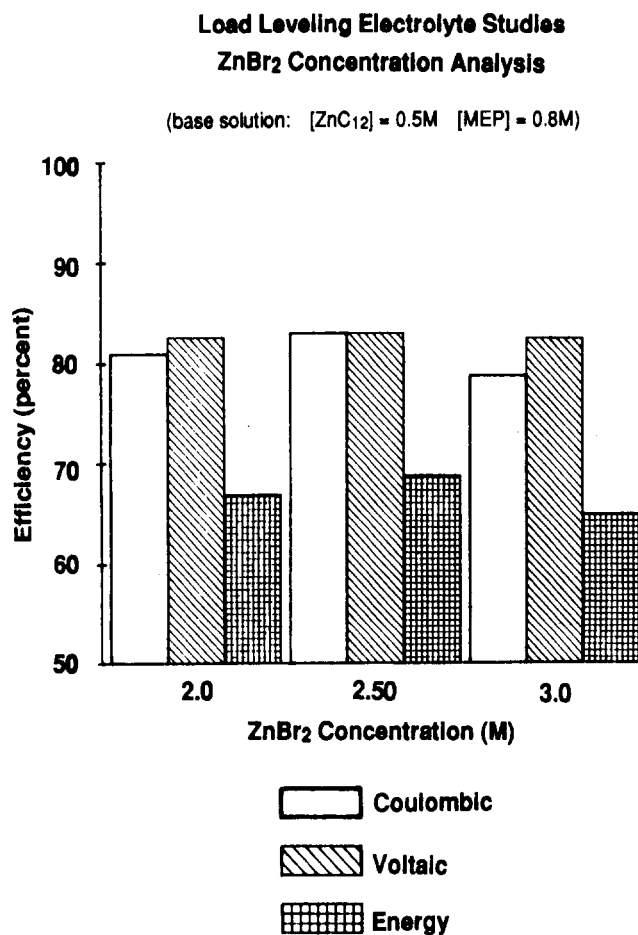


Figure 2-9. Zn/Br₂ Concentration (M)

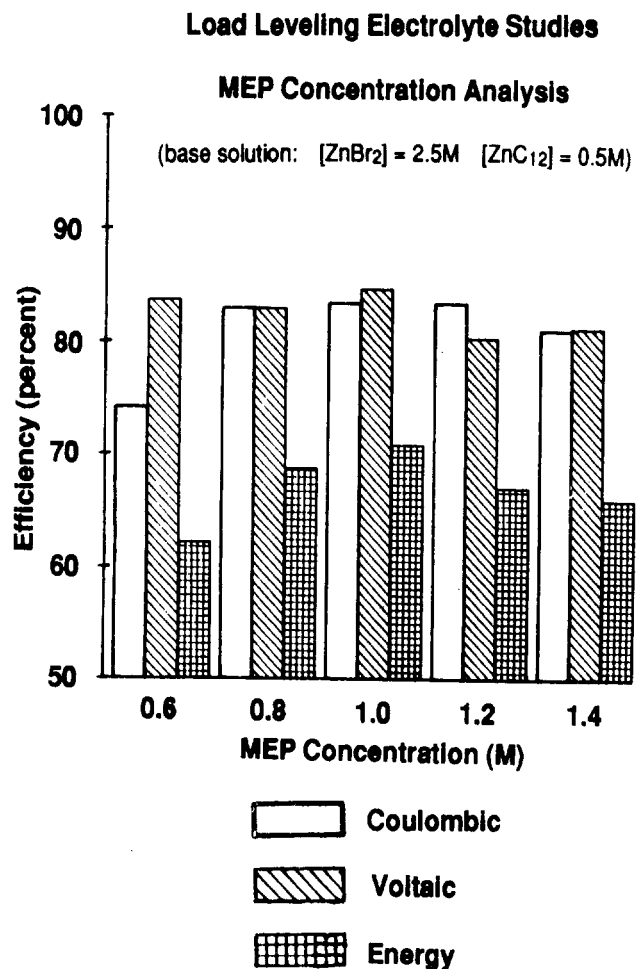


Figure 2-10. MEP Concentration (M)

thickness, and catholyte gap thickness. Studies at JCI showed that the effect of electrode thickness with a 1.0-ohm/cm resistivity carbon plastic is minimal for the cycling conditions anticipated (3-h discharge). Selection of the electrode thickness was based mainly on warpage considerations.

With separators of the type recently developed, the thickness for optimum energy efficiency is about 0.025 in. This separator has a resistivity of 12.1 ohm/cm ($\approx 25\%$ less than the present separator, 15.7 ohm/cm), and a bromine transport of $1.1 \times 10.8 \text{ M/s-cm}^2$.

The effect of the electrolyte gap width is appreciable—thinner gaps are favorable. With the new V-design flow frames, JCI will have the ability to test various electrolyte gap widths, changing in the electrode thicknesses. The first batteries will be made with electrolyte gaps of 0.025 in to avoid potential difficulties in maintaining uniform electrolyte flow.

Test results are shown in Table 2-1.

Z-20LL

The Z-20LL battery is the 20-kWh load management battery located at the JCI Keefe Facility. The Z-design battery consists of two stacks of 78 cells each, with an adhesive and bolt assembly. The battery incorporates posted Daramic separators and polypropylene electrodes.

Table 2-1.
V-Design Flow Frame Parameters

<u>Thickness</u>	<u>Width (in)</u>
Electrode	0.030
Separator	0.025
Anolyte gap	0.025
Catholyte gap	0.020

After completing 159 cycles, with the battery performing at 60% energy efficiency, the electrolyte was changed to reflect advances in electrolyte composition. The new electrolyte contained the same components but with a different quaternary ratio and lower concentrations. The original electrolyte had 2.0-M zinc bromide, 0.5-M zinc chloride, and an MEP:MEM (N-methyl, N-ethyl morpholinium bromide) quaternary ratio of 1:1. The new electrolyte was composed of the same compounds but with the total quaternary concentration lowered and the ratio changed to 3:1, MEP:MEM. The higher ratio of MEP to MEM is based upon investigations that show MEP is a more efficient bromine complexing agent than MEM. The lower total concentration of quaternary agents decreases the electrolyte resistivity. The battery efficiencies from before and after the electrolyte change are summarized in Table 2-2.

Nine cycles were run after the electrolyte change. As Figure 2-11 shows, the coulombic and energy efficiencies declined. Energy efficiencies with the new electrolyte ranged from 47% to 52%, compared to the range of 57% to 60% seen in earlier cycles. Coulombic efficiencies dropped from about 80% to about 65% and electrical problems were encountered. This performance drop was attributed to an air bubble in one of the shunt current protection tunnels. Repairs were made, and the battery was cycled again.

Continued testing of the new electrolyte showed a 2.4% increase in energy efficiency over the original electrolyte. Table 2-1 compares the efficiencies of the 10 cycles before the electrolyte change with 10 continuous cycles after the electrolyte change.

The slight decrease in coulombic efficiency with the new electrolyte is more than compensated for by a large increase in voltaic efficiency, giving a net gain of 2.4% energy efficiency. The voltaic improvement results from more efficient bromine complexation by the 3:1 quaternary mixture and by decreased electrolyte resistivity from the lower overall quaternary concentration.

No significant change in battery efficiency was noted when 100 liters of electrolyte were removed from

Table 2-2. Electrolyte Comparison Studies

<u>Electrolyte</u>	<u>Coulombic Efficiency</u>	<u>Voltaic Efficiency</u>	<u>Energy Efficiency</u>
2.0 M ZnBr ₂ , 0.5 M ZnCl ₂ , 0.5 M MEP, 0.5 M MEM	80.31	71.89	57.73
2.0 M ZnBr ₂ , 0.5 M ZnCl ₂ , 0.6 M MEP, 0.2 M MEM	78.90	76.22	60.14

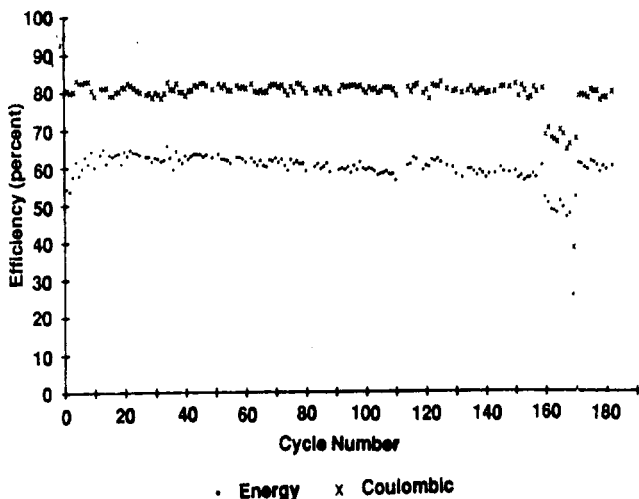


Figure 2-11. Zinc/Bromine Battery - Load Management Cycle Efficiencies

the battery at cycle 177. Before this, the battery had been cycling at 38% zinc-bromide utilization (theoretical) with 400 l. With the reduced electrolyte volume, the battery cycled at 51% electrolyte utilization.

During cycle 182, a short circuit caused the battery to fail. Revival efforts have not yet been successful. This battery performed 82 cycles longer than the original 100 cycles anticipated.

Nickel/Hydrogen Battery Development - JCI

Background

A program to design and develop a multikilowatt-hour nickel/hydrogen battery for storing electricity from photovoltaic or other power sources is continuing under a cost-sharing contract between JCI and SNL. The nickel/hydrogen battery has been successfully used for more than a dozen years in aerospace photovoltaic systems. The challenge is to reduce dramatically the first-cost of the battery to make its life-cycle costs economically competitive with other energy storage batteries in terrestrial applications without compromising the characteristics that make nickel/hydrogen so useful in photovoltaic systems.

The advantages of nickel/hydrogen batteries include a significantly longer cycle life than any other battery system, no maintenance, and a high tolerance to abuse. This last characteristic is possibly the most important because there may be no need for a charge controller to sit between the solar array and the battery. Since controllers are the least reliable component in a photovoltaic system, their removal benefits the long-term reliability and long-term cost of an installation, especially in remote areas where photovoltaics can play an important role but where skilled maintenance people are often unavailable. It also means that one can take full advantage of the maximum output of the solar array, in contrast to what happens with many other installations in which the controller isolates the battery during maximum insolation. Coupled to the battery's excellent energy efficiency, there can be a significant reduction in the size of the array required for the application.

Technical Effort for 1988

The technical effort under contract No. 53-8334 concluded March 31, 1988, and effort under contract No. 57-4683 commenced July 1, 1988. A final report was prepared in the interim.

The major emphasis of the contractual effort is to reduce component costs without compromising performance. Previous studies indicated that competitive life-cycle cost is achievable and pointed to the negative catalyst, the porous fluoroplastic film on the negative electrodes, the asbestos separator, the thickness and number of nickel electrodes, and the pressure vessel as having the most addressable impact on cost. Thus, the contractual efforts in 1988 centered on reducing the costs of these components. Improvements will be demonstrated in an 8-kWh battery to be designed and delivered in 1989.

The standard catalyst has been 10% platinum on carbon at a loading of about 0.5-mg platinum per cm^2 . Two approaches to reduce the catalyst cost were pursued: (1) a reduction in the quantity of catalyst used per electrode and (2) a cheaper catalyst.

Electrodes with reduced quantities of 10% platinum-on-carbon catalyst were characterized by polarization testing. Satisfactory performance was indicated with loadings as low as 0.2-mg platinum per cm^2 . A standard, full-size 160-Ah cell (Figure 2-12) was then assembled and tested to verify the results of this screening test under actual operating conditions. The lower platinum loading has performed well to date. After several hundred cycles at 80% depth of

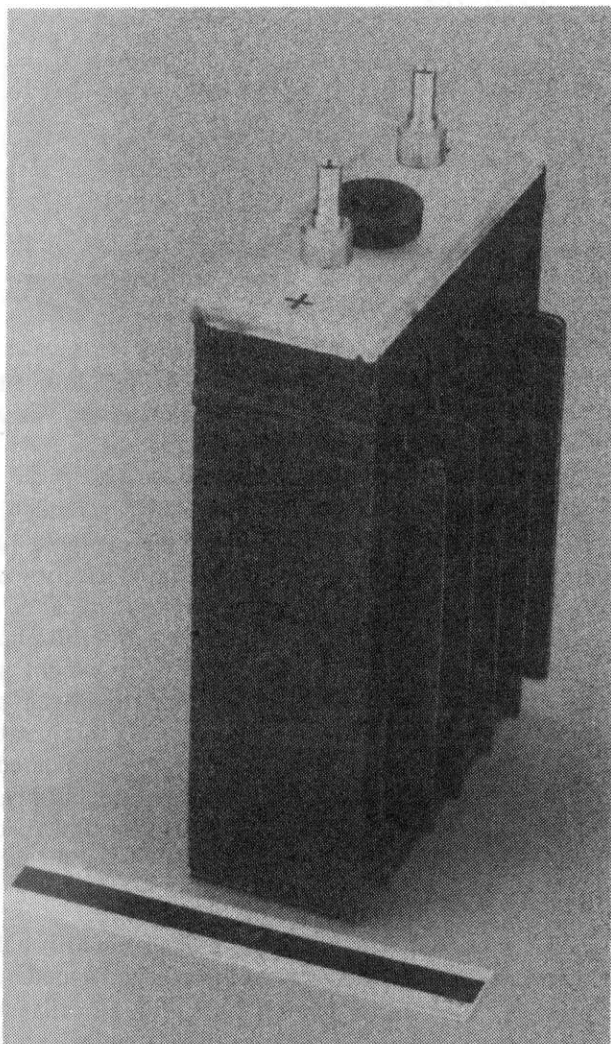


Figure 2-12. Standard 150-Ah Cell

discharge (DOD), this cell is delivering in excess of 160 Ah with an energy efficiency of 81%.

A lower cost alloy-on-carbon (AOC) catalyst was obtained and used, at various loadings, in the fabrication of electrodes. Above-average performance was achieved in the polarization tests, even with low loadings. These screening tests indicated that electrodes with AOC catalyst perform better than electrodes with the 0.2-mg platinum/cm² catalyst. In addition, the material costs would be 25% less. The AOC catalyst should be even more stable than the platinum catalyst. Another 160-Ah cell was assembled, incorporating electrodes with the AOC catalyst. Initial cell test results have been very promising.

Two approaches reduced the cost of the porous fluoroplastic films. In one approach, full-size electrodes were prepared using three times the normal quantity of fluoroplastic binder instead of the films, which reduced battery cost by about \$50/kWh. The increased hydrophobic property provided by the additional binder was predicted to prevent flooding of the catalyst with electrolyte, despite the absence of the fluoroplastic films. A 160-Ah cell was assembled using the electrodes with the 3X binder. After 200 cycles at 80% DOD, the cell is delivering in excess of 160 Ah with an energy efficiency of 84%. This approach looks promising, but more than 500 cycles will be required to determine the long-term effect.

The second approach was to replace the purchased fluoroplastic films with less expensive films prepared by JCI. Again, this approach reduced the battery cost by about \$50/kWh. A process for preparing films was developed, and electrodes incorporating these films were prepared. The test bed of these electrodes is another 160-Ah cell, which is performing very well; 165 Ah are being delivered with an energy efficiency of nearly 87% after 160 cycles.

Environmental concerns about the use of fuel-cell grade asbestos separator material and its uncertain availability, and possibly its escalating cost, have prompted the effort to find a replacement. Continuing throughout the year were screening tests of candidate nonasbestos materials from Celanese Co., Gelman Co., Zircar Products Co., and NASA-Lewis, as well as a full-size cell test of a separator material from W.R. Grace Co. The screening tests indicated that full-size cell testing of several candidates is warranted. Cell tests of the Celanese, Gelman, and a new candidate material from Pall RAI, Inc., are planned. The material from Zircar Co. is very expensive and, although it demonstrated good performance, would be used in a terrestrial battery only as a last resort. The separators from W.R. Grace and NASA-Lewis also demonstrated good performance but are no longer available. These separators are comprised of potassium-titanate (KT) fibers. The only producer of these fibers, a Japanese company, discontinued selling the material because of safety concerns (the aspect ratio of the KT fibers is the same as that of asbestos). The cell with the W.R. Grace separators continues to perform well after 1,000 cycles.

The primary objective in developing a thicker positive electrode is to reduce cost and, secondly, to improve energy density. Cost reductions would be achieved by using fewer cell components. The theoretical capacity for a cell stack containing fourteen 90-mil electrodes is about 210 Ah, whereas the theoretical

capacity for the same size stack containing eighteen 70-mil electrodes is about 190 Ah. Thus, fewer cell components of the 90-mil electrodes would not adversely affect cell/battery capacity, while at the same time reducing costs. In practice, the capacity delivered by the 90-mil electrodes in flooded cell tests, using half-cell reference electrodes, was 14% below theoretical. Characterization capacities of 70-mil electrodes, cycled in the same manner, were typically theoretical. In addition, the mid-discharge voltage of cells with 90-mil electrodes was slightly lower, resulting in a 3% reduction in energy density. Currently, the scope of the study for the impregnation of 90-mil porous nickel plaque is being broadened to improve the uniformity of distribution of active material throughout the thickness of the plaque. Process control, plaque pretreatment, and impregnation bath composition are also being studied with the goal of preparing a more efficient positive electrode.

Also, less costly substitutes for the sintered nickel plaque such as fiber and foam materials will be sought, remembering that the sintered positive electrode contributes to the long life of this battery system that offers life-cycle cost advantages.

The pressure vessels for the 8-kWh battery were designed to be rugged to ensure complete safety and zero maintenance (no hydrogen leaking or permeation), at the expense of weight and cost. The vessels were not meant to be opened; therefore, the design deviates from that of the previously used boiler-plate vessels and benefits by significant weight and cost savings. Three vessel configurations were considered: an all-fiber-reinforced-epoxy vessel, an all-metal vessel, and a fiber/epoxy reinforced metal-shell vessel. The third was selected, and drawings were submitted to vendors. The conceptual design is based on previous vessel designs with the exception of the cylindrical portion of the metal liner. Since the battery operating pressure is low, the liner will not be stressed beyond its yield point. As a result, the liner will be rolled and longitudinally welded, which simplifies the design. The end domes will be spun and will have plugs welded in place before assembly. The electrical and other feed-throughs will penetrate the end plugs. The end plugs will also support the vessel during filament wrapping. A preliminary drawing of the vessel is shown in Figure 2-13. The safety of this type vessel is assured by sufficient wraps with the fiber/epoxy while the metal liner limits permeation of hydrogen. A full complement of tests is planned for completed vessels to verify adequacy of design and manufacture.

The two other configurations remain viable candidates. Off-the-shelf mild steel vessels offer proven

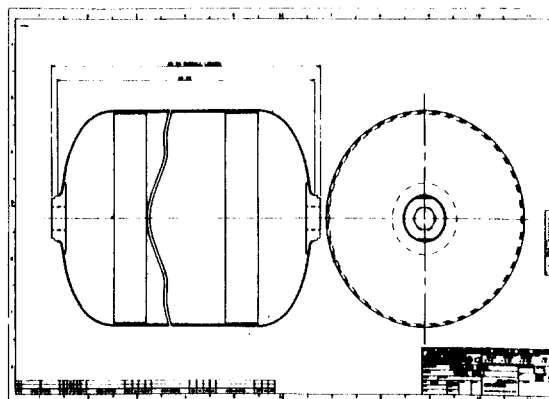


Figure 2-13. Preliminary Design of Stainless Steel Liner for Filament-Wound Hydrogen Pressure Vessel

safety and low cost, but the possibility of embrittlement of the steel by the hydrogen must be explored fully before these vessels can be used. The fabrication of a device to test the steel under conditions typical of the battery environment has been started. The all-plastic vessel offers ease of fabrication and light weight, also at an acceptably low cost. However, hydrogen permeates most plastics at unacceptably high rates. Polyvinylidene chloride (PVDC) is being considered as a restriction to hydrogen permeation. An all-plastic vessel incorporating PVDC is being designed, and hydrogen permeation tests are planned for the completed vessels.

A photovoltaic test system was set up in Milwaukee that consists of a solar array, a battery, and a load. The array is comprised of two modules with 35 cells each. The battery consists of five cells, has a nominal voltage of 6.25 V, and a capacity of 160 Ah. It was built to verify component selection and operation before building the 7-kWh battery delivered to SNL. The initial load was two incandescent lamps, which drew 500-mA current full time. The system was originally connected in parallel with no controller. While the system works well during high insolation, the capacity of the battery is drained during extended cloudiness (Figure 2-14).

To alleviate this problem, a simple energy management system (EMS) was connected to the system. The EMS on the small solar installation takes advantage of the fact that the state of charge (SOC) is directly related to the pressure of hydrogen in the pressure vessel. Four inexpensive pressure switches were installed on a common manifold, which was connected to the pressure vessel housing the battery. The load was changed from one 500-mA load to four 250-mA loads, each connected to the battery through its own pressure switch. The switches were adjusted to turn off at various states of charge, in this case 75%, 50%, 25%,

and 10% SOC. The inherent hysteresis in the switches prevents loads from toggling on and off line. This load-shedding system works by reducing the load on the battery when the SOC falls to certain levels and reconnecting the loads when capacity has recovered sufficiently (Figure 2-15).

Summary

A terrestrial nickel/hydrogen battery has been developed that appears to be ideally suited for remote solar applications. It is essentially maintenance-free, is tolerant to abuse, and has a projected life equivalent to

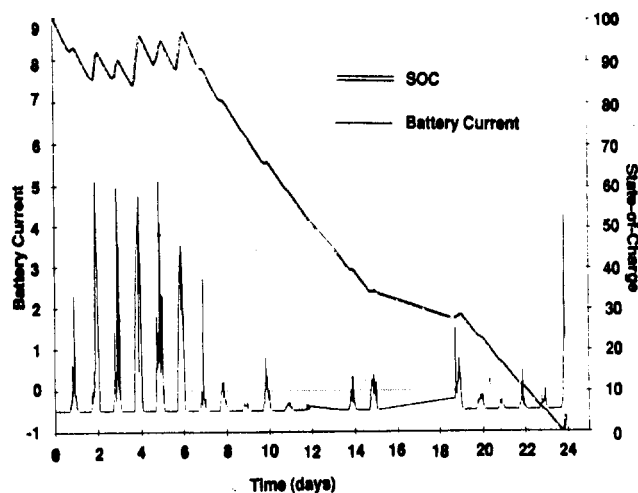


Figure 2-14. Battery Current and SOC vs Time (No Load Shedding)

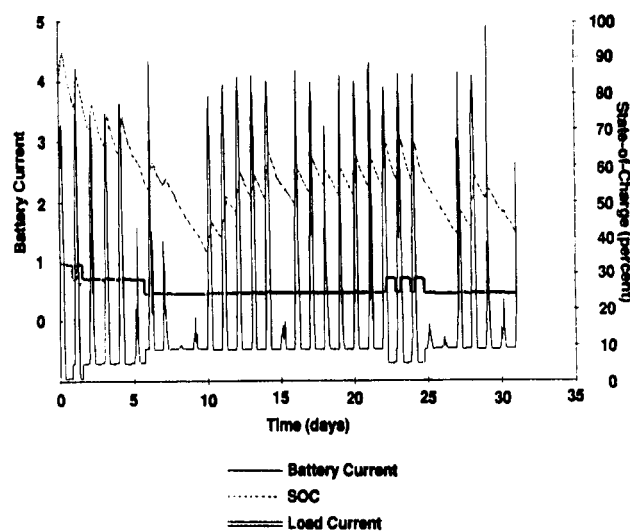


Figure 2-15. PV Array/Battery Performance, January 1988

solar panels. SOC can be accurately determined even after extended operation at a partial state of charge. The latest cells operate at up to 30°C without active cooling. The effort to reduce the initial cost and optimize performance is continuing.

Aluminum/Air Battery Development - Eltech

Introduction

An alternative to the secondary battery as the power source in an electric vehicle is a fuel cell, i.e., a cell that generates power by consuming a mixture of a fuel and oxygen from the air. Metals such as lithium, aluminum, zinc, and iron may be used in a fuel cell, and aluminum is a particularly attractive candidate. The metal has high energy and power densities, is environmentally acceptable (as are the products of the cell reaction), is easy to handle, and has a large industrial base for its production and distribution.

Aluminum is reactive and dissolves when discharged in an alkaline electrolyte to form a soluble aluminate species. It should be noted that alkali metal hydroxide is also consumed



so as the dissolution proceeds the conductivity of the electrolyte decreases. The metal also corrodes in the aqueous electrolyte both at open circuit and when polarized, forming hydrogen gas that must be safely handled within the battery system.

As the electrolyte becomes saturated with aluminate, precipitation of hydrargillite (Al(OH)_3) can replenish the electrolyte in terms of free hydroxide. Thus, a steady-state condition may be achieved with respect to the conductivity of the electrolyte, which will then contain crystals of hydrargillite. Aluminum cannot be electrodeposited from aqueous solutions, so the aluminum/air battery is not a true secondary battery. However, the anode can be mechanically replaced, requiring novel features in the design of the cell but offering relatively rapid refuelability.

The cathode reaction is the electroreduction of oxygen, which can be sustained at practical rates only by using a gas-diffusion electrode. A three-phase boundary between catalyst, electrolyte, and reactant oxygen must be established, and this demands a unique structure. The performance of the gas-diffusion electrode in alkaline electrolytes is sensitive to the

presence of carbon dioxide in the air-feed stream. Carbon dioxide must be reduced, probably to less than 100 ppm, to obtain acceptable, extended operation.

An aluminum/air battery is therefore a multicomponent system represented schematically in Figure 2-16.

Research Engineering In 1988

This program continues the research and development conducted jointly by the Department of Energy and Eltech Research Corporation since 1980, with the longer term objective being to install and evaluate the battery system in a vehicle. The present program, which combines cell designs, experimental studies, and mathematical modeling, addressed two phases:

- Phase I: Design and optimization of the aluminum/air cell
- Phase II: Design and optimization of the auxiliary systems (including heat exchanger, solids separation, control of carbon dioxide, and the disposal of hydrogen gas)

The wedge cell was primarily developed and evaluated in earlier programs (Despic and Milanovic 1979), (Maimoni, Meulder, and Hui 1985) to address the need for a rapidly rechargeable battery. Although

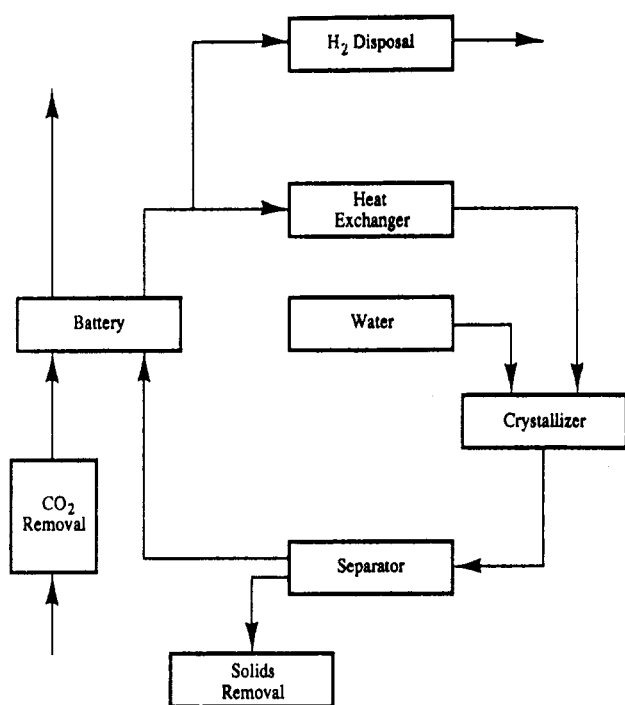
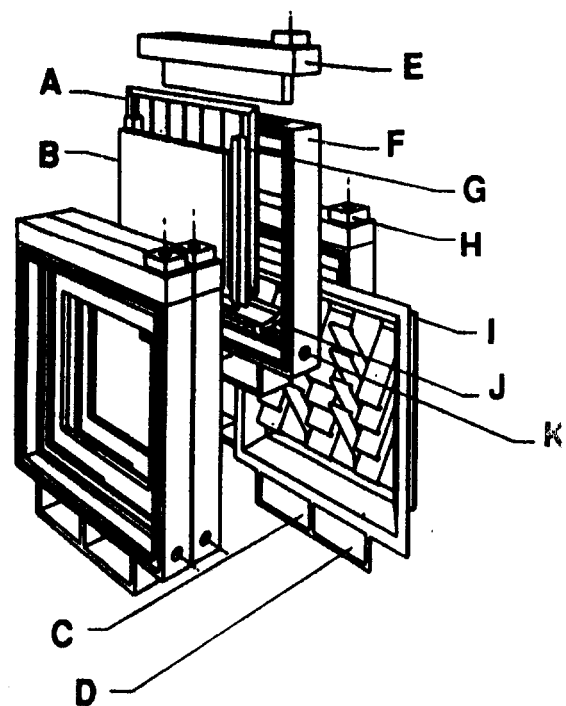


Figure 2-16. Aluminum/Air Battery Process Diagram

promising levels of performance were achieved with this cell design (Eltech Research Corporation 1987) the need for a sealed, lighter, and more compact battery was clearly identified. Eltech developed the B-300 cell (Figure 2-17), significantly reducing both weight and volume relative to the wedge cell, and this design was selected for the present program.

The characterization of the cell performance is being carried out at Eltech Research Corporation, including definition of operating conditions, electrolyte composition, and fluid flow rates. Modifications to the design of the cell and/or components of the cell as operating experience is gained are also being addressed at Eltech, together with those tasks focusing upon Phase II, the auxiliary system.



- A. Cathode Support Structure Assembly
- B. Aluminum Plate
- C. Air Inlet Plenum
- D. Air Discharge Plenum
- E. Anode Seal Block
- F. Cell Frame
- G. Discharge Plenum
- H. Electrolyte Outlet
- I. Anode Current Collector Assembly
- J. Inner Gasket
- K. Electrolyte Inlet

Figure 2-17. B-300 Aluminum/Air Cell

The following specific research tasks were sub-contracted by Eltech:

- (1) Development of a mathematical model of the B-300 aluminum/air cell—Case Western Reserve University, under direction of Dr. R. F. Savinell;
- (2) Characterization and optimization of Helipump fluidizer impeller (for separating fine particles of hydrargillite from the electrolyte)—Mr. Michael Petrik of Helipump Corporation;
- (3) Development of computer model of the Helipump fluidizer impeller—Case Western Reserve University, under direction of Dr. R. J. Adler; and
- (4) Analysis of shunt currents in the battery using the B-300 cell design—Case Western Reserve University under the direction of Dr. R. F. Savinell.

Eltech Characterization of Fluid Flow Rates in the B-300 Cell

A statistically designed experimental program was used to determine the dependence of the performance of the cell (energy density and power density) upon the flow rates of electrolyte and air. The test matrix was arranged such that the first eight tests represented a full factorial design. These data were analyzed and yielded the following equations:

$$\text{Energy Density} = 3.52 - 3.08 (\text{Current Density}) + 0.02 (\text{Air flow rate})$$

$$\text{Power} = 0.152 + 0.42 (\text{Current Density})$$

where current density is expressed in A/cm² and air flow rate in terms of the stoichiometric requirement at a particular current density.

The analysis showed that over the ranges of values selected for the matrix, the cell performance was insensitive to fluid flow rates. Operation of the battery at significantly lower fluid flow rates may be cost effective, and therefore additional studies were completed. It was shown that

- The cell could be operated at electrolyte flow rates as low as 0.5 l/min without significant effect upon performance.
- Operation at air flow rates lower than 3X stoichiometric caused a decline in performance, particularly at current densities above 400 mA/cm².
- At the lower electrolyte flow rates, a temperature gradient of 6-7°C was developed across

the cell when operating at high current densities.

Eltech Electrolyte Composition

It is planned to operate both a single B-300 cell and a multicell battery using a "batch" electrolyte approach and to establish a series of "steady-state" compositions as a function of the operation conditions. Note that the mass and energy balances in the battery system are also being determined for both approaches. In addition, a simulated B-300 cell and flow system are being used to determine the physical (abrasive) effects of circulating the hydrargillite slurry.

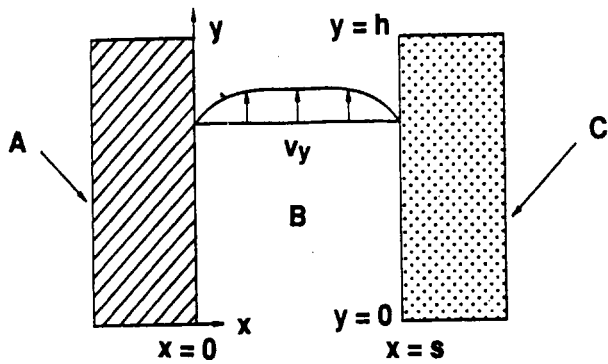
Preliminary to this task, modifications were made to the B-300 cell, particularly with regard to the modular air cathode. Extended operation of the modified cell established that uniform current distribution was consistently realized and the reliability of the seals in the cathode was significantly improved. (Note that these modifications will be incorporated into the 12-V battery to be tested early in 1989).

It was also necessary to identify an acceptable "cathode assembly," or the support material inside the modular unit and metal screens laminated to the gas-diffusion electrode. Several anode-cathode separator materials were also evaluated to allow replacement of the plastic tines used in the earlier studies. This segment of the work has been completed.

The single cell has been operated using the "batch electrolyte" approach, that is, using a solution of only the alkali metal hydroxide into which aluminum is dissolved until precipitation of the aluminum hydroxide is imminent. These cell tests have also been extended in efforts to obtain a "steady-state" electrolyte composition. Preliminary experiments indicate that the "steady-state" electrolyte composition may be determined by the operating conditions such as current density, temperature, operating cycle, and volume of electrolyte. Furthermore, thermal cycling from 60°C to room temperature does not readily promote crystallization of hydrargillite.

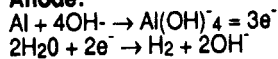
Case Western Mathematical Model of the B-300 Cell

The aluminum-air cell was considered as a parallel-plate electrochemical reactor (Figure 2-18). Two approaches were explored to develop the mathematical model: (1) the finite difference method and (2) the boundary layer method. Although the former approach is the more fundamental, it is limited by parameters that are difficult to measure. By comparison, the

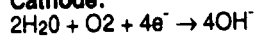


- A. Aluminum
 B. $K^+ Al(OH)_4^- OH^-$
 C. Air Cathode

Anode:



Cathode:



- Mass transfer limitations even at low flow rates (superficial velocities of 0.5 - 1.0 cm/s) are avoided because of the generation of hydrogen bubbles at the anode surface.
- The effect of electrolyte velocity upon cell performance predicted by the model agrees closely with the results obtained in the experimental study.
- An optimum concentration of hydroxide ion exists between 4- and 8-M potassium hydroxide. This suggests that there may be an advantage to operation at a higher inlet hydroxide concentration.
- The presence of solid particles and/or gas bubbles affects the conductivity of the electrolyte but the impact upon cell performance is small.
- The anode-cathode gap will be determined primarily by the mechanical construction and assembly of the cell.

Case Western Analysis of Shunt Currents

In the B-300 cell stack, a common electrolyte is fed in parallel to the individual cells within the stack. Because there are common electrolyte paths, the possibility of shunt currents (currents that bypass the cells, dissipate energy, and create nonuniform consumption of reactants) exists.

The shunt currents in the B-300 battery were estimated by formulating an analog model of the stack (Kaminski and Savinell 1983). The parameters in the model were determined by the cell geometry, fluid properties, and operating conditions. Power losses because of shunt currents in the B-300 battery were less than 0.3%, but the cell-to-cell current may vary by several percent of the load current, suggesting that the centrally placed anodes dissolve more rapidly than those in end positions. Nonuniform current distribution close to the entrance and exit ports was not considered.

Characterization of the Solids Separator by Helipump

The Helipump impeller fluidizer (Figure 2-19) is a device for separating, contacting, and pumping solid-liquid slurries. A locally confined fluidized bed of particles is dynamically held within the vessel by the interaction of centrifugal forces and convection, both produced by an impeller-driven flow. The radial pressure gradient generated allows either clear liquid or

Figure 2-18. Schematic of the Aluminum/Air Battery

boundary-layer method is more direct and was therefore adopted for this task.

The electrochemical kinetics at the anode and cathode were described by the Butler-Volmer equation, modified to account for resistive components arising from the presence of a surface film at the anode (Brown and Whitley 1987) (MacDonald, Real, and Urquidi-MacDonald 1988) on the one hand and the microporous structure of the gas diffusion electrode (Srinivasan 1987) on the other. The changes in the concentrations of the various product and reactant species were accounted for by equations for convection, diffusion, and migration. Gas bubbles at the anode surface (since hydrogen is generated by the simultaneous corrosion reaction) and the resultant changes in boundary layer conditions were also considered in the model.

The ability of any model to predict performance depends on the availability of fundamental input data. For this system, and particularly the anode, kinetic data are limited, and therefore the cell is difficult to represent. However, simulated cases were studied, and the distributions of current, potential, and concentrations were determined for them. This allowed the following conclusions:

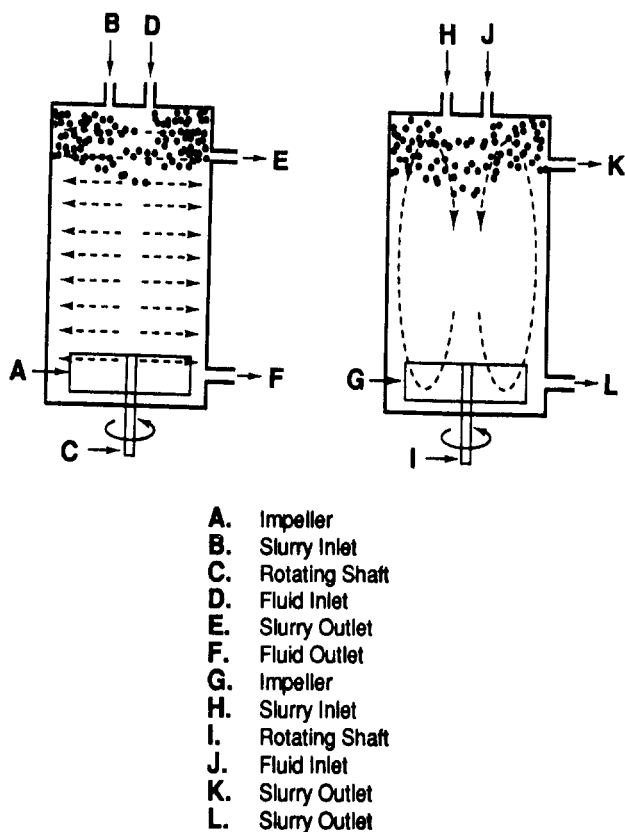


Figure 2-19. Mechanism of Fluidization

concentrated slurry to be pumped into and from the separator.

The characterization of the fluidizer impeller was completed using an experimental design study to determine the effects of six variables upon the separation efficiency. A convenient test solution for these tasks was an aqueous slurry of alumina particles of sizes ranging typically from 5 to 10 microns, with solids of either 5 or 30 wt%.

Analyses of the data indicated that the separation efficiency was significantly affected by (1) the wt% solids in the slurry, decreasing as the solids content increased, (2) the ratio of vessel length to diameter, with higher ratios being preferred, and (3) the particle size.

However, the separation efficiencies were all low, ranging from 55% to 65%. Neither changes in the vessel size and geometry nor changes in the impeller blade led to substantial improvement in the separation efficiency. It was concluded that the Helipump could not efficiently separate fine particles (i.e., particles of less than 10 microns) as presently operated. This conclusion

was supported by the results of tests with a slurry of hydrargillite in potassium hydroxide.

Mathematical Model of the Helipump by Case Western

The model of the impeller fluidizer used an assumed fluid flow field and classical momentum balances on a particle. The method adopted was to track a single spherical particle within the device and to analyze the trajectory of that particle to determine the spatial distribution of an ensemble of particles. Fluctuations because of turbulence and the effects of substantial particle concentrations were considered. The model includes particle density, fluid viscosity, impeller speed, vessel dimensions, and inlet and outlet flow rates as parameters. The values of the parameters were selected to match those used in the parallel experimental program. The fluid flow field was tuned using a single adjustable parameter, the strength of pumping in the axial direction, to achieve separation efficiencies similar to those of the experimentally tested unit.

The model successfully correlated the results of the experimental program and clearly indicated the limited separation with particles smaller than 10 microns. Further analyses of the secondary (recirculating) flows and turbulence intensity are presently progressing. This will define the conditions that may lead to more efficient separation of the fine particles. The question will be whether these conditions can be realized in a practical device.

Eltech Heat Exchange In the Battery System

Various designs of heat exchangers may be considered for this battery system such as direct electrolyte-air exchangers as presently used in the automobile. However, direct cooling was rejected because of the prohibitive cost of manufacturing a "radiator" from nickel (recommended because of the corrosive nature of the electrolyte), possible plugging of the "radiator" by the hydrargillite particles in the electrolyte, and the safety hazard if a pinhole leak developed.

Thus, an electrolyte-water-air system consisting of a conventional liquid-liquid exchanger, using water to remove heat from the electrolyte and then a "radiator" to cool the water was considered more practical.

Heat duty cycles for a 12-V B-300 battery were calculated based upon a thermodynamic analysis of the cell reactions such as metal dissolution, corrosion, and oxygen reduction and crystallization of the

aluminum hydroxide. Convective and evaporative heat losses from the battery are probably negligible. The heat duty cycles were determined to be 1,980 W at an operating current density of 400 mA/cm² and 3,470 W at 600 mA/cm². Two heat-exchanger designs were evaluated in terms of size, weight, cooling water flow rates, pressure drops in the unit, ease of maintenance, and likely manufacturing cost. The two designs selected were a shell and tube unit and a plate and frame unit.

The plate and frame heat exchanger, fabricated with nickel plates and EPDM frames, was preferred and is therefore recommended for use in a prototype vehicle battery. The pressure drops through both the electrolyte side and water side of the heat exchanger unit were small. The presence of dissolved aluminum in the electrolyte (up to 1.5 M) affected the cooling water flow rates only for the higher heat duty cycle.

Summary

This program continues the research and development conducted jointly by the DOE and Eltech Research Corporation since 1980 and it addresses two phases:

- Phase I: Design and optimization of the aluminum/air cell
- Phase II: Design and optimization of the auxiliary systems

Eltech Research Corporation independently developed the B-300 cell, and this design was selected for the present program. The fluid flow rates have been

characterized and electrolyte composition is being defined for optimum performance. Modifications to the design of the cell and some of the components have been identified and implemented.

A mathematical model of the B-300 cell, based upon a boundary layer approach, has been developed by Dr. Robert Savinell at Case Western Reserve University. The model correlated the results obtained from the study of the fluid flow rates and has been used to identify operating-conditions and cell-design features that affect performance. The shunt currents in a B-300 battery were estimated, and the power losses were shown to be less than 0.3%.

The design of a prototype heat exchange unit for the aluminum/air battery system has been recommended. An electrolyte-water-air system was selected and, based upon the results obtained from a simulated 12-V battery system, a plate and frame exchanger design was recommended.

The Helipump fluidizer impeller, a device potentially capable of efficiently separating fine particles of hydrargillite from the electrolyte, was characterized using a statistically designed experimental program. The dependence of the separation efficiencies upon operating conditions and upon the design of the Helipump fluidizer was quantified. In all cases, the efficiencies of separating fine particles (sizes less than 10 microns) were low, ranging from 55% to 65%. A mathematical model of the device was developed by Dr. Robert Adler, at Case Western Reserve University, and the model clearly indicated this limitation. Additional analyses of the secondary flows and turbulence intensity in the Helipump unit are progressing.

Chapter 3. Nonaqueous Battery Development

In 1988, the nonaqueous battery development activities within the ETD project were devoted exclusively to the sodium/sulfur technology. This system remains a leading candidate for mobile and stationary energy storage applications because of its potential for low cost, good efficiency, long life, and reliable operation.

The primary ETD development program for the sodium/sulfur technology is being performed through a cost-shared contract with Chloride Silent Power, Ltd., (CSPL), Runcorn, England. A 4-year contract with CSPL was placed in September 1985. CSPL is cost-sharing 35% of this \$8.5M effort. The objective of the program is to advance the state of the technology with respect to components, cells, and small batteries for both stationary and mobile applications. The final product of the program will be a subscale battery module suitable for evaluation in a stationary-storage environment.

Support to the CSPL development program was provided by Science Applications International Corporation (SAIC) and ANL. SAIC has a major subcontract with CSPL to conduct a number of cell and battery performance studies. ANL performs posttest analysis on selected CSPL cells to help identify ways to improve cell reliability and lifetime.

A description of the results from the CSPL program and the supporting SAIC and ANL studies are given separately in the remainder of this chapter.

Introduction

In September 1985, a 3-year contract was awarded to CSPL to advance the state of the art of sodium/sulfur technology in components, cells, and batteries. This Core Technology and Battery Engineering program was intended to parallel an effort sponsored by EPRI. The EPRI contract, to develop and construct a 500-kWh sodium/sulfur battery for the BEST facility, commenced in December 1985 but was substantially reduced in 1986 and plans to construct a 500-kWh battery were deferred.

The contract with CSPL was extended by one year in 1986 to reduce the annual program costs. The construction of the main deliverable, a 100-cell battery, was deferred to the fourth year. However, the schedule for

the primary Core Technology tasks was maintained. An 18-kWh electric vehicle (EV) module was removed from the deliverable schedule to complete the cost adjustments.

The program is divided into two tasks:

- Task 1. Core-Technology Research and Development
- Task 2. Battery Engineering and Testing.

Task 1 is devoted to research and development in the areas that are generic to both stationary and electric vehicle applications. The major emphasis of this task is to improve cell performance, reliability, safety, and cost. The following subtasks are included in the Core-Technology task:

- 1.1. Electrolyte Research and Development,
- 1.2. Materials Development and Qualification,
- 1.3. Cell Development,
- 1.4. Cell Testing and Posttest Analysis,
- 1.5. Module Development and Testing.

The Task 2 effort is directed towards the design and fabrication of batteries for stationary applications.

SAIC has a major subcontract with CSPL for both tasks. The SAIC results of each task for 1988 are reported separately following the next section. In June 1988, at a design review meeting, the decision was made to increase the size of the final contract deliverable from a 100-cell XPB battery to a 200-cell battery. Also this battery will be tested at a CSPL facility rather than a DOE facility. Finally, an extension of the program was approved in late 1988 to continue the Core Technology task through the fourth year of the contract.

Background

The CSPL sodium/sulfur cell design strategy is based on a family of cells designated the "PB cells." Two specific sizes are currently being developed, a 45-mm-diameter by 45-mm-high cell called the PB cell and a 45-mm diameter by 110-mm-high cell called the Extended PB (XPB) cell. Both cells are central sodium

designs based on identical components as far as possible, particularly in the seals.

The intention of the program is to develop generic cell technology. This generic technology will enable the commercialization of optimized cell designs that are close in size to those currently under evaluation. Selection of cell size is a complex issue that involves battery voltage, battery capacity, cell reliability, vertical dimensions of the battery enclosure, and life-cycle cost. The XPB cell is better suited by size, energy, and power to stationary applications, and the PB cell is better suited to EV applications.

CSPL has a long-term technology data base from testing earlier central sulfur, 150-Ah NaS7 and 30-Ah Technology Demonstration (TD) cells. These cells have been on test for up to 6,300 deep discharge cycles. The longest-lived cell operating at the time of writing has completed more than 54,500 h on test (>6 years). The longest-lived PB cell has completed 1,900 cycles, and the longest-lived XPB cell has completed 1,400 cycles. Several networks of PB cells have exceeded 500 charge/discharge cycles.

During 1987, the production capability of PB cells was increased to 350 per week. A substantial proportion of the output was used in the construction of a battery for the Bedford CF delivery van. This vehicle completed more than 100 miles on its second road trial and added considerably to CSPL's experience with battery performance under actual driving conditions.

A significant milestone for CSPL was reached in 1988 when approval was given for the construction of a pilot production facility at Chloride Industrial Batteries Clifton Plant. This pilot production module has been specified for the production of 5,000 cells per week of either PB or XPB design. The output will be used in the construction of batteries for extensive field trials.

Core Technology Research and Development

Overview

The overall objective of Task 1 is to advance generic sodium/sulfur cell technology for both utility and EV applications. Specifically, the basic research, cell development, cell testing, materials studies, quality control, and computer modeling required to support a battery program directed to the fabrication of a 200-cell

XPB battery is being performed. The issues of performance, reliability, safety, and cost are being addressed.

During 1988, there were two major endeavors in the Core Technology aspects of the program: 1) to refine the PB cell following performance analysis from extensive testing and 2) to advance the technical status of the XPB cell in preparation for construction the 200-cell XPB battery.

Extensive design synergy was achieved between the PB and XPB designs with concepts being transferred between each cell. The majority of the seal, electrolyte, and sulfur electrode development was conducted on the PB cell. The safety activities from the XPB program were transferred back to the PB cell and yielded substantial improvements. In addition, a significant amount of F/T testing was completed in 1988, and over 300 F/T cycles were accomplished in one experiment.

During 1988, the testing emphasis began to change from single cells to 120-cell banks (or modules). These units consist of thirty 4-cell, series strings and are a basic building block of CSPL's larger battery designs. By March 1989, a facility to test 10 such banks should be functioning, and an option to test up to 34 banks has been planned for late 1989. Although the new test facility was not funded by this contract, the underlying technology that allows routine testing of such banks has been substantially supported.

The PB-cell development was embodied in the fabrication of an intermediate EV battery (funded by DOE/OTS through SNL). This unit was shipped to ANL in early 1989 and is being tested. Further refinements to the PB design were made following the fabrication of this battery. At the time of writing, the latter cell design was undergoing abuse safety testing by crushing and immersion in water.

Initially, some difficulty was experienced when the PB technology was transferred to the XPB cell, causing some delay to the development of the larger cell. However, once improved production techniques of the latest PB cell were implemented, they were rapidly transferred back to the XPB design. This enabled a scoping trial of 50 cells to be constructed for single-cell, safety, and module testing. This experiment gave the most consistent XPB performances to date and enabled thermal management studies to be commenced using a 16-cell module. F/T studies were also initiated on the XPB cells, and the encouraging results enabled a cold maintenance operation to be successfully completed on the 16-cell XPB module.

Electrolyte Research and Development

During 1988, all aspects of electrolyte fabrication were further developed with an emphasis on improved yield, cost reduction, and performance. Larger scale developments were instituted under CSPL funding using previous progress under this contract as the basis for the expanded capability. An example is the development of machinery for automatic electrophoretic deposition (EPD) and green shape extraction.

The improvement in yield was sustained during 1988 as indicated in Table 3-1. A target of 50% yield with an output of 500 ceramics per week was set for 1988. This was accomplished and 20 out of 29 batches had yields over 50%. To pass CSPL's quality criteria, ceramics must exhibit no visible defects on dye penetrant testing as well as passing all dimensional, chemical, and physical property testing. The highest batch yields achieved were 74%, 70%, 68%, and 67%. The 1988 output was limited because of a reduction in demand while PB design refinements were made.

Other methods of testing ceramic strength were studied. One objective was to simplify the testing methodology so that it could be incorporated into a routine production line test. Comparisons were made of the strength measured by a four-ball biaxial technique and compressive C-ring testing. Finite-element modeling was used to examine the effect of out-of-plane forces and distorted base shapes upon the results.

A group of cells containing beta"-alumina toughened by the addition of zirconia commenced test before the start of the contract. A failure in a cell containing a nonoptimized zirconia addition occurred in 1986 at 949 cycles (*ETD Annual Report for 1986*, page 47). Since that time, the remaining cells have continued to cycle and have been supplemented with more cells (*ETD Annual Report for 1987*, page 58). The total population was 20 and all are 30-Ah, central-sulfur, TD

cells. The status of the experiment is shown in Table 3-2. A cell failed in 1988 at 3,383 cycles and another failed in early 1989 at 3,005 cycles. The longest running cells have exceeded 4,000 cycles, and the accumulated cell-cycles are 62,350, i.e., more than 3,000 per cell average. After almost 4 years of testing, it is still not possible to compute meaningful Weibull statistics although the eventual values will be in excess of any produced by cells containing nonzirconia ceramics.

Attempts were made in 1988 to manufacture a high-zirconia formulation on a continuous production basis. This trial lasted six weeks and highlighted the problems that had previously been identified: moisture sensitivity and loss of tetragonal phase.

Materials Development and Qualification

The major objective of this subtask is to qualify cost effective candidate materials for cell and system design. The subtask includes the following activities: alpha-alumina to beta"-alumina glass seals, alpha-alumina ceramic to metal seals, sulfur electrode and sodium electrode design, and sulfur-electrode containment.

A materials performance data base had been established before the start of this contract. This was based on CSPL's NaS7 and TD cell designs that contain materials and materials combinations pertinent to the present PB family of cells.

Alpha-Alumina to Beta"-Alumina Glass Seals

A glass joint is used to hermetically seal the alpha-alumina seal header to the beta"-alumina. CSPL's longest-lived cell contains a glass (formulation 668-barium aluminoborate modified with silica) in a TD type of cell. The cell contains two glass seals, one at each end of the electrolyte, and it had completed 6,406 deep discharge cycles to 1.76 V open circuit in 54,072 h (6 yr 1 mo) at the time of writing.

The present composition, employed in all standard production cells, is glass (formulation 2112, an aluminoborosilicate). This has been tested for 5,856 cycles in 40,392 h.

A study of SNL-developed CABAL glasses was concluded during 1988. Two types were studied, CABAL 12 and CABAL 5. Both glasses were tested for sodium resistance at cell operating temperatures, but neither was satisfactory because of poor wetting to the alpha-alumina header, which produced a poor quality joint. Better progress was made with composite glass and inert ceramic mixtures and this option was being

Table 3-1.
CSPL Electrolyte Output and Yield

Year	PB Output	Yield (%)
1984	101	12.0
1985	391	17.4
1986	3,709	28.5
1987	14,765	36.7
1988	12,470	44.6

Table 3-2. Cycle Status - High Zirconia TD Cells

Cell No.	Storage Conditions	Days Stored	Resistance (mohms)	Capacity % Theo.	Cycles
5982	NR	NR	—	—	953 (F)
5983	—	—	13.05	74.40	4,087 (C)
5984	—	—	14.36	68.70	4,027 (C)
5985	—	—	11.91	75.90	3,383 (F)
5986	—	—	13.14	74.80	4,027 (C)
5987	—	—	14.10	75.20	4,027 (C)
5990	—	—	14.04	73.80	4,087 (C)
5993	—	—	12.15	72.60	4,087 (C)
6013	50% RH in glass	50	11.09	76.60	2,939 (C)
6014	50% RH in glass	50	12.05	78.70	3,126 (C)
6025	50% RH in glass	50	11.32	79.70	2,261 (R)
6047	50% RH in glass	100	10.62	75.70	3,056 (C)
6012	0% RH over silica gel	50	14.29	72.80	3,126 (C)
6015	0% RH over silica gel	50	13.06	79.13	3,126 (C)
6024	0% RH over silica gel	50	13.23	74.90	3,056 (C)
6038	0% RH over silica gel	100	11.99	75.30	3,056 (C)
6016	0% RH in N ₂	50	22.40	81.40	2,331 (R)
6048	0% RH in N ₂	100	10.76	70.40	3,005 (F)
6011	25% RH in N ₂	50	11.16	80.76	2,331 (R)
6039	25% RH in N ₂	100	11.19	79.70	2,261 (R)

pursued following encouraging results from sodium exposure testing.

Metal to Alpha-Alumina Seals

The ceramic to metal seal component is of critical importance to the satisfactory life and performance of any sodium/sulfur cell. Two concepts have been studied at CSPL: a direct metal to ceramic bonded seal (funded by CSPL) and one employing an aluminum interstrate between a chromized steel component and the ceramic header. The former concept was employed on cell designs designated MkII and MkIIa; the latter was known as the MkI seal. In 1986 a hybrid of the two seal concepts was selected for further development and designated the MkIII. This seal contains a direct-metal-bonded sodium electrode closure and a sulfur-electrode closure employing chromized mild steel and an aluminum interstrate. The MkIII design was refined during 1987. An independent design and cost study carried out by a team of consultants found in favor of the MkIII design over the MkIIa design.

The MkIII became the production standard in 1988 and the majority of seals were made to this design. The sulfur-side seal of the MkIII is stiffer than that of the MkIIa, and concerns were expressed about the effect of this on F/T performance. Tests conducted during 1988 on both cells and seal/electrolyte subassemblies showed that the F/T performance of the seal is good. A group of 82 cells was F/T cycled in a variety of discharge states. The results clearly differentiate between F/T at top of charge and end of discharge as shown in Table 3-3. The surviving cells in this group (12 cells) continued on test after 312 successful F/T cycles. A hazard plot of the data is shown in Figure 3-1. The line intersects the horizontal cycle axis at 100, predicting a low probability of failure before that time. The cell work was supported by thermal cycling of subassemblies consisting of the MkIII seal with a glass seal and electrolyte. This latter study was part of a seal parameter optimization intended to refine the conditions for manufacture of seals and to study the precise time and nature of thermal cycle failures. The results have enabled proposals to be made for screening out seals that might be susceptible to

thermal-cycle failure. This would further improve the statistics.

Sodium Electrode

The design of the sodium electrode interacts strongly with the performance of the cell under both normal and failure conditions.

During 1987, a greater degree of synergy was achieved between the sodium-electrode safety features of the PB and XPB designs. The use of a totally enclosed safety containment vessel within the electrolyte/seal subassembly was progressed and initial trials conducted. During 1988, the design was refined and its safety performance thoroughly validated. In each of two 24-cell modules, every cell was successively failed by deliberate application of an over-voltage. This was

followed by a 10-A charge and discharge current application to drive the reaction to completion. The failure exotherms of the above cells, a further 24-cell module, and 14 single cells are plotted in Figure 3-2. One of the modules and a cell string are shown after the completion of safety testing in Figure 3-3.

After testing, cells from the 24-cell modules were examined and shown to be externally intact, although x-radiography revealed disintegration of the ceramic and complete reaction of the electrodes. The cells were subsequently subjected to a variety of charge and discharge tests designed to reveal their electrical characteristics. This was followed by F/T testing between ambient temperature and 350°C. Five of the cells survived 123 F/T cycles before seal failure. The Weibull statistics for the F/T behavior are a characteristic (F/T) life of 226 and a modulus of 1.2.

Table 3-3. Freeze/Thaw of MkIII PB Cell

Cell Discharge State (OCV)	No. of Cells	Weibull Statistics					
		Characteristic Life Freeze/Thaw Cycles		Modulus			
2.074 (Top of Charge) 1.76 V*	30	296	445	670	1.5	2.8	5.5
	5	44	102	238	0.5	1.2	2.7

* Normal PB cell operation is terminated at 1.9 V.

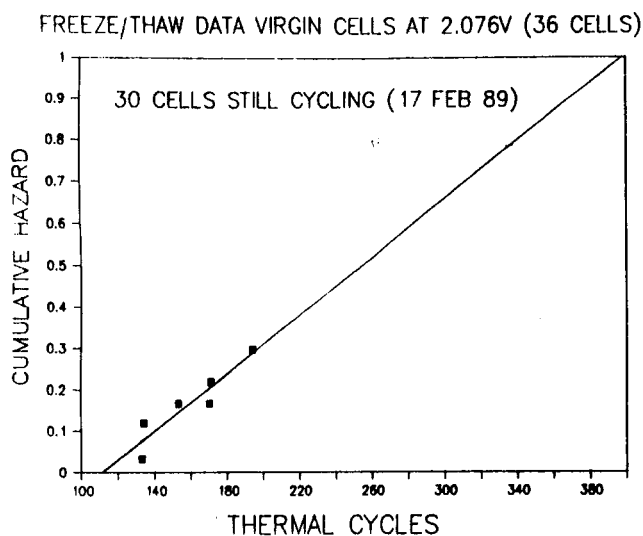


Figure 3-1. Peak Power at Depth of Discharge, Cell 469

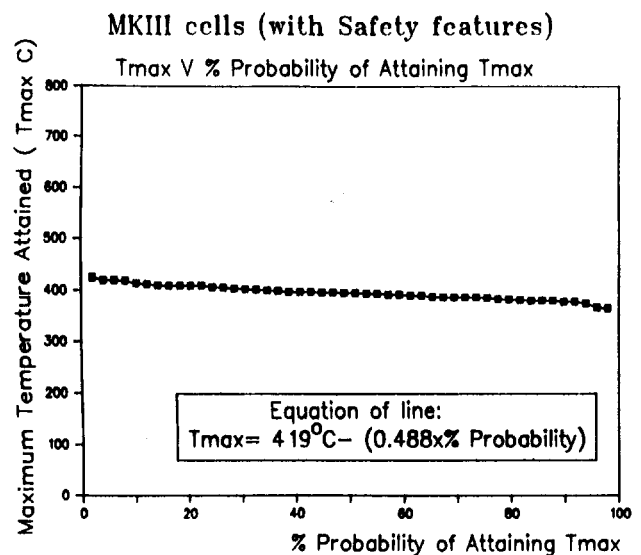


Figure 3-2. Temperature Exotherms Resulting from Safety Testing of MkIII PB Cells Containing Safety Features

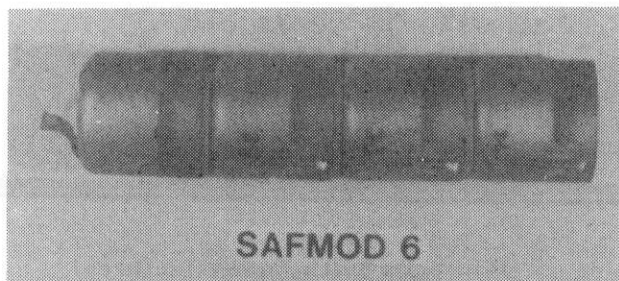
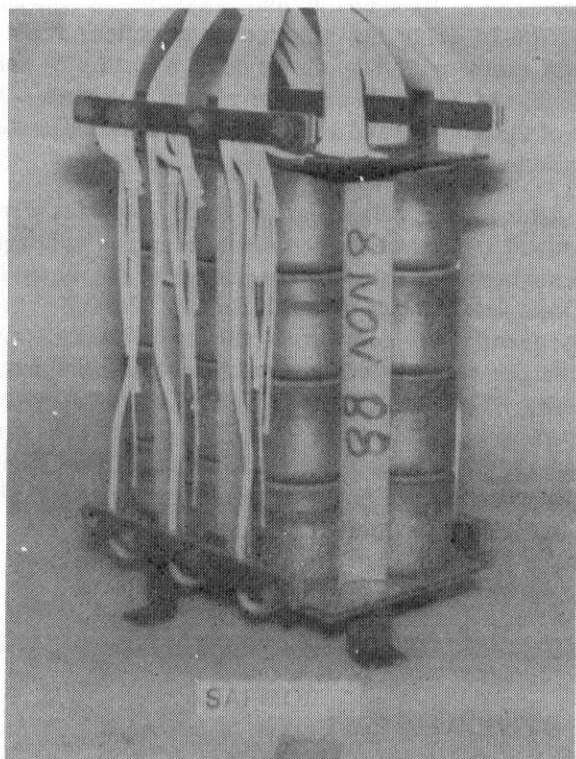


Figure 3-3. 24-Cell PB Module (upper) and One String (lower) After Safety Testing

Abuse safety was also commenced in early 1989. PB cells were impacted from the side by a steel spike until fracture of the electrolyte occurred. Although these tests were at an early stage at the time of writing, five cells had been impacted without any reactant leakage. A posttest cross-section of one of the cells is shown in Figure 3-4.

Sulfur Electrode

A characteristic of the MkIIa cells used in the Bedford CF Battery was the presence of charge polarization. An intensive study was conducted throughout 1988 to learn more about the CSPL sulfur electrode

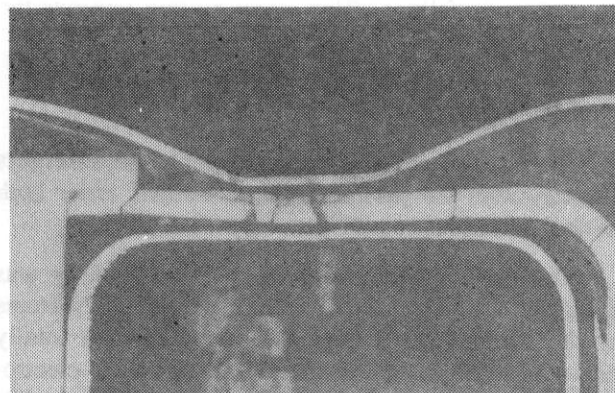


Figure 3-4. PB Cell After Side-Impact Testing

manufacturing and the effect that this had upon recharge performance. Many different molding conditions were studied and an improved set of parameters established. This was introduced as the production standard in 1988 and was employed in the cells for the intermediate EV battery. Electrodes made under these conditions have yielded satisfactory performance for normal EV operation, although some shortcomings are evident at high rates of charge pertinent to applications other than EV and load leveling. Table 3-4 shows data for PB cells operated at up to 4.76 A (1.75-h rate). The improvement in the recharge polarization index, R_c/R_d , for electrodes molded at higher temperature for longer times is evident. The recharge polarization index is the ratio of charge to discharge resistance 2.5 A from the top of charge (i.e., into the two phase sodium/sulfur polysulfide region). A value of <1.2 is desired.

The studies also showed an improvement in recharge polarization during the first 100 cycles of operation. This is thought to be because of beneficial effects of corrosion products in the electrode. Deliberate doping of electrode with metallic elements was demonstrated to reduce polarization.

Containment

The production of a long-term corrosion-resistant containment is one of the major challenges of this program. The presently preferred approach is the use of duplex chromized steel containers, which were employed on all cells made and tested in 1988. Other chromium-containing coatings were developed during 1988 at CSPL and in collaboration with SNL. The results of these tests were incomplete at the time of writing, but 50 cells were undergoing static corrosion testing and electrical cycling.

Table 3-4. High Recharge Current Testing of PB Cells

<u>Mold Conditions</u>	<u>Average Initial Recharge Current A</u>	<u>Rc/Rd ± 1sd</u>
Low Temp, Short Time	2.74 ± 0.28	1.35 ± 0.150
Low Temp, Short Time	3.68 ± 0.22	1.23 ± 0.160
Low Temp, Short Time	4.04 ± 0.12	1.40 ± 0.170
High Temp, Long Time	2.76 ± 0.25	1.06 ± 0.020
High Temp, Long Time	4.07 ± 0.29	1.06 ± 0.043
High Temp, Long Time	4.76 ± 0.04	1.13 ± 0.060

Cell Development

The objective of subtask 1.3 is to develop cell designs for both stationary and motive power applications, and to establish the cell performance, reliability, safety, cost, and F/T survivability.

PB Cell Development

Several versions of the PB cell were developed and tested during 1988. The seal variations are described earlier under the section on ceramic to metal sealing. In addition, cells that contain no safety features in the sodium electrode were tested as well as cells that had a mild steel container in the sodium electrode. This device was tested in a variety of forms. However, the basic concept remained the same in that a mild steel cup acted as an internal sodium container and formed a wick between itself and the beta"-alumina.

Reliability

By the end of 1987, the number of PB cells that had exceeded 500 cycles was 282. In 1988, this value almost reached 500 and the progress made since 1986 is shown in Figure 3-5.

A fall in the reliability of cells was detected in late 1987 following the scale-up of cell manufacture. The scale-up had involved changes to the methods of production in several areas. Analysis of test data showed a relationship between cell resistance and characteristic life, with high resistance cells exhibiting shorter lives. Investigations in the development program suggested that variability in sulfur electrode properties and electrolyte surface properties/sodium wetting were the most likely contributors to variable cell resistance and hence to poor reliability. Improvements in these areas were observed by changing the molding conditions of the sulfur electrode and by modifications to the production of the MkIII sulfur-electrode seal.

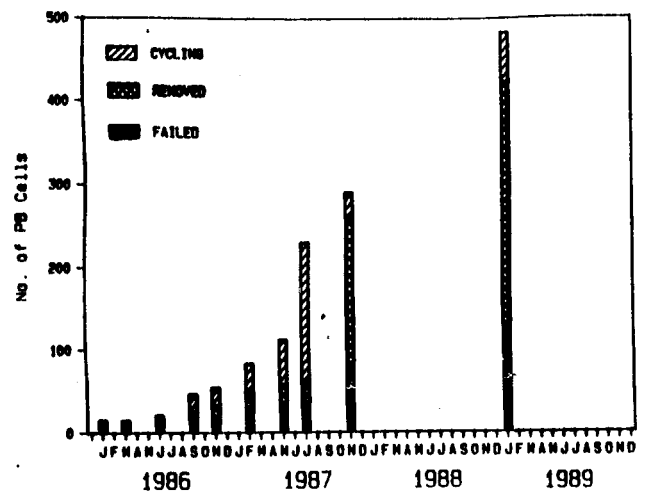


Figure 3-5. Number of PB Cells Exceeding 500 Cycles

An evaluation of cell reliability (Reliability Trial) was then performed to address the issues above and another area of concern, namely, the incidence of cell failures in the region of the glass seal. Variables in the experiment included sulfur-electrode molding conditions (considered to interact with cell resistance and rechargeability), electrolyte storage time (considered to interact with surface properties/sodium wetting), seal type (MkIII seal manufacture involved special heat treatment of the electrolyte), sulfur-electrode length (shorter electrodes limit the possibility of current intensification in the glass-seal region), and the amount of glass used to form the glass seal (additional glass was shown to improve seal quality). The Reliability Trial included 40 special cells (four groups of 10 cells), 10 standard production MkIIa cells and 10 standard MkIII production cells. The structure of the experiment is shown in Table 3-5.

The status of the experiment in early 1989 is shown in Figure 3-6. Meaningful Weibull statistics could only

Table 3-5. PB Cell Reliability Trial

Group Number	Experimental Sulfur Electrode Group Length Conditions	Number of Moulding Cells	Electrolyte Storage (days)	Sulfur Seal	Glass* Seal	(mm)
1	Standard Production low temp/short duration	10	84	MkIII	Not Preglazed	22
2	Standard Production low temp/short duration	10	84	MkII	Not Preglazed	22
3	Reliability high temp/long duration	10	7	MkII	Preglazed	20
4	Reliability high temp/long duration	10	7	MkII	Not Preglazed	20
5	Reliability high temp/long duration	10	7	MkIII	Preglazed	20
6	Reliability high temp/long duration	10	7	MkIII	Not Preglazed	20

* Preglazed seals used twice the standard quantity of glass.

**Mark IIa - Mark III Repeatability Trial Status
February 28, 1989**

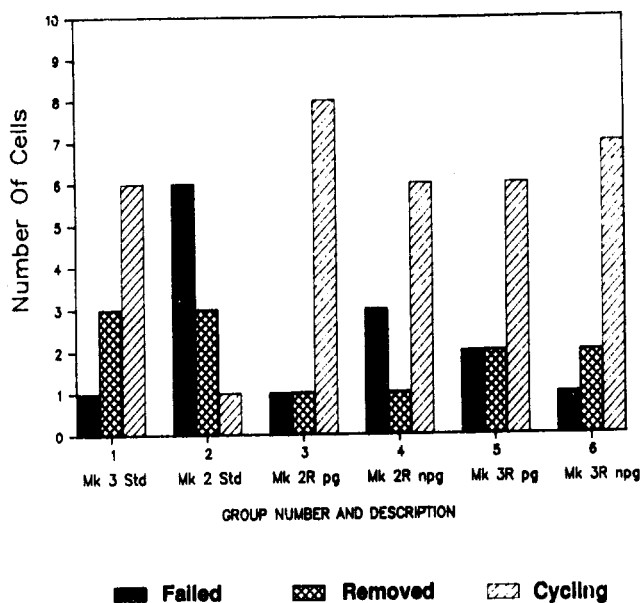


Figure 3-6. Status of MkIIa - MkIII Reliability Trial

be computed for the MkIIa groups. These statistics are listed in Table 3-6.

Failures in the MkIII design groups (1, 5 and 6) have occurred at 63, 307, 488, and 697 cycles. The failure at 63 cycles was shown by posttest analysis to be because of poor sodium wetting, a problem that has been resolved in subsequent designs (see performance below). If this failure is censored from the data, then the cell failures at various cycle lives are as shown in Table 3-7.

Overall the experiment showed that identical process changes would allow the reliability of the MkIIa design to be improved to pre-1987 levels. This improvement is shown in Table 3-8.

An additional benefit from the reliability trial experiment was the data collected on cell performance. It was apparent that cell resistance was rising as discharge progressed. Subsequent analysis and real-time radiography performed at SAIC showed that dewetting of the beta"-alumina was occurring and that effective electrode area was being decreased. This problem was solved when the safety feature was added to the sodium

Table 3-6. Weibull Statistics for MkIIa Cells in MkIIa - MkIII Repeatability Trial

Group	Weibull Statistics					
	Characteristic Life			Modulus		
Group 2	542	665	816	2.1	3.9	7.3
Group 3 and 4	740	893	1,078	2.3	4.1	7.3

electrode and the effects of this change on performance are described in the performance section below.

As well as the MkIIa - MkIII experiment, 271 MkIII cells were tested in single cells, strings, and modules. None of these cells contained a safety feature in the sodium electrode. The reliability of the MkIII PB cell without safety features has been predicted using the life data of all 311 cells. The data used in the analysis are shown in Table 3-9.

The 23 cell failures from the 311 cell population occurred at cycle lives between 63 and 837 cycles. The accumulated number of cell cycles is over 148,650. The Weibull analysis of the data in Table 3-9 yields the following parameters:

- Characteristic Life (Cycles): 1,774
- Shape Parameter: 2.02

Posttest analysis and other diagnostic studies have confirmed that the early failures are not associated with the MkIII sulfur electrode seal. The major cause of the early failures is associated with inadequate wetting of the electrolyte by sodium. When those failures associated with poor wetting are excluded from the analysis, the Weibull prediction gives a characteristic life of 1,340 cycles and a shape parameter of 2.85.

The reliability/performance data base for the MkIII PB cell with safety features includes over 600 cells, tested as single cells, strings, 24-cell modules, and 120-cell banks. Nonstandard (i.e., electrolyte and sulfur electrode development cells) safety cells were tested but are excluded from the reliability/performance data base. The baseline group of cells consisted of four 120-cell banks, two 24-cell modules and 73 cells tested as single cells or 4-cell strings, as shown in Table 3-10.

With only 18 cell failures (at between 126 and 439 cycles) out of 601 cells tested, only tentative estimates of the Weibull parameter could be made. The predicted characteristic life was 1,270 cycles with a shape parameter of 2.2.

Table 3-7. Failure of Cells in MkIIa - MkIII Reliability Trial

Cycle Life	Failures	
	MkIIa	MkIII
250	0	0
500	1	1
750	10	2

Electrical Performance

The electrical performance of the PB cell remained at the same level during 1986 and 1987. An overall improvement was made in 1988 following the introduction of the MkIII cell and the sodium safety features. The improvement in discharge resistance of the cells containing safety features is illustrated by Figure 3-7. The average cell resistances were reduced as follows. The discharge resistance of the MkIIa cells in the 36-cell experiment in 1987 was 34 ± 2.7 mohms. The discharge resistance of the MkIIa in the reliability trial was 39.0 ± 2.3 mohms and for the best MkIII cells, 40.3 ± 2.7 . The best MkIII cells with the safety feature had a discharge resistance of 30.14 ± 1.2 mohms.

A MkIII group of cells with safety features and special electrolytes was built near the end of the reporting period. This group is highlighted because it showed an average discharge resistance of 29.8 ± 2.07 mohms with one a cell that had a resistance of 25.8 ± 2.07 mohms, the lowest ever achieved in a PB cell.

The long-term resistance stability of the PB cell is illustrated in Figure 3-8 which shows the performance of three MkIII cells while the safety features were being developed. These cells have completed more than 750 cycles.

The capacity retention of cells was improved during 1988, particularly the values beyond 500 cycles where

Table 3-8. Comparison of Standard Production and Reliability Groups

Cell Groups	Weibull Statistics					
	Characteristic Life (cycles)			Modulus		
Standard Production (Groups 1 & 2)	678	952	1,336	1.4	2.5	4.6
Reliability (Groups 3, 4, 5 and 6)	877	1,287	1,889	1.3	2.4	4.5

Table 3-9. Life Data on MkIII PB Cells (No Safety Features)

Experiment	No. of Cells	Maximum Cycles Completed	No. of Failures
120 Cell Bank (B53)	120	510*	8
120 Cell Bank (B61)	120	472	6
21 Cell Scoping Trial	21	1,100	4
Reliability Trial	30	860	5
Sulfur Evaluation	20	575	0
Total	311	1,100	23

* Testing Complete

Table 3-10. Life Data on MkIII PB Cells (with Safety Features)

Experiment	No. of Cells	Maximum Cycles Complete	No. of Failures
120 Cell Bank B74	120	22	0
120 Cell Bank B89	120	24	0
120 Cell Bank B87	120	188	5
120 Cell Bank B75	120	283	3
24 Cell Bank B78	24	143	0
24 Cell Bank B70	24	377	1
Cells/Strings	73	747	9
Total	601	747	18

the MkIIa design had started to show a capacity loss because of corrosion. The capacity of the MkIII cell with safety features is also illustrated to 750 cycles in Figure 3-8.

Battery Performance

Although the intermediate EV battery delivered to ANL did not form a direct part of this program, the cells

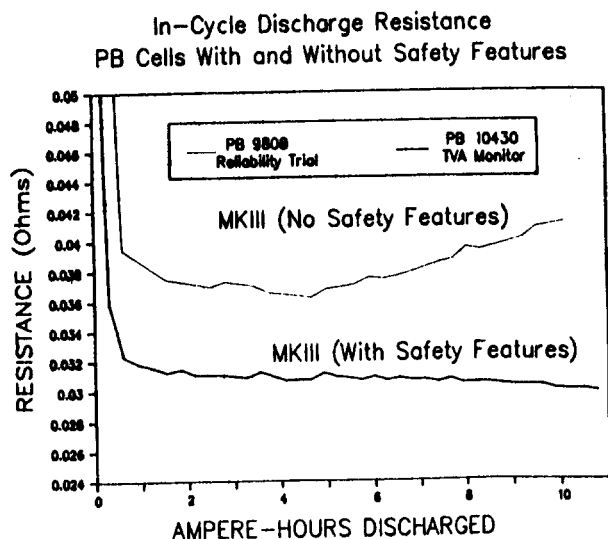


Figure 3-7. Comparison of PB Cell Discharge with and without Safety Features

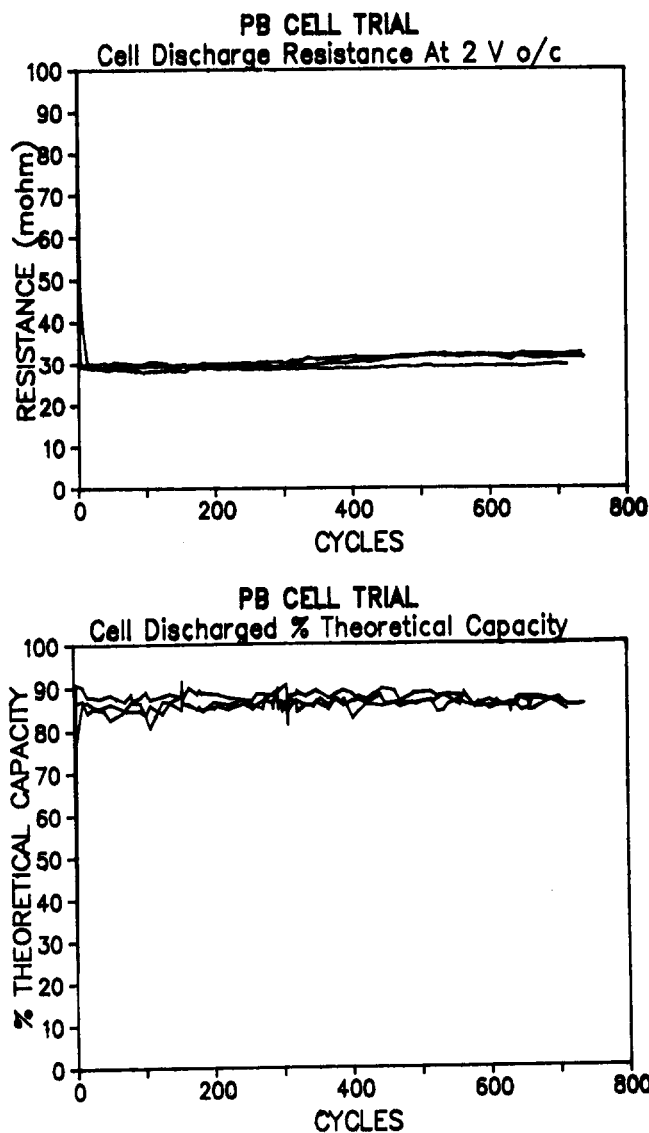


Figure 3-8. Resistance and Capacity of MkIII Cell with Safety Features

from which the battery was constructed embodied the Core Technology developments made under this contract. The preliminary performance of the battery was verbally reported by De Luca at the Society of Automatic Engineers Detroit Meeting (March 2, 1989), and a summary graph of the ANL testing is shown in Figure 3-9. At the time of writing, this 960-cell battery had completed 70 electrical cycles conducted under a wide variety of discharge profiles. No cell failures had been detected. The cells were built into the battery and dispatched to ANL in the virgin state (i.e., no prior break-in electrical testing was conducted at CSPL). Based upon the performance of the battery, ANL constructed a table of projected ranges for different simulated driving profiles, comparing the range obtained with sodium/sulfur with other battery systems.

CAPACITY HISTORY CSPL 64-V Na/S EV BATTERY

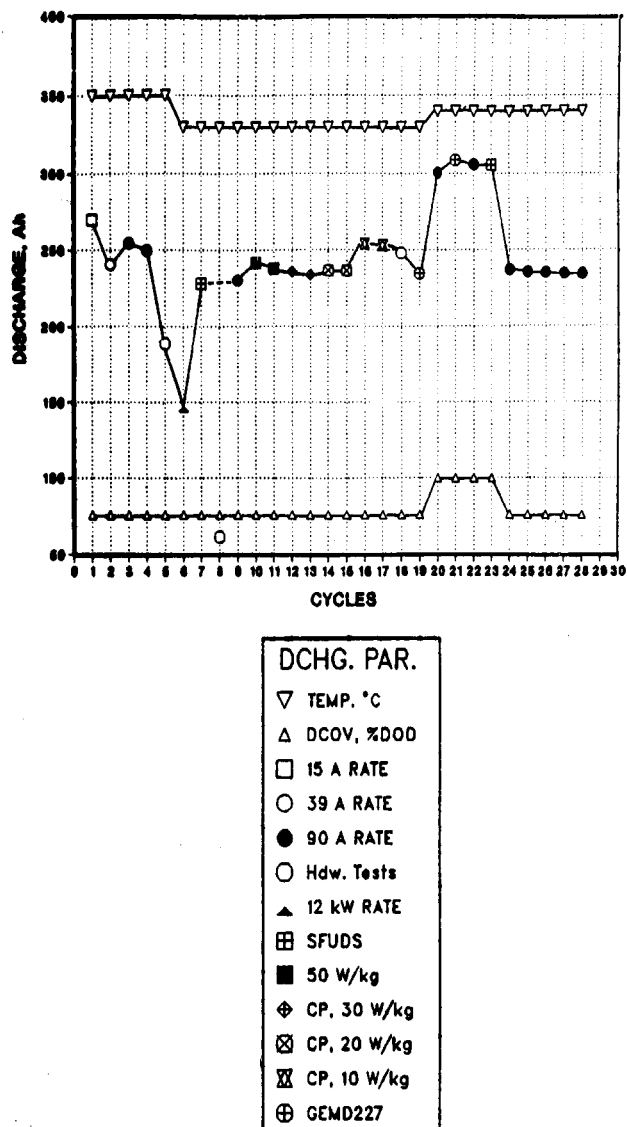


Figure 3-9. Capacity History of DOE/SNL EV Intermediate Deliverable Battery

The advantages of the sodium/sulfur system are evident in these data (Table 3-11). Based upon the performance of the CSPL battery at ANL, ranges of 148 miles and 182 miles were projected for the various electric vehicles.

XPB Cell Development

At the beginning of 1988, a group of 60 XPB cells was undergoing test. Three sodium container designs were under consideration that share a common spout configuration to connect the containers to the seal. Even when infant mortality was censored from the analysis, the reliability of the cells was inadequate (Weibull characteristic of 500 cycles combined with a modulus of 1). Posttest analysis confirmed that problems experienced during cell building had resulted in damage to the glass seals. To address the problem, the development effort was intensified. This was accomplished and, once resolved, the new fabrication methods and equipment were used on a 50-cell XPB build. The cells were tested as single units, a 16-cell module, and a safety-test group.

All of the cells were warmed up successfully, an improvement upon all previous cell builds, and the cells produced the lowest and most consistent resistances demonstrated to date. The single-cell test data are summarized in Table 3-12. All of the cells were given a F/T cycle after 27 electrical cycles to enable a cell to be removed from the test bath for transfer into the 16-cell

module. All cells survived the F/T cycle; some of them exhibited a small capacity rise and resistance fall. F/T testing was conducted on other cells made before the 50-cell build. Two cells each survived eight thermal cycles with no detectable change in performance during the electrical cycling, which was conducted between the thermal cycles.

The foregoing tests were conducted at 350°C at the 3-h discharge/9-h recharge rate. As well as these tests, a series of parametric tests was completed to characterize the performance of XPB cells at various temperatures and under different charge and discharge regimes. Temperature rise tests were also conducted under various discharge conditions to provide baseline information for the 16-cell module and Task 2 battery design efforts.

XPB Safety Testing

Ten XPB cells from the 50-cell build were each subjected to overvoltage failure. Figure 3-10 shows the temperature profile at the point of failure and immediately afterwards. The results of a statistical analysis of the data are shown in Figure 3-11. The least squares line lies slightly above that generated in a similar manner for the PB cell, and in view of the additional reactant load, this was an expected result.

Further testing of XPB cells that had leaking seals showed a significant probability of unacceptable

Table 3-11. Projected Ranges for Simulated Driving Profiles

Part I					
<u>Schedule</u>	<u>Vehicle</u>	<u>Weight (kg)</u>	<u>Avg. Speed (mph)</u>	<u>Peak Power (W/kg)</u>	<u>Avg. Power (W/kg)</u>
SFUDS79	IDSEP	695	19.0	79	9.9
J227aD	IETV-1	488	28.3	48	12.0
J227aC	G-Van	1,180	15.1	36	7.3

Part II			
<u>Battery</u>	Projected Range in Miles (Discharge Ah/kWh)		
	<u>SFUDS79</u>	<u>J227aD</u>	<u>J227aC</u>
Na/S (EV Intermediate)	148 [306/17.6]	182 [308/17.8]	TBD
Ni/Fe (NIF220)	75 [166/0.95]	98 [194/1.10]	93 [185/1.11]
Lead-Acid (3ET205)	47 [143/0.76]	54 [146/0.77]	5 [181/1.02]

Table 3-12. Summary of XPB Single-Cell Test Data for Cycle 55

Cell No.	Cell Resistance (mohm)	Capacity (Ah)	Capacity % of Theoretical
10352	10.26	30.1	87.5
10353	10.06	30.2	86.2
10354	10.12	30.5	87.6
10355	10.43	30.0	85.1
10356	10.77	28.1	82.6
10357	9.77	29.0	86.2
10358	9.86	29.0	86.5
10359	10.05	29.4	85.7
10360	11.02	30.4	85.4
10361	9.89	29.3	82.7
10362	10.09	29.6	88.4
	10.20 ± 0.4	29.6 ± 0.7	

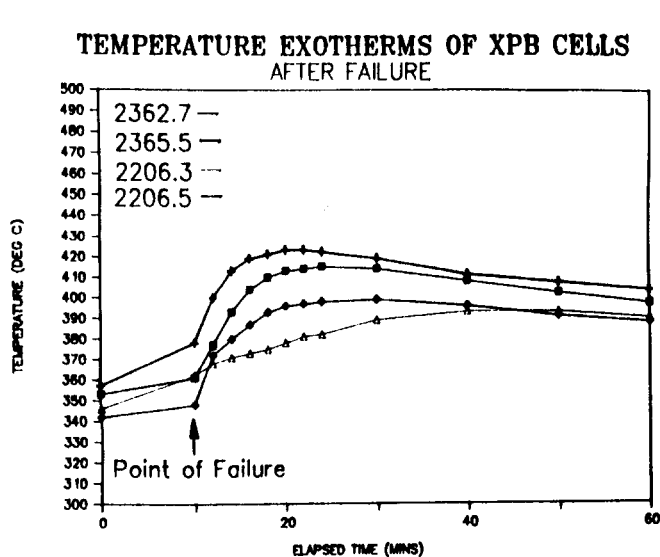


Figure 3-10. Temperature Profiles of XPB Cells After Safety Testing

exotherms, and further refinements to the design were under development at the time of writing. However, the overall safety performance of the new design was sufficient to enable test of a 16-cell XPB module to commence. Concerns about safety of previous XPB designs had led to the abandoning of the original 16-cell module test in early 1988.

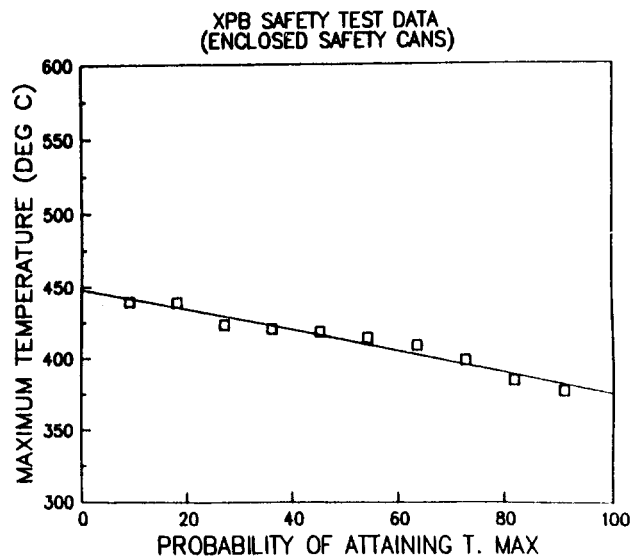


Figure 3-11. Statistical Analysis of XPB Safety Test Data

Cell Test and Posttest Analysis

The objective of this subtask is to provide test support and posttest analysis for other subtasks and as such the result of the effort is reported in the relevant sections.

Module Testing

The objective of this subtask is to develop and test submodules of larger battery designs in order to explore the interactions of cell connection strategy and to test groups of cells against application-specific requirements. Other objectives are to study the effect of cell failure interactions and the effect that varying cell performance has in an interconnected group of cells.

Module testing increased during 1988. A total of 19 modules was given the following tests: qualification, high-rate discharge, safety, and F/T, and XPB thermal management evaluations were performed.

PB Module

The number of PB cells in modules tested was in excess of 950, and the cumulative cell cycles were in excess of 210,000. The 120-cell bank (shown in Figure 3-12) became the preferred size of module for qualification testing. These banks consist of thirty, 4-cell strings arranged to deliver 8 V nominal and are subunits of CSPL's EV battery designs. The standardization of components between battery production and development testing improves the speed with which the development modules can be constructed as well as simulating the battery production methods for intercell terminations and bank plate construction.

The additional instrumentation that is applied to the development banks enables the consistency of cell performance to be monitored, particularly the string resistance. A typical example is shown in Figure 3-13, which is from a F/T test regime. The bank resistance

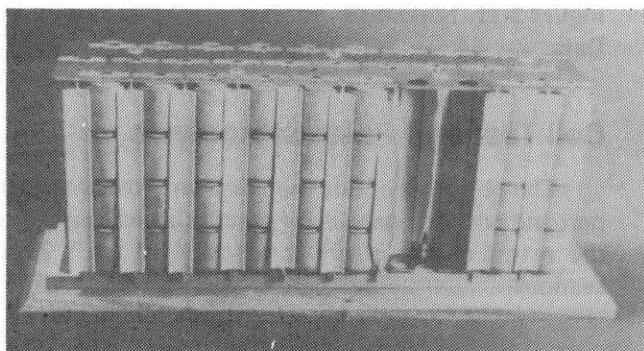


Figure 3-12. Typical 120-PB Test Bank

and capacity are also shown. In this trial, intended to establish the susceptibility of the PB cell to F/T failure early in battery life, no cells failed.

The 120-cell banks were also used for longer term cell testing. Bank B53, shown in the *ETD Annual Report for 1987*, page 69, completed more than 500 cycles before testing was voluntarily terminated. Typical longer term bank stability is shown in Figure 3-14. The cells in this bank were MkIII PB type with safety features. A significant statistic for the latter cell is that 1,448 of them were warmed up for test in 120-cell banks, 24-cell modules, and the intermediate EV battery without a single failure early cycle.

XPB Module

A 16-cell (4 series x 4 parallel) module of XPB cells was constructed in January 1989 and commenced testing. The module completed 7 cycles, with a discharge capacity of 110 Ah to 8 V_{oc}, before a cell was observed to polarize markedly on discharge at approximately 20 Ah discharged from the cell. This was considered to indicate a sodium electrode feed problem. After 14 cycles the module was cooled and the cell was replaced with one from the population on test as single cells. The module capacity fully recovered. All the cells survived the thermal cycle. The success of this operation opens up the possibility of using maintenance on the 200-cell battery should it be necessary.

The cell terminations and current shunts provided a significant contribution to the total resistance of 20 mohms to 25 mohms. Equivalent cell resistances (less terminations) were measured and shown to be similar to those of single cells (11 mohms). Different interconnections have been developed that contribute only 2.5 mohms to the cell resistance, and future modules with similar interconnections are expected to exhibit a resistance of approximately 13.5 mohms.

The module had completed 43 electrical cycles at the time of writing. These included a series of parametric tests to determine the thermal uniformity obtained with the convective air, recirculatory cooling system shown in Figure 3-15. In the first series of tests, the module was discharged at 43 A, and the cell temperatures monitored under three conditions:

- Without air recirculation
- With pre-heated air recirculation
- With air recirculation (no preheat).

The temperature behavior of the cells during discharge under the various cooling conditions is shown in Figure 3-16. Significant observations were as follows:

120 MkIII PB Safety Cell Freeze/Thaw Bank

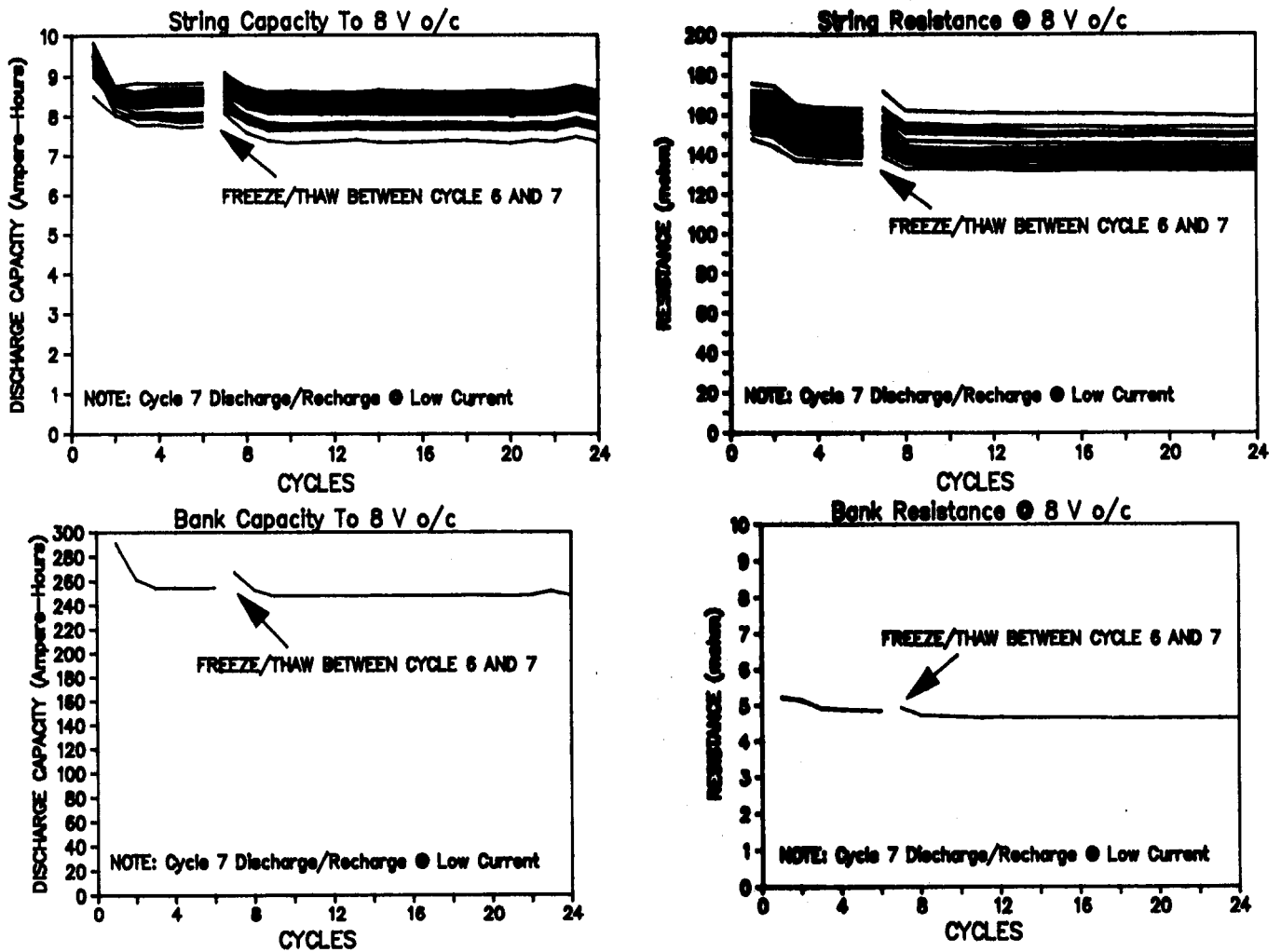


Figure 3-13. Typical Performance Characteristic of 120-Cell Bank

SANDIA DELIVERABLE BATTERY - QC BANK

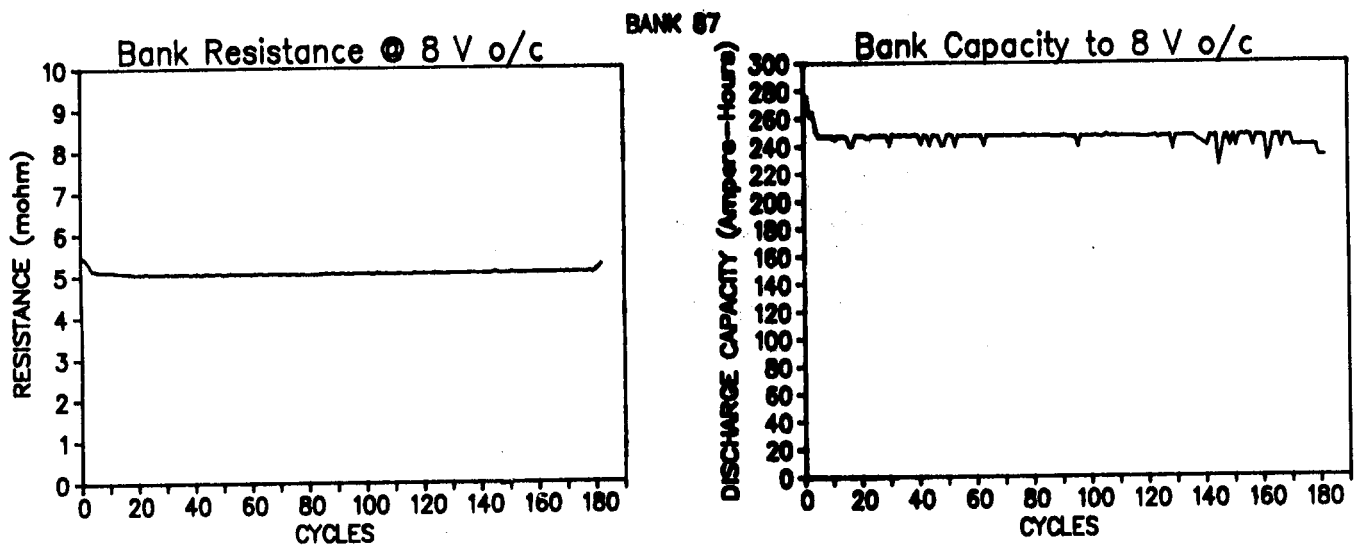
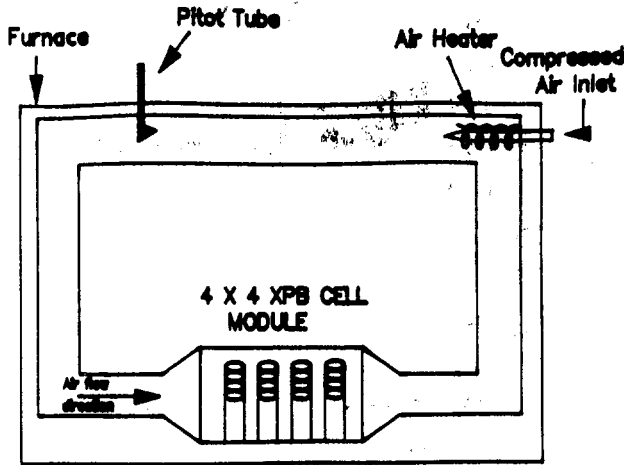


Figure 3-14. Resistance and Capacity of 120-Cell Bank B87

Schematic Diagram of Thermal Management Arrangement used on XPB Bank (B66)



Cell Arrangement In XPB Module
Shunt Resistors

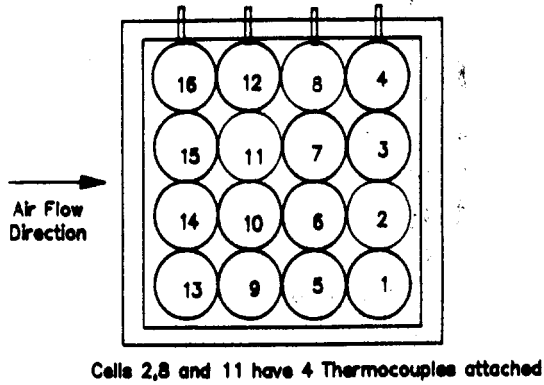


Figure 3-15. Thermal Management System - XPB Cell Module

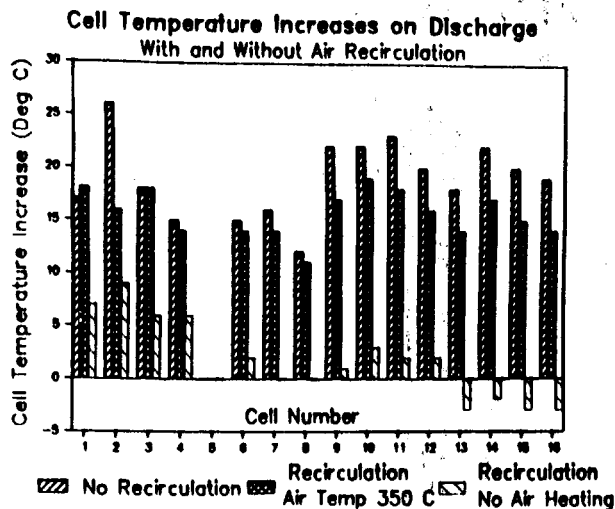


Figure 3-16. Cell Temperature Distribution - XPB Cell Module

- A mean temperature increase of 19°C (standard deviation = 3.7°C) was obtained when the module was discharged without air recirculation.
- The use of preheated air recirculation reduced the mean temperature increase to 14.4°C and also improved temperature uniformity (standard deviation = 2.8°C).
- Recirculating nonheated air actually cooled some of the cells during discharge and produced an average temperature increase of only 2°C. The variability in temperatures observed during the test indicated a need for further baffles to improve temperature uniformity.

Temperature distributions along the lengths of cells 2, 8, and 11 were also monitored during testing under the various cooling conditions. The significant observations are listed below and illustrated in Figures 3-17, 3-18, and 3-19.

Cell No.2 Temperature Distribution

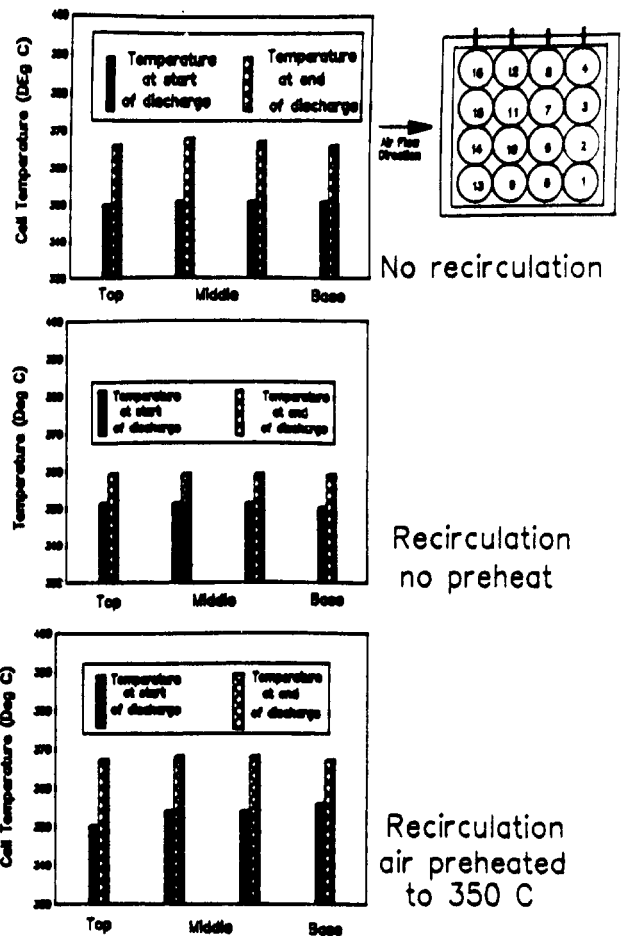


Figure 3-17. Temperature Distribution of Cell 2 - XPB Module

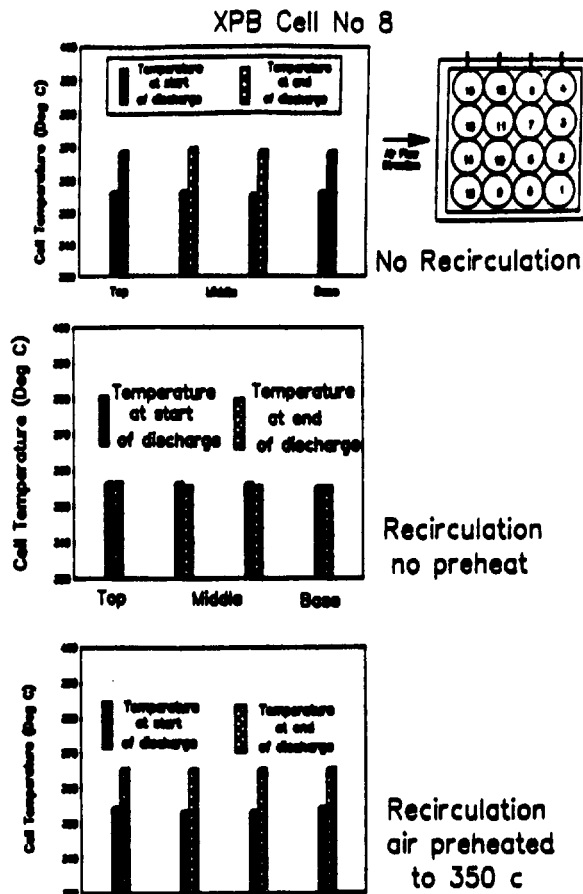


Figure 3-18. Temperature Distribution of Cell 8 - XPB Module

- The axial temperature distribution was uniform under the three test conditions.
- The axial temperature distribution was independent of position in the module.
- Absolute temperatures were skewed towards the air plenum.

Battery Engineering and Testing

The original design concept for utility batteries was based upon a proposal to EPRI (RFP 2123-4) in which a 100-MWh unit consisted of ten 10-MWh circular unit batteries. Originally, a 500-kWh battery in the BEST facility was scheduled in the EPRI-funded program. As stated in the introduction, this program was deferred, but the primary deliverable for this contract remained a 100-cell subunit. The design of this unit was based on several stationary battery concepts and contained the development experience of the Core Technology task.

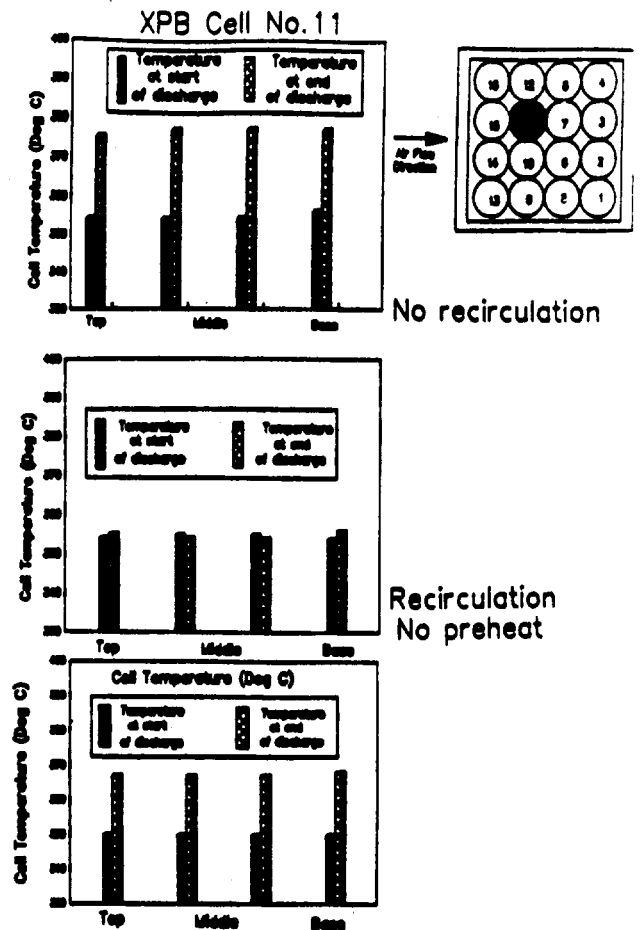


Figure 3-19. Temperature Distribution of Cell 11 - XPB Module

The surviving effort in the EPRI contract, designated "Phase P," consisted of commercialization and costing studies. To proceed, a clearer idea of the 100-MWh design concept was needed. This work was carried out in conjunction with CSPL's Runcorn and Wayne, PA, offices, SAIC, Stone and Webster Engineering Corporation, and Electrochemical Engineering Consultants, Inc. A lower footprint battery plant was proposed with a notable difference from earlier designs, from circular 10-MWh unit batteries to a more rectilinear approach.

The 100-MWh design concept that was developed is depicted in the artist's sketch shown in Figure 3-20. A major subunit of the 100-MWh plant is a thermal management system (TMS) that services four modules (shown in Figure 3-21). Each module consists of 10,320 XPB cells configured to deliver 72 V nominal and rated at 0.714 MWh. The module is subdivided into trays that contain a 26 x 10 cell flat array of vertically arranged XPB cells. A key feature of the design is the inclusion of an open-circuiting intercell device that

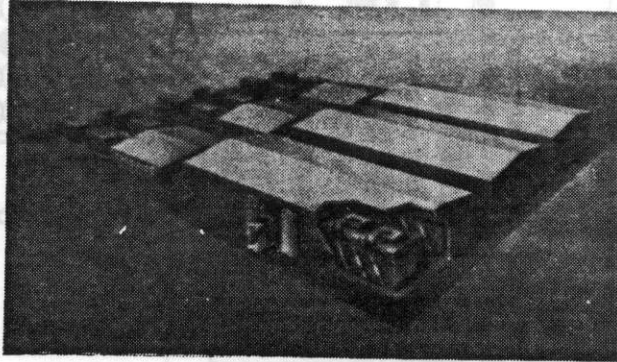


Figure 3-20. Artist's Sketch of the 100-MWh Utility Load Leveling Battery Developed in Phase P of EPRI Contract No. 2123-4

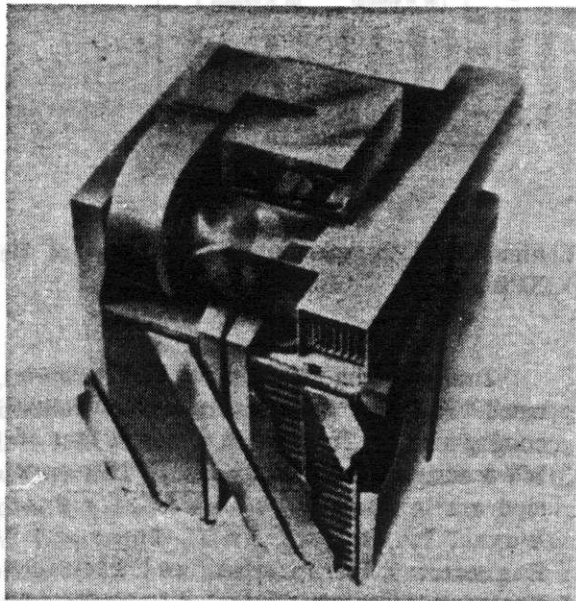


Figure 3-21. Artist's Sketch of Four-Module Thermal Management System for 100-MWh Utility Battery

ensures that cells fail open. Such a device enables an all-parallel electrical connection to be made.

The foregoing EPRI-sponsored study represented the starting point from which the design of the 100-XPB cell battery was commenced. The TMS concept relies upon the use of a moving airstream to maintain temperature uniformity, and an intercell spacing of 10 mm was calculated for the 26 x 10 cell array in that concept. The

direction of the air is such that it flows through an aperture 26 cells wide and through two sets of 10 cells (i.e., two trays) before emerging into the return air plenum. To maximize the information obtained from the deliverable battery, it was judged advantageous to keep the cells in a single vertical level and to release the 100-cell constraint so that more of the tray area could be simulated. At the present time, an open-circuiting device is not available, so batteries designed for near-term testing rely on the 4-cell series string approach. This concept is well tested at CSPL and has been demonstrated in battery sizes from 24 to 3,584 cells. It does however impose limitations on design freedom, leading in the presently preferred option to the use of an 8-V system.

The number of 4-cell strings was selected on the basis of expected battery reliability and synergy with the module design from the EPRI program. The ideal array would consist of a 26-cell-wide array arranged with two 10-cell runs. This was judged to be too large and incompatible with the desire to use 4-cell strings. For these reasons, an array of 8 cells wide by 25 cells deep was selected and is shown in the general arrangement drawing Figure 3-22.

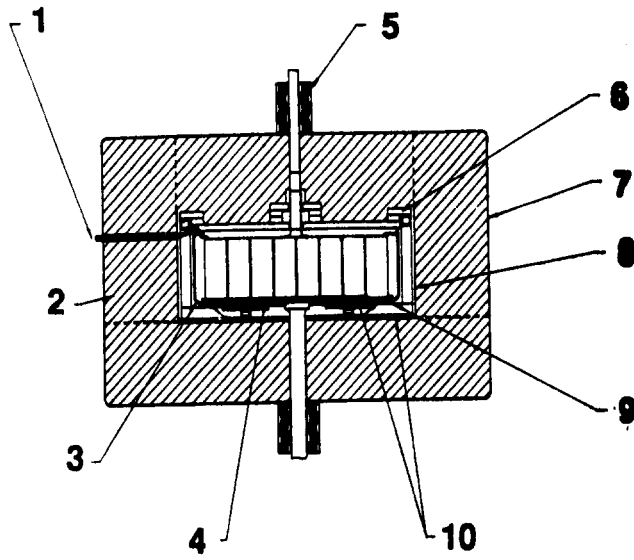
Four concepts were considered for the air flow management of the 200-cell battery. These include:

- Single Pass Air Flow System
- Single Pass with Heat Recovery Heat Exchanger
- Recirculatory Air Flow System
- Oven-Based Recirculatory System

As discussed in the previous section, the initial option chosen for testing in the 16-cell module was the recirculatory air system driven by a small fan. This was shown to be capable of delivering an adequate supply of air, but test experience led to the adoption of a system in which the air stream was driven by compressed air from the utility line in the laboratory. This proved to be more reliable than the fan-based system, although for future larger-scale batteries, the commercially available fans are adequate for the proposed service environment.

Sodium/Sulfur Battery Development - SAIC

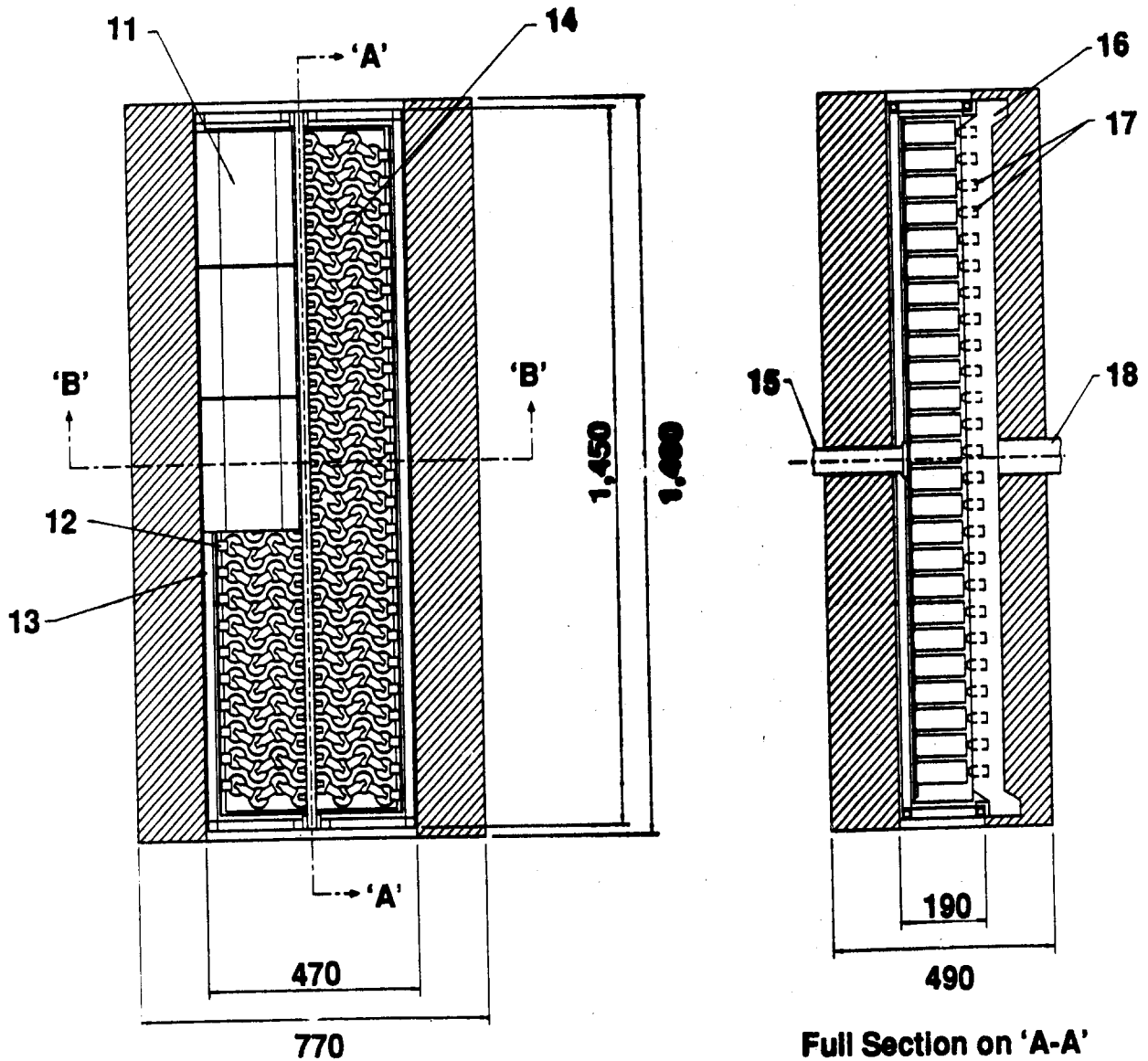
SAIC is the major subcontractor to CSPL on the ETD-sponsored development of the sodium/sulfur technology. The overall objective of the SAIC effort is to



Full Section on 'B-B'

Notes:
Cell Array Consists of 50 4-Cell Strings Mounted Side
By Side. Total Number of Cells = 200.

1. Thermocouple/Shunt Instrumentation Lead Through's
2. Insulation Material
3. Positive Busplate
4. Cell Location/Insulation Board
5. Wrap Round Heater on Busbars to Minimize Heat Loss
6. Rigid Insulation Material (removable)
7. Outer Box
8. Inner Box
9. Standby Plate Heater
10. Insulation Pads
11. Rigid Insulation Board (removable)
12. String to Busbar Connections
13. Mounting Framework
14. Cell Array
15. Positive Busbar Take-Off
16. Negative Busbar
17. String to Busbar Connections
18. Negative Busbar Take-Off



Full Section on 'A-A'

Figure 3-22. General Arrangement of 200-XPB Cell Array

support CSPL with the design of electric vehicle and utility load-leveling battery systems based on PB and XPB cell designs.

During 1988, the SAIC activities focused on four principal areas:

- Design support for the final contract deliverable: a load-leveling subbattery
- X-radiographic analysis of the performance characteristics of PB cells
- Development of a cell-failure device
- Mathematical modeling of battery performance.

A summary of the results for each area is presented in the following sections.

Battery Design Support

The BATREL computer model was used to model the capacity of an XPB subbattery design as a function of time and of the failure characteristics of the cells. The battery consisted of 200 cells arranged as 50 parallel 4-cell strings. For this initial set of simulations, only the capacity degradation from cell failures was considered. No consideration was made of capacity degradation from cell age, resistance rise, or other effects.

An example simulation is shown in Figure 3-23. Here the average capacity degradation with a cell lifetime of 1,300 cycles and shape parameter (β) of one, two, three, and four are given. Many simulations were performed, and Table 3-13 summarizes the overall results. The average lifetime cycles of the battery to 80% of the initial capacity is given for each of the cell lifetimes and shape parameter values. Using the current best estimates of cell parameters, which are a lifetime of 1,300 cycles and a β of 5.37, the current design would be expected to reach 80% of its initial capacity after about 700 cycles. This represents over 2.5 years of cycling in a utility load-leveling battery operated at 250 cycles per year.

The results indicate that the incremental increase in battery lifetime decreases with increasing shape factor value. Between shape parameter values of one and two, the increase in battery lifetime is over 300%, but between two and three, it drops to about 60-70%. However, between three and four, the increase is still significant at about 25%. The effect of the characteristic lifetime is relatively small.

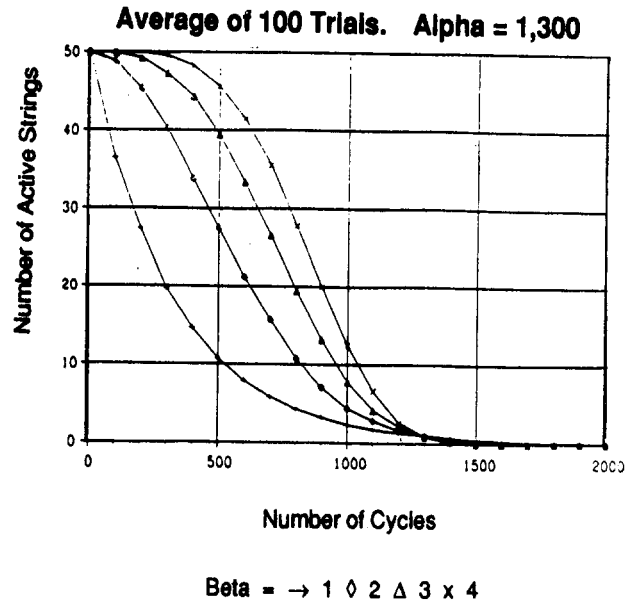


Figure 3-23. Comparison of Battery Capacity Degradation Curves for Alpha = 1,300

Table 3-13. Battery Capacity Modeling Results

Characteristic Lifetime (cycles)	Weibull Shape Parameter	Avg. Lifetime to 80% of Initial Capacity (cycles)
1,300	1	70
1,300	2	300
1,300	3	500
1,300	4	620
2,000	1	100
2,000	2	470
2,000	3	760

X-Radiography Analysis

The performance characteristics of several PB cells were analyzed in 1988 with real-time x-radiographic techniques developed in 1987 and later modified. Five cells were analyzed. Some of their characteristics at the time they were received are listed in Table 3-14.

These five cells were selected by CSPL for evaluation. Cell 9867 was meant to provide more information

Table 3-14. Characteristics of PB Cells Analyzed with X-Radiography

<u>Serial No.</u>	<u>Description</u>
9867	New cell, of the current state-of-the-art components. New specification sulfur barrier thickness and sulfur remold conditions, 20-mm side segments.
9547	250 cycles. Thick sulfur barrier, standard sulfur remold conditions.
9665	89 cycles. Thick sulfur barrier, standard sulfur remold conditions.
9559	308 cycles. Old standard thickness sulfur barrier, standard sulfur remold conditions.
9255	729 cycles. Old standard thickness sulfur barrier, standard sulfur remold conditions.

about break-in of new cells, and to provide a comparison to the data obtained from the new cell that was observed last year during break-in (cell 8815). It was also expected to show recharge polarization. Cell 9547 was tested to determine the cause of high discharge resistance that had been observed by CSPL. Finally, cells 9665, 9559, and 9255 were chosen for testing as cells that showed recharge polarization, in order that the processes producing that effect could be observed and identified.

Similar to the 1987 testing, the 1988 x-radiography studies produced useful data on cell operation, as well as observation of some additional unexpected phenomena. The detailed results are beyond the scope of this report and contain proprietary information. However, the following specific observations and conclusions are worth noting: bubbling in the sulfur electrode was observed throughout the charging of cells in the 1987 tests. In the latest tests, bubbling was observed to cease at the same time that recharge polarization began to occur (the cells in the 1987 tests did not show recharge polarization). This suggests a possible link between convective motion in the sulfur electrode and low cell recharge resistance.

Evidence of poor wetting of the sodium on the electrolyte was observed in both the earlier tests and the new series of tests. In several cells, the sodium meniscus was observed to "stick" at some locations and deform from a fully wetted shape. In one cell, blobs of sodium were observed to form above the visible meniscus of the sodium on the walls of the electrolyte during charging and then to fall into the central pool of sodium. In two others, a mass of material appeared to exist in the upper portion of the sodium container, on which the sodium appeared to hang up on discharge. These

observations suggest that wetting problems may be more complex than initially thought.

One cell (9867) was accidentally overdischarged to an open-circuit voltage of 1.74 V. Upon being slowly recharged, it recovered all of its previous capacity and showed no signs of damage. In fact, although the cell had displayed a large amount of recharge polarization in previous cycles (on the order of 100 mohms), the cell showed practically no sign of recharge polarization in the cycles that followed. The recharge resistance continued to improve over the next several cycles, never exceeding 40 mohms before the cell was almost charged. This behavior indicates that recharge polarization problems may be related to activity in the sodium electrode, as well as the sulfur electrode.

Two cells failed during the x-radiography testing. Although neither event was captured on film as it occurred, images of both cells were taken before and after the events so that changes that occurred during failure could be observed.

Development of Cell-Failure Device

An effort to develop cell failure devices was performed. First, characteristics of cell failures in various electrical network configurations were studied. Then, new ideas for failure detection and switching were generated and evaluated. Finally, the proposed failure switch systems were compared and rated, and additional device development was carried out on promising concepts identified in the study. Circuits for failure protection using high-temperature semiconductor devices were analyzed, and prototype circuits were fabricated and tested. Also, a stressed-glass thermal fuse

concept was defined in more detail. Two reports containing this material were written but are not reported because both contain proprietary information.

Battery-Performance Model Development

The battery statistical model BATREL was used to perform capacity degradation analyses for two EV battery configurations. The analyses compared a battery made of four series banks of thirty 4-cell strings with one consisting of one bank of 120 4-cell strings. Although the single-bank battery did show measurably better performance, it was not significantly more than the normal statistical variation between the two batteries.

A later series of analyses was performed using the battery capacity degradation model RELSIM. The configuration of interest was 30 cells in parallel and 96 cells in series. Four-cell strings, single-cell banks, and full series battery configurations were investigated. In one analysis, the lifetime of a battery to 80% of its initial capacity was related to the cell failure parameters (for an example, see Figure 3-24). In another, the number of active strings was related to the number and percentage of cell failures in the battery (see Figure 3-25). The results of these analyses were used to evaluate the capacity degradation of a small battery comparable to a vehicle battery.

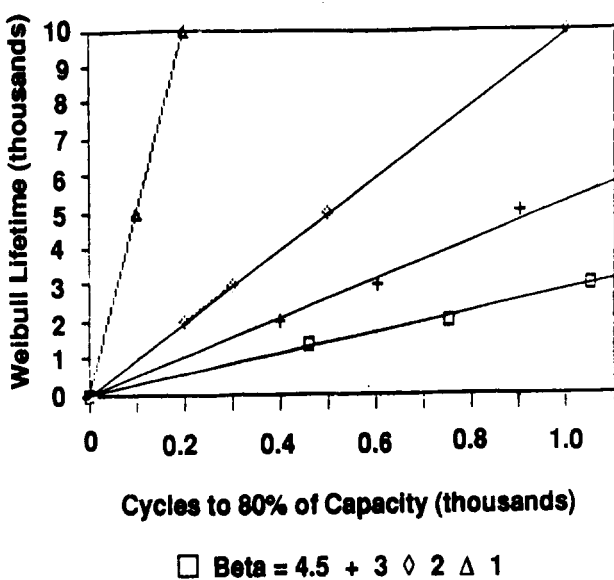


Figure 3-24. Four-Cell Strings - Weibull Lifetime vs Cycles to 80% of Capacity

Final modifications to the BATSIM code were made during 1988. BATSIM was developed for detailed simulation of sodium/sulfur battery modules. Figure 3-26 shows an overview of the BATSIM program. BATSIM is a comprehensive model that calculates both the electrical and thermal responses of a battery module to an externally imposed load. Among the applications for which the model is intended are detailed prediction of battery performance, evaluation of the effects of cell failures and failure devices on battery operation, thermal management studies, and

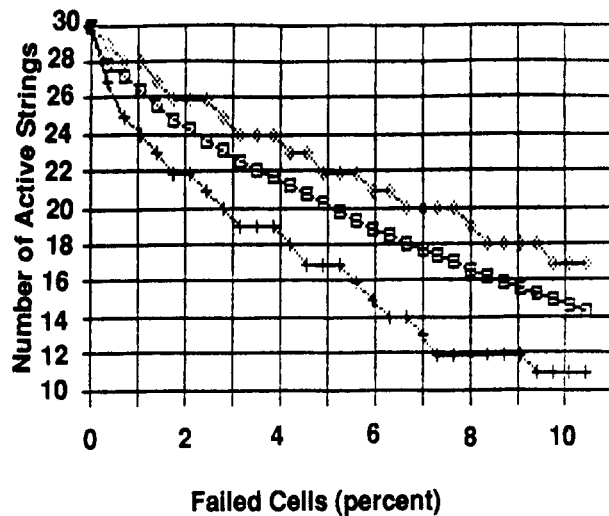


Figure 3-25. Four-Cell Strings - Number of Active Strings vs Percent of Failed Cells

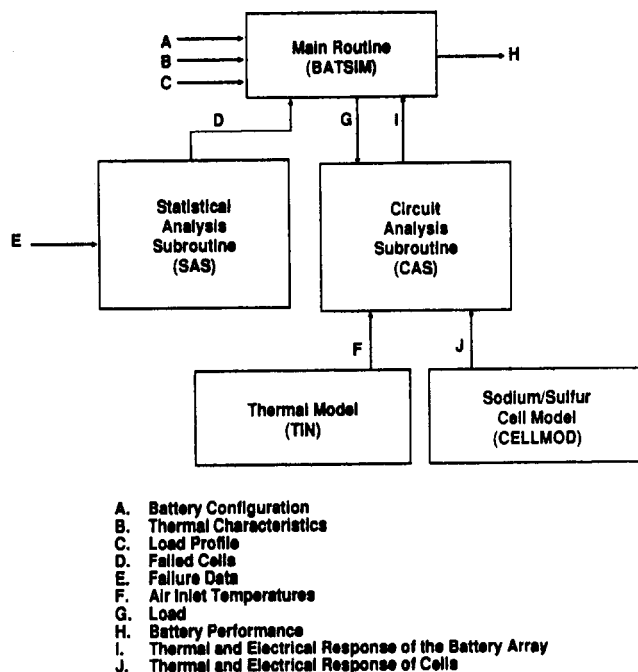


Figure 3-26. Overview of BATSIM Program

development and testing of sodium/sulfur battery control strategies.

terminated prior to failure. A summary of the test conditions and posttest observations is provided in Table 3-15. These findings are discussed further in the following sections organized by specific cell components.

Posttest Analysis of CSPL Sodium/Sulfur Cells

Specific CSPL cells were selected for detailed examinations using specialized facilities at ANL. These evaluations were performed to support CSPL's effort to improve cell performance and reliability and involved studies of the sulfur electrode, performance of cell hardware, and potential failure mechanisms. In 1988, examinations were conducted on three PB cells and two XPB cells. Operation of all five cells was voluntarily

Positive-Electrode

The final four cells listed in Table 3-15 were terminated in the charged state (2.076 V), and their positive electrodes shared several characteristics in spite of differences in cell design and operation. Sulfur, the primary phase in the electrodes, occupied roughly 45% of the available space. Sodium pentasulfide (Na_2S_5) was a minor constituent that filled about 5% of the electrode volume. These percentages were

Table 3-15. Summary of Posttest Findings for CSPL Sodium/Sulfur Cells

<u>Cell</u>	<u>Design</u>	<u>Cycles</u>	<u>Major Findings</u>
8815 ¹	PB	6	Terminated in the discharged state. Sodium polysulfides in the base of the positive electrode contained more sodium. Porosity in the cap-to-case weld.
8015 ²	PB	20	Thermal cycling induced a partial fracture through the glass seal. Shallow cracks on sodium side of the electrolyte. Extended periods in discharged state accelerated corrosion of the cell case. H_2S , COS , SO_2 , N_2 , and CS_2 were the major constituents of the gas in the sulfur electrode.
7835	PB	699	Sealing glass exposed to sodium developed spalling-type fractures from compositional changes. Build-up of calcium on the inner electrolyte surface. Corrosion penetrated 90% of the chromized layer at the base of the cell case. Minor deposition of NaCrS_2 on the outer surface of the electrolyte base. H_2S , CO_2 , COS , and N_2 were the major constituents of the gas in the sulfur electrode.
9343 and 9345	XPB	424	Weak metal-to-ceramic bonding for the MkIIa seals. Sealing glass exposed to sodium developed spalling-type fractures from compositional changes. Minor deposition of FeS_2 on the outer surface of the upper electrolyte. Reduced levels of calcium on the inner electrolyte surface.

¹ Tested by SAIC as part of their real-time radiographic imaging program.

² After electrical cycling, the cell was subjected to static corrosion tests at potentials of 1.76, 2.074, and 1.9 V for periods of 13, 28, and seven days, respectively. Interspersed within these tests were two periods of thermal cycling totaling 147 F/T cycles.

consistent with the values found during prior examinations of cells operated for 60 cycles and indicated that extended cycling did not result in a decline in rechargeability.

A general trend also existed in the concentration of active materials within the electrode. For XPB cells 9343 and 9345, nearly 90% of the active material was in the lower half of the electrode. Similarly, the volumetric percentage of active materials was three times greater for the base section of the 7835 electrode than for its cylindrical section. The examination dissection of cell 8815 revealed two distinctive zones of coloration. The cylindrical section had a yellow-green color and consisted primarily of sodium tetrasulfide (Na_2S_5). The bulk of the base section was orange. X-ray diffraction determined that this zone contained three phases, one sodium tetrasulfide and two metastable polysulfides, that have been designated as K-phase and M-phase. Both of these phases contain more sodium than sodium tetrasulfide. The composition of M-phase has been bracketed between 35.5 and 38 wt% sodium in past studies. An SEM-EDS scan across the base section revealed a gradient in the composition of the orange zone. The sodium content was $\approx 4\%$ greater at the electrolyte than at the cell case. These findings indicated that more sodium was transported through the base of the electrolyte, at least in the initial stages of cycling.

Mass spectroscopy was used to determine the composition of the gases present in the positive electrode compartments of the PB cells. Unfortunately, an adequate seal could not be maintained during penetration of the case of cell 8815. The attempts to sample cells 7835 and 8015 were successful, and the results are summarized in Table 3-16. Residual quantities of atmospheric gases (N_2 , O_2 , Ar, H_2O , and CO_2) were expected in the sulfur compartments because the vacuum maintained during welding was on the order of 10^{-3} torr. However, this source alone would not explain the high gas contents found in these electrodes. The total gas volumes were estimated to be 7 and 10 cm^3 (STP) for cells 8015 and 7835, respectively.

The gas compositions were somewhat different for the two electrodes. For cell 7835, the ratio of atomic hydrogen to atomic oxygen in the electrode gases was about 1.9 to 1. This ratio was consistent with a previously formed hypothesis that absorbed water in the positive electrode reacts with the sodium polysulfides formed during discharge. This reaction would form H_2S and liberate oxygen that, in turn, would react with the graphite fibers to form gases like CO_2 and COS. Similar findings were made during a past analysis of a cycled cell. For cell 8015, the ratio of hydrogen to oxygen was 2.9 to 1, which is too high to fit this hypothesis. The

Table 3-16. Gases Found Within the Sulfur Electrode Compartments

Gas	Volume Percent	
	Cell 8015	Cell 7835
H_2	0.60 ± 0.10	0.25 ± 0.05
H_2O	0.14 ± 0.10	0.15 ± 0.10
N_2	4.80 ± 0.10	4.00 ± 0.10
O_2	N.D.*	0.60 ± 0.30
H_2S	59.80 ± 1.50	60.00 ± 1.80
Ar	0.04 ± 0.01	0.03 ± 0.01
CO_2	29.60 ± 1.50	7.80 ± 0.60
COS	5.00 ± 0.20	24.2 ± 1.20
SO_2	0.02 ± 0.01	0.09 ± 0.03
CS_2	0.03 ± 0.01	2.90 ± 0.30

* N.D. stands for not detected.

relative amounts of CO_2 and COS were also reversed in comparison to the amounts for cell 7835. Two factors could be responsible for these differences. The 20 electrical cycles may not have provided enough time for equilibrium conditions to be established. Alternatively, the 147 F/T cycles may have influenced the gas chemistry.

Sulfur Container

The cell cases and top caps were fabricated with low-carbon steel and were thermally chromized to increase their corrosion resistance. The chromizing process produced a duplex layer on the surfaces that consisted of a thin outer layer of chromium and chromium carbides and a thicker alloy layer of iron and chromium. Initially, corrosion of the outer layer formed a porous scale of sodium thiochromide (NaCrS_2), but as corrosion of the outer layer continued, the scale became multiphased with compact interior layers of chromium sesquisulfide (Cr_2S_3) and trichromium tetrasulfide (Cr_3S_4). When corrosion progressed into the ferromanganese layer, iron disulfide (FeS_2) formed in addition to the chromium sulfides.

Corrosion was significantly less for the top cap and upper walls of the cell case and was most severe for the base of the case. The accelerated attack undoubtedly reflected the exposure to the more corrosive electrode melt formed in the adjacent region of the electrode. As described in the above section, sodium polysulfides of

higher sodium content form and remain concentrated beneath the base of the electrolyte during discharge.

Sufficient corrosion data were collected from these and prior examinations to project the expected lifetime of this type of cell case. Figure 3-27 plots the maximum depth of corrosion found for the base of the cell case as a function of cycle life. The curve in Figure 3-27 illustrates that portions of the high chromium layer were penetrated within the first 300 cycles. The ferrochromium layer, which was five times thicker, was projected to last nearly 500 more cycles before sections of the steel substrate became exposed. Because the cases were chromized on both sides, cells operated under these conditions would not develop breaches through the cases during the first 1,600 cycles of operation. It should be emphasized, however, that the data used in Figure 3-27 were derived from cells operated under the following conditions: continuous cycling under constant load, one charge/discharge cycle every eight hours (after break-in cycling), and discharge to a fixed open-circuit voltage. The temperature extremes ranged from 346 to 359°C for these cells. Examinations of other cells showed how deviations from these test conditions can measurably alter the corrosion rate.

Electrolyte

None of the cells experienced electrolyte failures, but SEM-EDS studies were used to identify subtle forms of degradation. Calcium contaminated the inner electrolyte surface of these cells, especially the PB cells with long cycle life. Calcium is considered a source of increased electrolyte resistance. The highest calcium

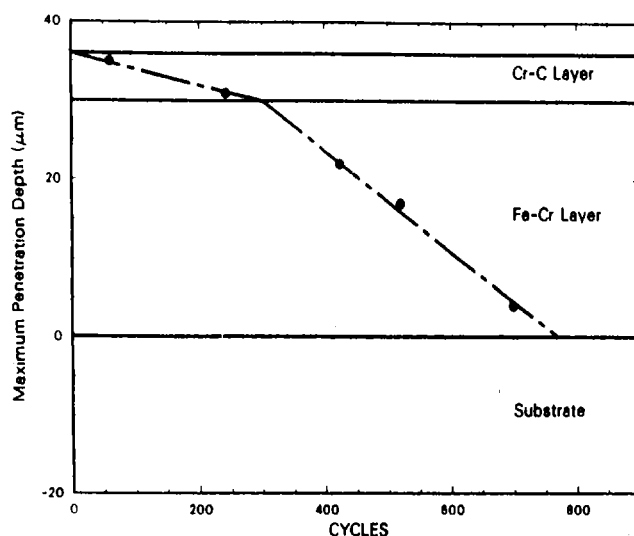


Figure 3-27. Corrosion Penetration for the Chromized Cell Cases

levels were found at the bottom of the electrolyte. Calcium contamination also increases with cycle life for these and previously examined cells. For the PB cells, the calcium level initially showed a near linear increase over the first 200 cycles before reaching a plateau value of about 7 at.% for the maximum calcium level. The limited data for XPB cells fell far below this value. The divergence resulted from differences in the two cell designs. The PB cells used aluminum powder as an infill material within the electrolyte to help distribute sodium. The XPB cells used a safety tube and an alumina wick in place of the infill material. The alumina components also served as a getter for calcium, and the wick apparently provided better gettering action than the powder.

The electrolyte from cell 8015 was the only one to exhibit physical damage from its testing regime. The thermal cycling induced shallow cracks along the inner wall of the electrolyte. These cracks always terminated on the inner surface, producing small fragments of electrolyte. The depth of penetration never exceeded 30 μm. These fractures probably developed because of nonuniform stress imparted to the electrolyte surface during freezing and melting of sodium. This mode of cracking would be unlikely to cause a sudden failure of the ceramic.

Glass Seals

The glass seal between the electrolyte and alumina cap was characterized by good adhesion to both ceramics, complete filling of the horizontal sections of the joint, and filling of the upper vertical section. A low-grade reaction was evident, however, for cells with long cycle life. The reaction was restricted to the glass within the sodium compartment, and the depth of the sodium reaction was less than 50 μm beneath the exposed surfaces. For cell 7835, SEM-EDS measurements found a substitution of over 20 at.% sodium for silicon and the other elements. For cells 9343 and 9345, which used a different sealant, the increase in sodium was comparable.

Thermal cycling induced a more serious fracture in the glass seal from cell 8015. The fracture developed in the seal glass between the flat of the alumina cap and the rim of the electrolyte. Interaction occurred at the surface exposed to sodium and propagated through the horizontal section of the joint. The fracture developed no branch cracks and made a complete circuit around the seal circumference. Both of these characteristics are typical of thermal shock fractures. In addition, the glass near the fracture showed no discoloration and no significant shifts in composition. Generally, the crack

growth was arrested in the glass seal before it could propagate horizontally through the lip of the insulator, but in one section, the fracture deflected upward and continued into the insulator. For cell 8015, the 147

thermal cycles were insufficient to complete the fracture, and the cell passed nondestructive inspection at CSPL because the ceramic components still maintained a physical barrier between the sodium and the sulfur.

Chapter 4. Battery Technology Evaluation

Introduction

Rechargeable cell and battery testing was performed within the Battery Technology Evaluation Element. Work was carried out at ANL and SNL. Evaluation tasks consisted of standardized cell and battery testing at ANL and specialized cell and battery testing at SNL.

The objective of these activities was to provide independent prototype testing. Most units tested were deliverables from the major OESD battery development projects. Cells and batteries were evaluated from CSPL, Ceramtec, ERC, JCI, and Eltech. The test results were used in part to verify developer claims and predictions. Additional tests were conducted to characterize each prototype fully. These results assisted in identifying the strengths and weaknesses of each technology. In some cases, problem areas were identified for additional research and development, either by the developer or SNL. These evaluations provided essential information for judging the technical progress of each development project. In virtually all cases, the evaluation activities provided new performance and design information.

These data and results were distributed to DOE and national laboratory program managers. All tests were conducted with the close cooperation of the respective developers, and the results were shared on a timely and open basis to provide the maximum benefit to each project.

At SNL in 1988, evaluations continued on CSPL and Ceramtec sodium/sulfur cells, ERC zinc/bromine batteries, and JCI nickel/hydrogen cells and batteries. Testing was initiated on an Eltech aluminum/air cell. A key finding of these tests was that new MkIII CSPL cells demonstrated good performance and long life, but that charge acceptance was impaired compared to earlier deliverables. The Ceramtec cells performed well and delivered expected capacities. The cycle life of an ERC zinc/bromine battery was shown to be 100 cycles, a significant increase compared with prior ERC deliverables. Electrolyte flow uniformity was identified as the key to extending battery life for this technology. A nickel/hydrogen 7-kWh battery was successfully operated with a photovoltaic array. Finally, an aluminum/air cell was assembled and operated during the

last half of 1988, establishing the feasibility of the present design.

At ANL, testing was completed on several CSPL sodium/sulfur single cells, and evaluations were started on two 24-cell modules. Over 1,200 cycles were achieved before failure on one of the single cells, verifying SNL data. The first 24-cell module was removed from test after only 14 cycles because of several unexpected cell failures. A second 24-cell module was successfully tested later in 1988 and demonstrated excellent performance.

The rest of this chapter presents these results in detail.

Battery Evaluations at ANL

During 1988, EV battery evaluations were performed at the ANL/ADL for the DOE/OESD and Office of Transportation Systems (OTS), and EPRI. The results of the OESD technology evaluations are discussed here.

The ADL conducted performance and life characterization tests on single cells and 24-cell modules. The status at the end of 1988 and performance of these cells and modules are listed in Table 4-1. Composite plots of sodium/sulfur, showing available specific energy vs discharge specific power level and specific peak power vs DOD, are given in Figures 4-1 and 4-2, respectively. The values of specific peak power were derived from driving profile discharge data and are plotted as a function the DOD during that discharge. The ranges projected using various driving profile discharges are listed in Table 4-2. These results and others are discussed below.

As part of the DOE/OESD sodium/sulfur (Na/S) battery development program with CSPL, the ADL completed life tests on eight cells and initiated the evaluation of two 24-cell modules. Eight 10-Ah, 20-Wh rated cells were received and placed under test in 1987. Four of the cells underwent performance characterization followed by life-cycle testing. The other four cells were only life tested. The cells had not been cycled before shipment and were of a 1987 MkII, PB design that previously exhibited premature seal failures.

Table 4-1. Performance Data for Sodium/Sulfur Cells and Modules Tested at the ADL from January 1 Through December 31, 1988

Sponsor Battery Type (Mfr.)	ID No.	Max. S.E. (Wh/kg)	PPSD ¹ 50%/30 s (W/kg)	Accum. Cycles ²	Δ from Prev. Qtr.(Cycles)
DOE/OESD/SNL Program					
(a) Sodium/Sulfur Cells (CSPL)					
Characterization and Life	7495	132.0	200.0 ⁴	(1221)	290
Characterization and Life	7494	131.0	220.0 ⁴	(1194)	292
Life	7464	125.0	207.0 ⁴	(1012)	300
Life	7472	135.0	—	(820)	13
Life	7440	127.0	—	(973)	281
Life	7438	139.0	—	(734)	210
Life	7437	128.0	—	(795)	266
(b) Na/S 24-Cell Module (CSPL)					
Characterization and Life	1	—	—	(14)	14
Characterization and Life	2	98 ³ /150 ⁴	140.0 ³	140	140

1 PPSD = Peak power sustained for 30 s duration at 50% depth-of-discharge; derived from SAE J227aD/IETV-1 driving schedule unless noted otherwise.

2 Parentheses indicated evaluation completed during the reported period.

3 For module weight of 4.382 kg (50% burden); S.E. at 10 W/kg CP discharge rate.

4 For naked module weight of 2.88 kg (120 g/cell x 24 cells).

COMPOSITE PEAK POWER PLOT

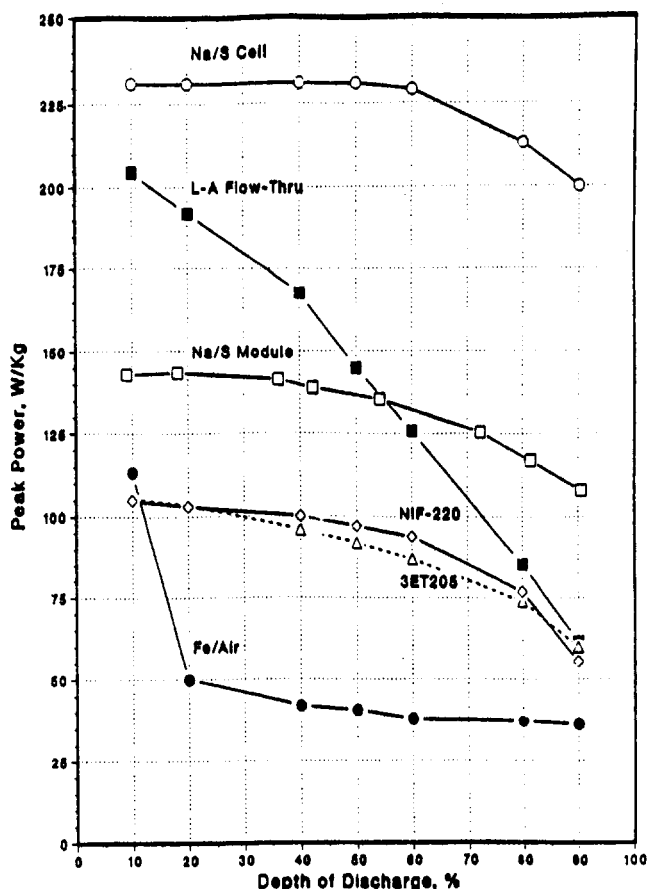


Figure 4-1. Peak Power of Four Advanced Battery Technologies as a Function of DOD Derived from Driving Profile Discharges

COMPOSITE RAGONE PLOT

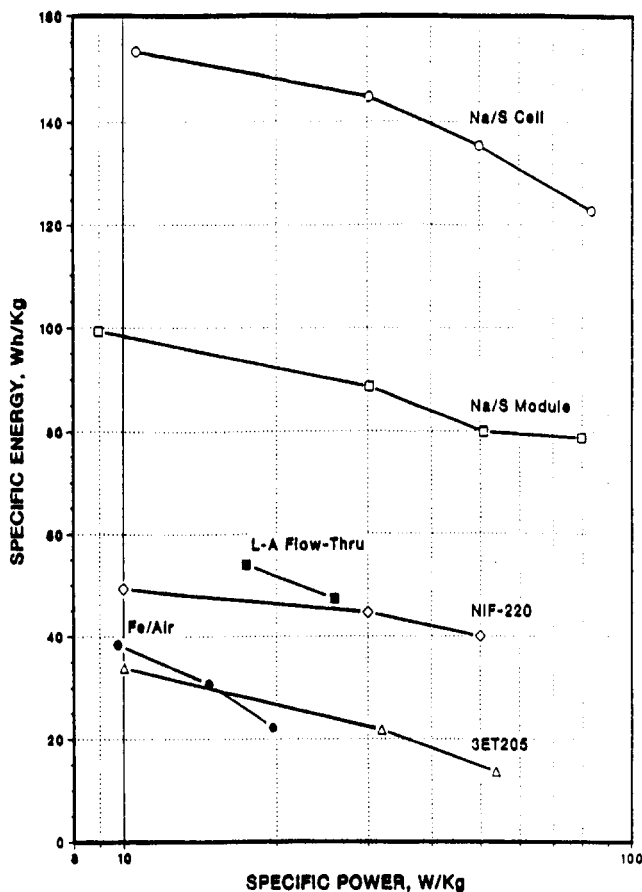


Figure 4-2. Effect of Discharge Specific Power on the Available Energy of Four Advanced Battery Technologies Evaluated at the ANL/ADL

Table 4-2. Projected Ranges for Simulated Driving Profiles

Technology (Developer)	Schedule→ Vehicle→ SFUDS79 IDSEP-Van (mi)	J227aD IETV-Car (mi)	J227aC GM-Van (mi)
Na/S 10-Ah PB-Cells (CSPL)	159 ¹	193 ¹	—
Na/S Module 60-Ah Na/S Module (CSPL)	168 ²	202 ²	196 ²

1 For total cell weight of 180 g (120 g mass and 60 g, 50% burden).

2 For projected module weight of 4.32 kg (includes 50% burden).

After conditioning, all eight cells demonstrated reproducible performance and achieved capacities of 8.2 ± 0.5 Ah (15.7 ± 1.0 Wh), resistances of 33 to 40 mohms, coulombic efficiencies of about 100%, and energy efficiencies ranging from 86 to 89%. The CSPL cells exhibited an average specific energy of about 131 Wh/kg at the 3-h discharge rate. The measurements were based on a discharge cut-off voltage algorithm of

$$V_{co} = 1.9 - 0.034 * I$$

and a cell weight of 120 g. The sodium/sulfur cell data plotted in Figures 4-1 and 4-2 are from discharges where a 0% weight burden was used (cell mass of 120 g).

Life cycling was performed with 100% capacity discharges at a constant-current 3-h rate. The eight cells operated for over 7,000 total cycles, and an average cell life of 892 cycles was achieved (from 388 to 1,221 cycles). One cell had a premature seal failure (in FY1987) after 388 cycles, and another was removed from testing before failure after completing 1,194 cycles so that a corrosion analysis could be undertaken. Testing of the remaining six cells was suspended when their capacity decreased to 75% of its initial level (average cell life of 926 cycles).

The first 60-Ah, 480-Wh CSPL sodium/sulfur module was tested in early 1988. The module contained 24 PB-cells of the MkII design, which were arranged in six parallel-connected strings of four series-connected cells each. This module was operated for only 14 cycles before being returned to CSPL. An initial capacity of 46 Ah (351.5 Wh) and an internal resistance of 29.9 mohms were exhibited. Cell string currents were matched at shallow DOD levels but varied by as much as $\pm 50\%$ at the end of discharge. During cycle 10 a cell apparently breached, and its string became an open cir-

cuit after a temperature excursion to 400°C (normal operating temperature, 350°C). Thereafter, the module was operated with only five strings, and a reproducible capacity of 35 Ah (275 Wh) was obtained for four cycles.

A second CSPL sodium/sulfur module was delivered for evaluation in September 1988. This module contained MkIIa PB cells, which have an improved seal design but no safety tube. Over 100 cycles have been accrued in this ongoing evaluation. A maximum capacity of 51.9 Ah (403 Wh) was obtained at a 15-A discharge rate (3 h) to a module IR-free cut-off voltage of 7.6 V (1.9 V/cell). A module resistance of 26.5 mohms was assumed in calculating the internal IR voltage drop, but a slightly higher resistance (≈ 28 mohms) is being measured at the end of discharge. Individual cell capacities remain matched as evidenced by uniform string currents ($2.5 \text{ A} \pm 6\%$) and cell voltages ($1.8 \text{ V} \pm 3\%$) at the end of discharge (15-A rate). The data in Figures 4-1 and 4-2 and the vehicle ranges listed in Table 4-2 are from discharges that used a module weight burden of 50%.

The second CSPL module exhibited a high resistance (coup-de-fouet effect) from 0 to 5% DOD after a full recharge. Module resistance was derived from measured variations in voltage and current during a driving profile discharge. The derived values of module resistance vs DOD level are plotted in Figure 4-3. The plot shows that the initial resistance is almost twice that measured at 15% DOD (23 mohms). At high initial discharge rates (>10 A), the resistance caused a large, temporary drop in module voltage to a value that could be less than the 100% DOD cut-off voltage level. With regenerative-braking currents, very high initial module charge voltages resulted. Our discharge termination al-

gorithm was modified to accommodate the large voltage drop, and a voltage clamp had to be installed to reduce the regenerative braking current and limit the module charge voltage during the coup-de-fouet.

conducted at the start and end of most discharges. The discharge rates during each scan ranged from 65 mA/cm² to 337 mA/cm². Occasionally, discharge was terminated by an unexpected low voltage. This was

Battery Evaluations at SNL

Flowing Electrolyte Battery Testing

Three flowing electrolyte battery units were tested electrically, chemically, and mechanically during 1988. A single aluminum/air cell (Eltech) and two zinc/bromine batteries (ERC) were evaluated. All three were placed on test in 1988, and one battery completed testing. Table 4-3 describes these units. Table 4-4 summarizes the test results.

Flow Battery Evaluation Procedures

A typical electrical cycle for the zinc/bromine batteries consisted of a timed, constant-current charge related to a theoretical zinc loading. After a 1-to-5-min open-circuit wait following charge, a constant-current discharge was imposed until the cell or battery voltage fell below a predetermined cut-off level, typically 1.0 or 1.2 V per cell. Periodically, it was necessary to discharge these units to the completely discharged condition (0 V). This was a maintenance requirement of the zinc flow technology. The frequency of this deep discharge depends on the cell design and varies from every cycle to every fifth cycle. The failure criteria for the zinc/bromine tests was less than 40% average energy efficiency for five consecutive cycles using baseline tests. Failure was also declared if the cell or battery became unserviceable because of leakage or component failures.

For the aluminum/air cell, a constant current discharge began immediately after the cell was charged by inserting an aluminum anode. Polarization scans were

Resistance of Na/S
8-V Module vs DOD

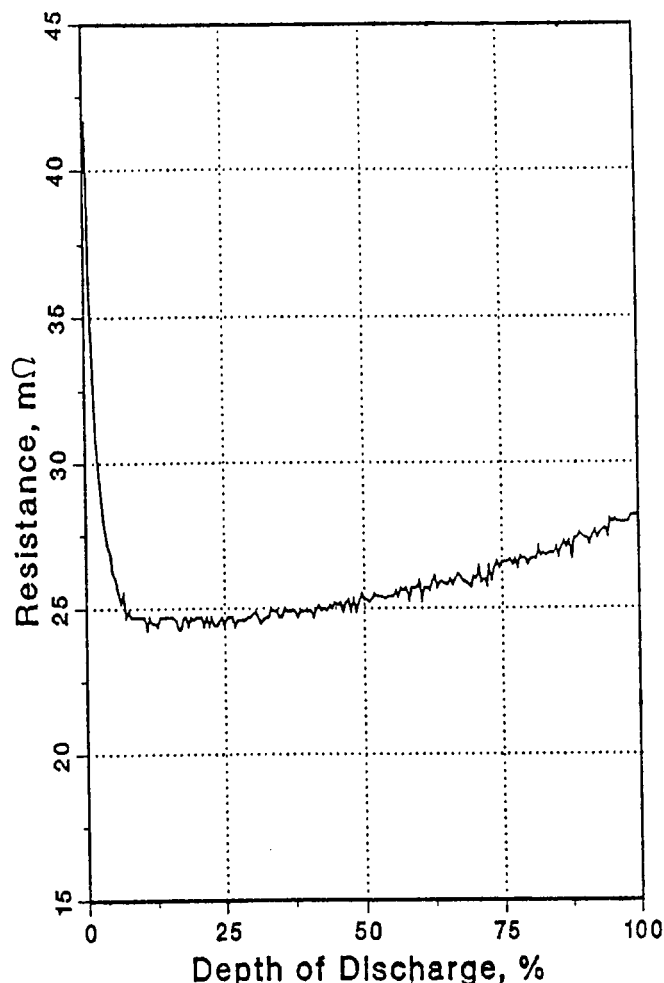


Figure 4-3. Internal Resistance of a 24-cell Sodium/Sulfur Module as a Function of DOD Level During a Driving Profile Discharge (J227aD/IETV-1)

Table 4-3. Flowing Electrolyte Cell and Batteries Tested at SNL in 1988

SNL ID No.	Type	Developer (ID No.)	Start/End Test Date	No. of Cells	Rated Capacity (Ah)	Weight (kg)
456	Zinc/Bromine	ERC (SNL-5-5D)	2-88/12-88	5	125 at C/3	200
459	Zinc/Bromine	ERC (SNL-30-ID)	2-88/—	5	125 at C/3	—
468	Aluminum/Air	Eltech (B-300)	6-88/—	1	600 at C/7	52

Table 4-4. Flowing Electrolyte Cell and Battery Data Summary, December 1988

Part I						
<u>SNL ID No.</u>	<u>Mean Coulombic Eff. %</u>	<u>Mean Voltaic Eff. %</u>	<u>Mean Energy Eff. %</u>	<u>Total No. of Cycles</u>	<u>No. of Cycles in 1988</u>	<u>Status</u>
456	86 ± 2	70 ± 1	61 ± 2	100	100	Failed
459	73 ± 3	71 ± 1	52 ± 3	66	66	On Test

Part II						
<u>SNL ID No.</u>	<u>Mean Al Elect. Eff. %</u>	<u>Al Energy Output (Wh/g)</u>	<u>Mean Al Util. %</u>	<u>Total No. of Runs</u>	<u>No. of Runs in 1988</u>	<u>Status</u>
468	76 ± 8	2.61 ± 0.2	47 ± 9	48	48	On Test

Part I Notes
 Uncertainties are expressed as 95% confidence limits.
 See Table 4-3 for battery identification.

Part II Notes
 Uncertainties are expressed as standard deviations.
 See Table 4-3 for battery identification.

caused by air leaks, cathode degradation, or high resistance in the anode current collector.

The measured parameters of all of these tests included cell or battery voltages, currents, temperatures, electrolyte conductivity, and electrolyte pressures or flow rates. Several parameters were calculated from these data, including amp-hours and watt-hours in and out of the battery, and coulombic, voltaic, and energy efficiencies for each charge/discharge cycle of the zinc/bromine batteries. All the efficiencies in this report are electrochemical only and do not account for power consumed by auxiliary devices. For the aluminum/air cell, discharge amp-hours and watt-hours were calculated, as were several parameters relating the discharge energy to the aluminum anode weight loss during the test run.

ERC Zinc/Bromine 5-Cell Battery (SNL ID 456)

One 5-cell ERC zinc/bromine battery was evaluated during 1988. It used the same improved electrolyte flow system as an ERC battery (ID 448) tested and reported on last year. It consisted of two pumps, in-line electrolyte filters, bromine mixing in the catholyte reservoir, and an electrolyte level sensor in the zinc

electrolyte reservoir. The cell stack clamping hardware was also modified to distribute compressive forces more evenly and to reduce the possibility of leaks. Battery electrolyte was supplied by ERC and was the baseline (H) solution. The cell stack design and materials were identical to previously tested ERC batteries with 872-cm² electrodes, except for improved structural supports on each end electrode.

The initial cycles were run at charge and discharge rates of 34 mA/cm² and 137 mAh/cm² of zinc loading on charge. After cycle 9, the charge and discharge currents were increased to 43 mA/cm², and the zinc loading on charge was increased to the design level of 170 mAh/cm². The end-of-discharge cut-off voltage was 6.0 V until cycle 57, when it was reduced to 4.0 V. Charge and discharge rates and zinc loading on charge were also reduced to 34 mA/cm² and 137 mAh/cm², respectively, from cycle 57 until the end of the test.

The battery operated for 100 cycles at SNL. Efficiency performance is plotted in Figure 4-4. Battery performance began at expected levels. The slight drop in voltaic efficiency at cycle 10 was because of the increase in charge and discharge rates described above. The inconsistency in coulombic efficiency between cycles 40 and 53 was because of the self-discharge rate

tests discussed below. Following a 48-hour charged stand test at cycle 53, subsequent baseline cycles exhibited reduced and inconsistent coulombic and voltaic performance. ERC recommended that the severity of the testing regime be reduced, and the changes described above at cycle 57 were implemented.

A transition period occurred between cycles 57 and 70, and then performance stabilized at reduced levels. At cycle 98, however, performance again dropped substantially. ERC suggested that the anolyte be replaced with a slightly different solution. Because of the possibility of precipitation of potassium salts from the original electrolyte, the replacement anolyte had a reduced potassium concentration. The last cycle was run after the new anolyte had been circulated in the

battery system for several days. Performance during the last cycle did not improve because of the electrolyte replacement: coulombic efficiency, 57%; voltaic efficiency, 45%; and energy efficiency, 25%; voltaic efficiency decreased about 9% compared to the previous cycle.

Polarization tests were run between cycles 23 and 28 to determine battery resistance. Over a range of 100 to 33% state-of-charge, battery resistance was relatively invariable and ranged from 30 to 33 mohms, respectively.

The self-discharge rate of the battery with the electrolyte pumps running was measured between cycles 31 and 43. The maximum open-circuit stand time

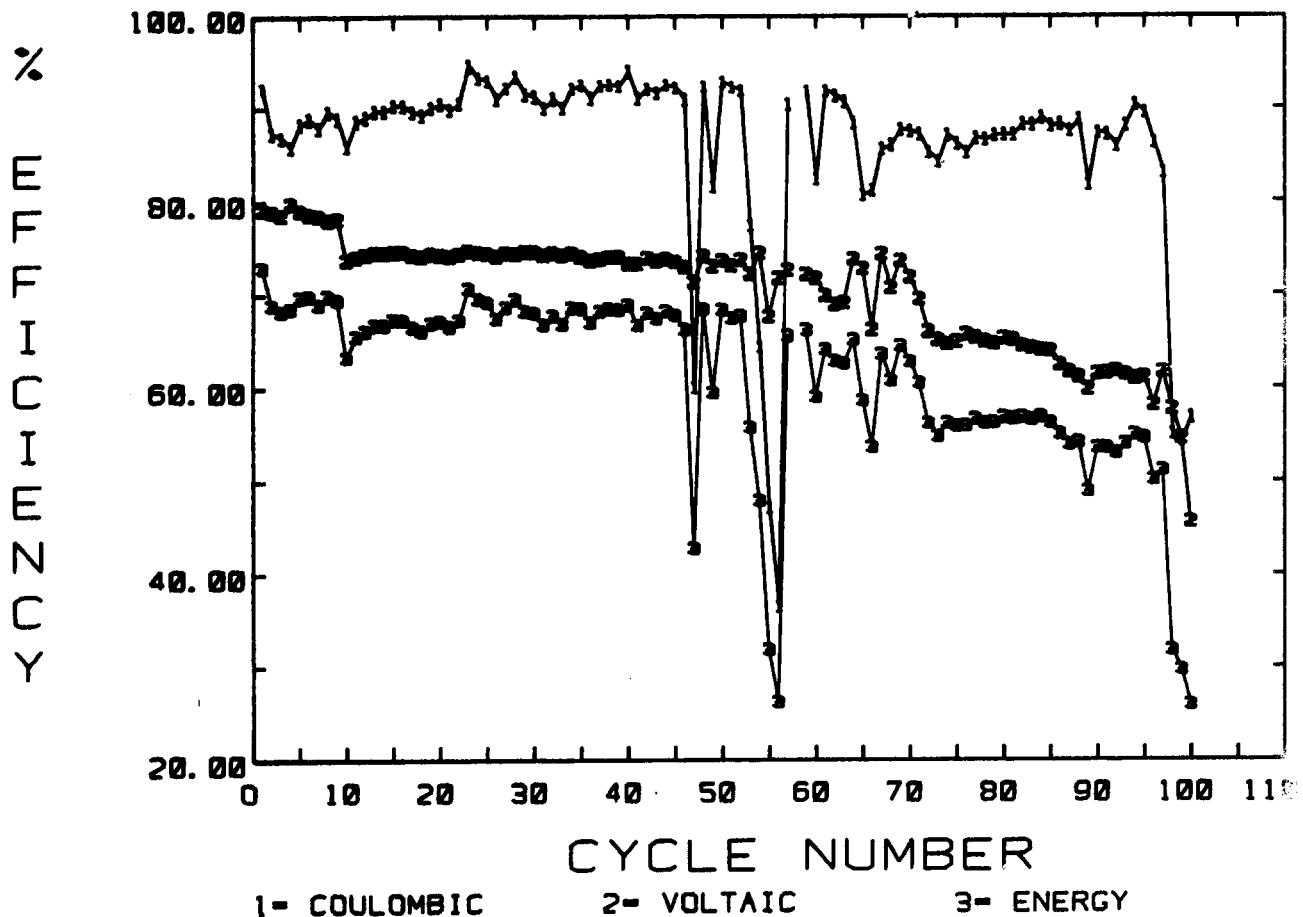


Figure 4-4. Efficiency Performance of ERC Zinc/Bromine Battery 456 at SNL

was 1 h, and self-discharge was not significant (less than 2% of the discharge capacity). Between cycles 47 and 53, self-discharge tests were run with the pumps off for periods of 24 and 48 h. The effect on capacity was significant with losses of 12 and 16%, respectively.

Electrolyte pH was maintained below 3.0 by the addition of hydrobromic acid. Approximately 5 ml of acid were added per cycle to maintain the desired pH between cycles 45 and 63. Between cycles 78 and 98, the battery required an average of 9.5 ml per cycle to maintain pH. This suggests that the performance reduction (possibly caused by reduced electrolyte flow) increased the rate of hydrogen evolution at the anodes and therefore increased the rate of pH increase.

Testing was terminated after the rapid drop in efficiencies observed at cycle 98. The cell stack was disassembled early in 1989; it is reported here for completeness. The battery had been left on open circuit after a complete discharge for several days before the tear-down. Its voltage, with the pumps off, was -1.0 V. Disassembly began at the positive (bromine) electrode end of the stack.

The separator between the bromine end electrode and the facing zinc electrode was dry and brittle and broke into two pieces when removed from the cell. Part of the separator had melted to the felt of the bromine end electrode. See Figure 4-5. Both sides of the separator were covered with salt deposits. The zinc side of the first bipolar electrode was covered with a white salt over about 70% of its area. All exposed electrolyte flow channels and holes were examined and no foreign materials were found. Close examination revealed a hairline crack along the length of the bromine end-electrode flow frame near the electrode. The crack went through the flow frame. It was similar to cracks observed in earlier ERC deliverables. The normally dry area behind the end electrode was completely wet with electrolyte because of this crack. The Hypalon gasket at the blind end of one of the zinc electrolyte manifolds was slightly deformed and raised, and may have blocked some flow channels.

The remaining electrodes and separators in the battery were examined, one by one. All appeared normal: no salts were present, and there was no evidence of residual zinc or bromine. There were no obstructions in any of the flow channels or manifold holes.

The zinc end electrode was in good condition. The end gasket (Hypalon) in the vicinity of the blind end of each bromine-electrolyte manifold was deformed and degraded. In each location, the gasket material had

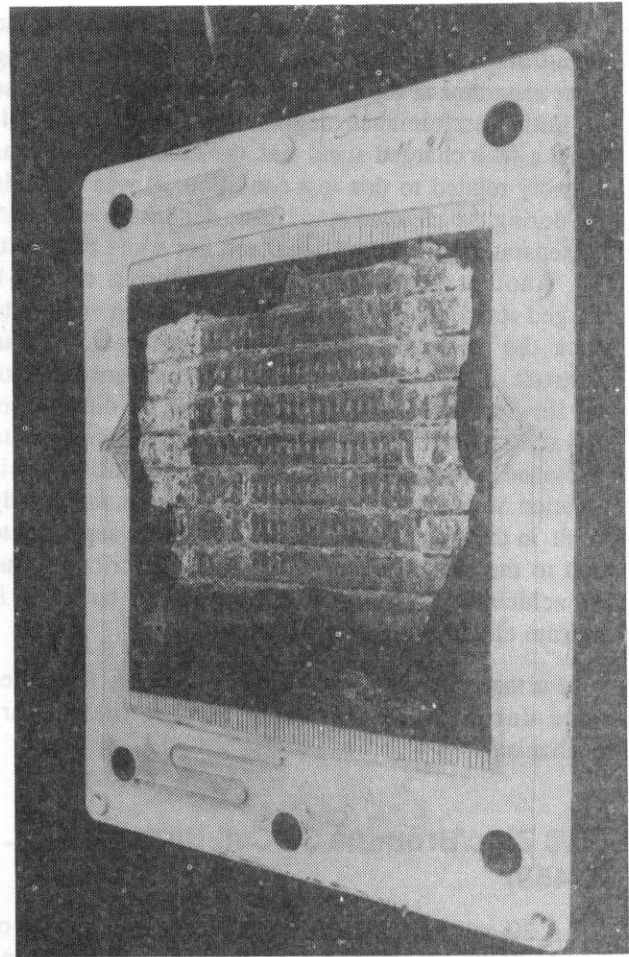


Figure 4-5. Bromine End Electrode of ERC Zinc/Bromine Battery 456. Note the broken piece of separator (covered with white salts) on the felt electrode. The bromine electrolyte inlet manifold is at the bottom left; the outlet at the top left. The blind ends of the zinc electrolyte manifolds are at the right. The deformed Hypalon gasket may be seen under the manifold hole at the top right. The crack in the electrode is not visible, but was located at the top of the electrode, in the groove between the parallel flow dispersing slots and the start of the single curved channel that leads to the manifold.

“bubbled” out into the manifold. It may have obstructed some flow channels. Also, in each case, the degraded areas had allowed brominated electrolyte to seep through the gasket and contact the PVC of the zinc end block. The dry felt and titanium current collector were

not contacted by electrolyte, based on visual observations.

In summary, there was no obvious cause for the nonuniform current distribution that led to the melting of the separator at the bromine end electrode. Because the initial performance degradation immediately followed a 48-h charged stand test, the nonuniformity was probably related to this test condition. It was possible that during the charged stand, zinc dendrites penetrated the separator and caused localized hot spots and melting. Another possibility was that during the 48-h charged stand, the Hypalon gasket deformed enough to block the flow channel leading to the bromine end electrode. This would also lead to nonuniform electrolyte flow and hot spots on the separator. In either case, with subsequent cycles, the localized melted areas led to increased nonuniform electrolyte distribution. This situation would tend to make itself worse and finally result in the general heating that caused the separator to melt to the electrode felt. Therefore, the critical issue for achieving long life in zinc/bromine batteries is uniform electrolyte flow distribution.

Further analyses will be performed on the failed parts during 1989 to define further this failure mechanism.

ERC Zinc/Bromine 30-Cell Battery (SNL ID 459)

A 30-cell ERC zinc/bromine battery was placed on test in 1988. It consisted of two electrolyte pumps, in-line electrolyte filters, bromine mixing baffles in the catholyte reservoir, and an electrolyte level sensor in the zinc electrolyte reservoir. Cell construction, most battery hardware, and the electrolyte were the same as described above for battery 456. The level sensor was connected to an anolyte pump controller that by changing the pump speed, automatically balanced electrolyte cross-over from one reservoir to another. This was a significant improvement compared to the manual flow adjustments required to balance the reservoir levels on other ERC batteries. However, the amount of headspace in the catholyte reservoir was limited, and minor electrolyte level variations significantly affected battery operation. It was necessary to maintain the proper level in this reservoir to avoid either overflowing of the reservoir or sucking of air into the catholyte flow system. The automatic pump control system worked well in this application, as long as a minimum catholyte level was maintained such that air would not be drawn into the catholyte pump intake.

A total of 66 cycles was run on the battery at SNL; it was still on test at the end of 1988. Figure 4-6 illustrates the efficiency performance during these tests. Initial performance was comparable to the expected levels, but the efficiencies became inconsistent late in 1988 and began to decrease.

Charge and discharge current densities during these tests varied from 34 mA/cm² to 43 mA/cm². Charge zinc loading ranged from 10 to 170 mAh/cm². Most cycles were run with zinc loadings on charge of 57 mAh/cm². Charge amp-hours were inconsistent because charging was terminated when the battery voltage exceeded 65 V, an upper limit specified by ERC.

Figure 4-7 illustrates battery voltage for three cycles. Cycle 5 was run early in life at charge and discharge rates of 34 mA/cm². Cycles 65 and 66 were run at the end of 1988 at 29 mA/cm². While the early cycles demonstrated expected voltage levels, the end-of-charge voltage rose steadily during the initial cycles until it began reaching the limit recommended by ERC at about cycle 25. Typical charge voltage performance is illustrated by cycle 65. Discharge voltage gradually degraded from the nominal performance exhibited by cycle 5 until the continuously decreasing voltage of cycle 65 was typical.

ERC suggested that the high end-of-charge voltage might be because of insufficient zinc ion in solution. Before the end-of-charge during cycle 54, one liter of a concentrated zinc solution was added to the anolyte reservoir. No noticeable effect was observed on end-of-charge voltage.

Between cycles 58 and 62, the end-of-charge concentration of zinc was analyzed for both anolyte and catholyte. The test cycle consisted of a 57 mAh/cm² charge; the end-of-charge voltage was near or at the high limit. The end-of-charge chemical analyses determined that the anolyte zinc ion concentration was about 1.75 molar while the catholyte concentration was about 2.0 molar. These values indicated that the high charge voltages were not caused by low zinc concentration.

Prior to cycle 66, the anolyte was replaced with a low-potassium formulation supplied by ERC. Certain data had suggested that potassium salts might precipitate out of solution at normal battery operating temperatures. The lower potassium concentration in the replacement anolyte reduced the likelihood of solids precipitation. As shown in Figure 4-7, voltage performance did not improve during cycle 66.

The battery required large volumes of acid to maintain the electrolyte pH below 3.0, and the volumes

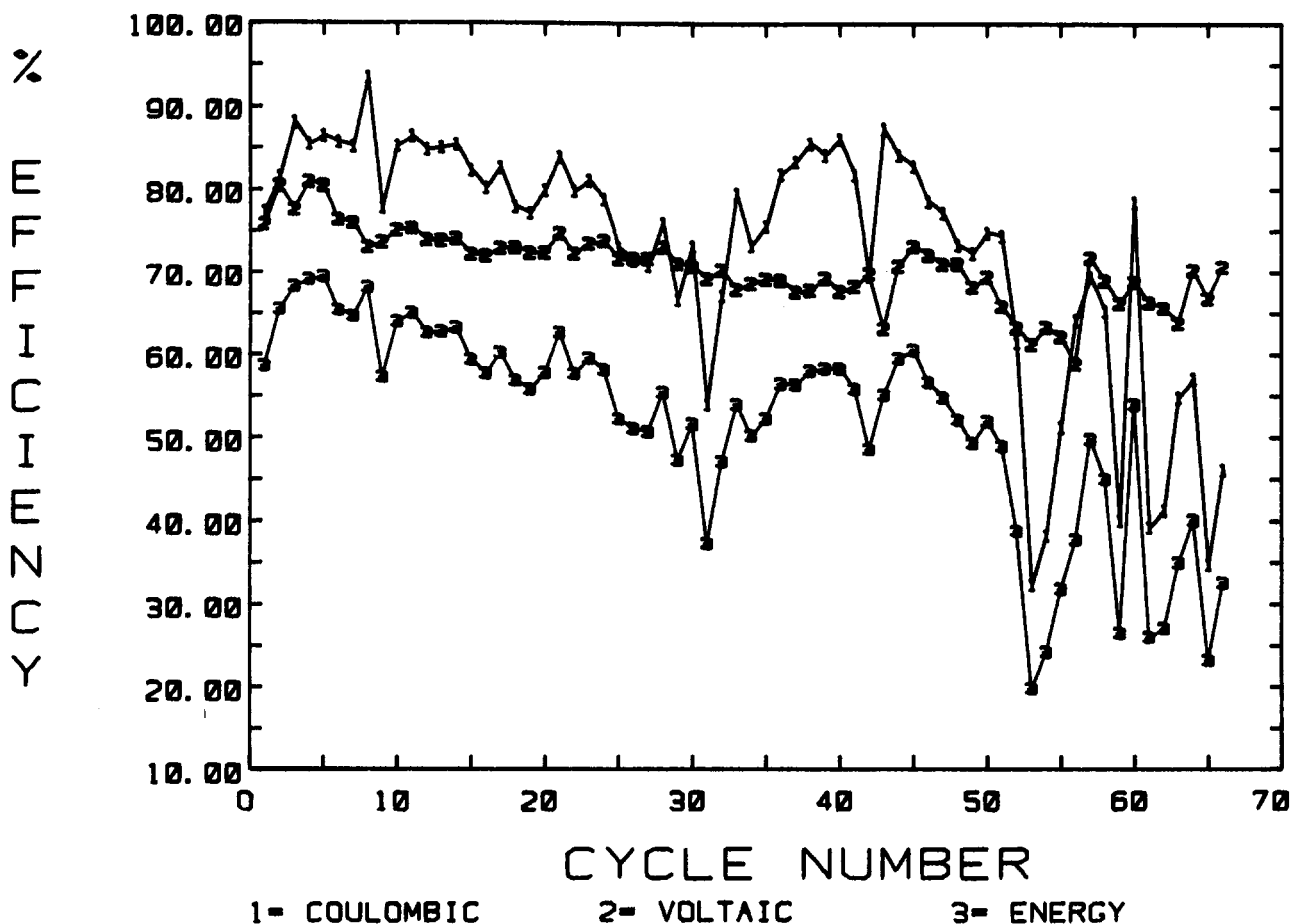


Figure 4-6. Efficiency Performance of ERC Zinc/Bromine Battery 459

increased as the battery aged. Before cycle 60, hydrobromic acid was added to the electrolyte to adjust the pH. At ERC's suggestion, after cycle 60, hydrochloric acid was used instead. From cycle 60 to 66, a total of 1,635 ml of hydrochloric acid was added to the battery to maintain the electrolyte pH below 3.0. This amounted to 272.5 ml per cycle, up from about 80 ml per cycle for cycles 23 to 35.

The evaluation will continue in 1989. Performance will be closely monitored in an attempt to determine the cause of the deteriorating performance.

Eltech Aluminum/Air Cell (SNL ID 468)

An Eltech aluminum/air cell was installed at Sandia during the week of June 20, 1988. A picture of the cell and its associated equipment is shown in Figure 4-8. Not shown is the carbon dioxide scrubbing column for

the air input stream. The unit consisted of a B-300 cell stack, one replaceable 99.995% pure aluminum anode (300 cm²), one electrolyte reservoir, one pump, a carbon dioxide scrubber, and associated plumbing and sensors. The cell stack weighed 6.9 kg dry, with an anode installed. Solids separation equipment was not included.

When fully charged with aluminum (≈ 350 g), the cell had a theoretical capacity of about 1,040 Ah. Approximately 600 Ah were routinely discharged using these anodes. Most tests were run at 175 mA/cm², with periodic polarization scans ranging from 64 to 337 mA/cm². The initial electrolyte concentration was 5 M KOH, with no dissolved aluminum. Approximately 36 liters of electrolyte (density 1.2 g/ml) were used. All tests were run with an electrolyte flow rate of 1.5 liters per minute and an air flow of four times the stoichiometric requirement. The cathode air backpressure was ≈ 24 inches of water.

ERC ZINC/BROMINE BATTERY 459

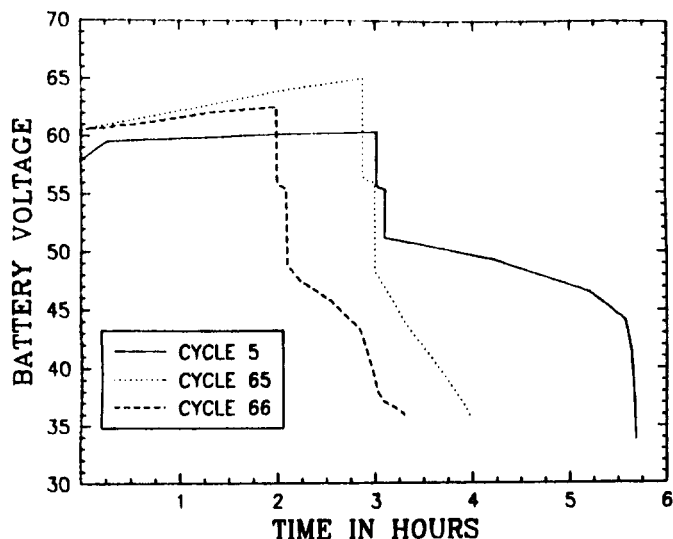


Figure 4-7. Voltage vs Time for ERC Zinc/Bromine Battery 459, Cycles 5, 65, and 66. Cycle 5 was run at 34 mA/cm² (charge and discharge rates); cycles 65 and 66 were run at 29 mA/cm² (charge and discharge rates).

During 1988, the aluminum/air cell was run a total of 48 times using 24 anodes for an elapsed run-time of 232 h. Recharge was accomplished mechanically using simple tools, in a short period of time, by removing the depleted anode and inserting a new one. The tests are summarized in Table 4-5.

The aluminum electrode efficiency varied from 70 to 90%, while the corrosion rate ranged from 20 to 80 mA/cm². Anode variability was the likely cause of the large range in corrosion rate. Aluminum energy output was consistent at about 2.6 Wh/g.

Anode utilization was limited to a maximum of about 57%. A reason for this limitation was the necessity of having at least 75 g of aluminum present in the cell at the end of a test to remove the spent anode. Smaller pieces were very difficult to pull out of the cell using the intended tools. Thus, a sizeable quantity of each anode was not utilized.

A total of 5,048 g of aluminum was dissolved in the electrolyte by the end of this year. Precipitates (hydrargillite, Al(OH)₃) were first observed while anode 10 was in the cell, after 1,770 g of aluminum had dissolved. The aluminum concentration in the electrolyte was about 1.8 molar when the precipitates began to form. The cell was operated with the solids present with

no noticeable effect on performance. The maximum weight percent of solids in electrolyte was about 2.6% during these tests. Solids did accumulate inside the cell body and in some of the electrolyte tubing. To avoid this, the plumbing was modified so that electrolyte was drawn into the pump from the middle of the reservoir instead of at the bottom. Then, when the cell was operated, the precipitates spontaneously settled out of the solution. The weight percent of solids in the electrolyte was ≈0.02% under steady-state conditions.

These results indicated that solids separation may require relatively simple equipment such as a baffle inside the electrolyte reservoir. After several runs, the precipitates were removed from the bottom of the reservoir and found to be a solid mass. Hydrargillite had compacted during the settling process and had to be scraped from the reservoir. Thus, the solids may be removed from a working battery in a single, solid piece.

A special test was run to determine the self-discharge rate of the anode. Following a normal test run, the anode was left in the cell overnight with the electrolyte pump off. About 2 g of anode reacted overnight, or about 1%. A related test was run in the same way except that deionized water was pumped through the cell before the overnight stand. In this case, the anode weight loss was about 1 g, or half the loss without a water rinse. The self-discharge rate appears to be low for this technology and can be reduced significantly using simple techniques.

The air cathode was replaced seven times during these tests. Each cathode degraded in performance at a different rate. Representative reference electrode data during polarization scans are illustrated in Figure 4-9. The air electrode voltage dropped noticeably during most tests. Variability in the aluminum electrode voltage may be caused by an increase in the anode/cathode gap that occurred during anode dissolution.

Another possible cause of voltage loss may have been the current-collector mechanism on the anode. Nickel foil was glued to the back of each anode. The foil was used to prevent corrosion and high resistance of the current-collector side of the anode. However, as the anode reacted, the adhesive between the foil and the anode loosened and corrosion of the back of the anode did occur. Once corrosion affected the entire back, the resistance of the anode increased, and the cell voltage dropped.

While the cell and associated hardware generally operated well, several mechanical problems were identified:

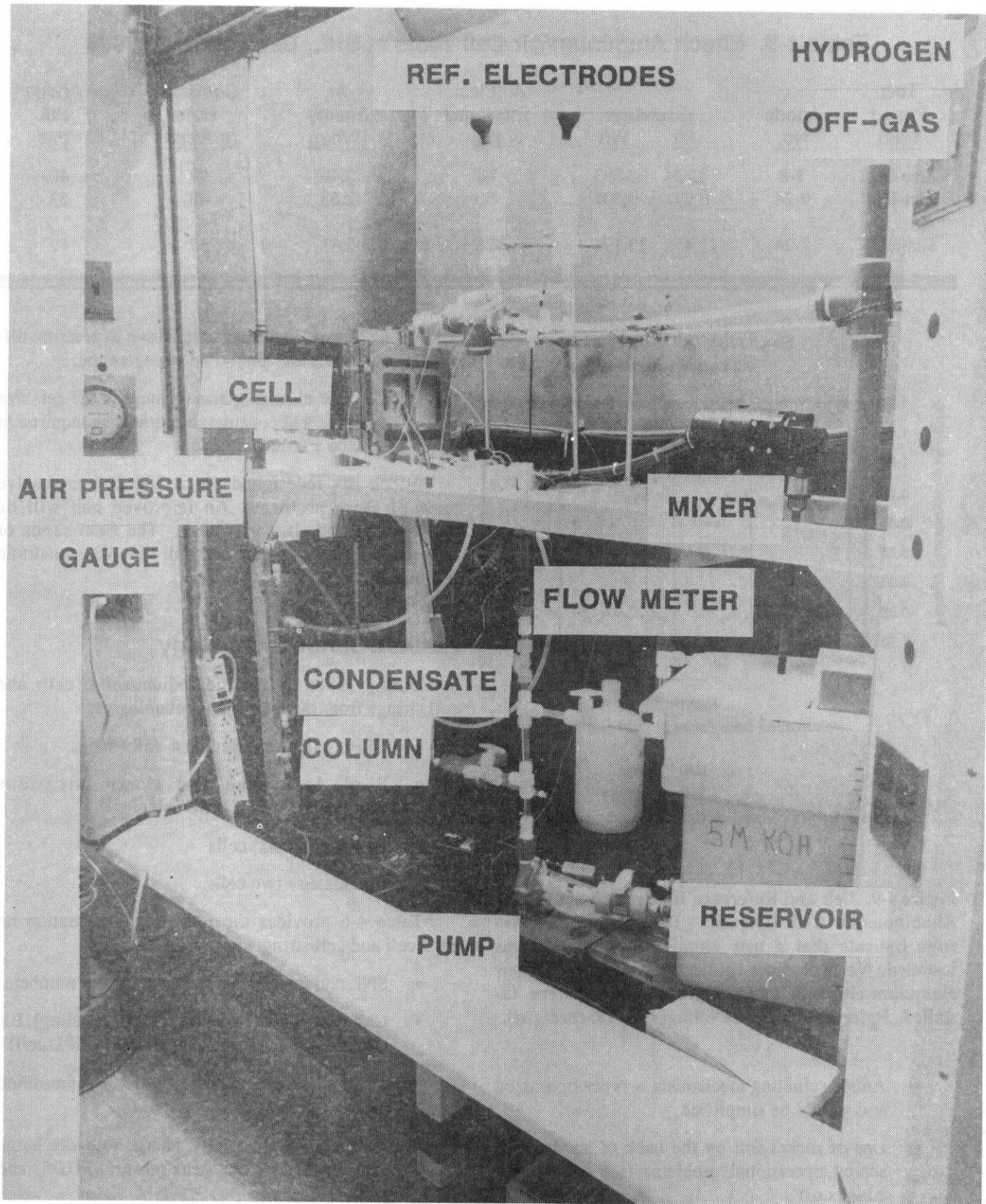


Figure 4-8. Picture of the Eltech Aluminum/Air Single Cell (SNL ID 468 on Test at SNL)

Table 4-5. Eltech Aluminum/Air Cell Tests at SNL, December 31, 1988

Test Period 1988	Anode No.	Discharge Ah	Discharge Wh	Al Elect. Efficiency (%)	Al Energy (Wh/g)	Corrosion Rate (mA/cm ²)	Anode Util. (%)
June-Sept	1-8	3,234	3,893	68	2.46	77	40
Oct-Dec	9-24	8,221	9,301	80	2.68	48	53
Summary	1-24	11,455	13,194	76	2.61	57	47

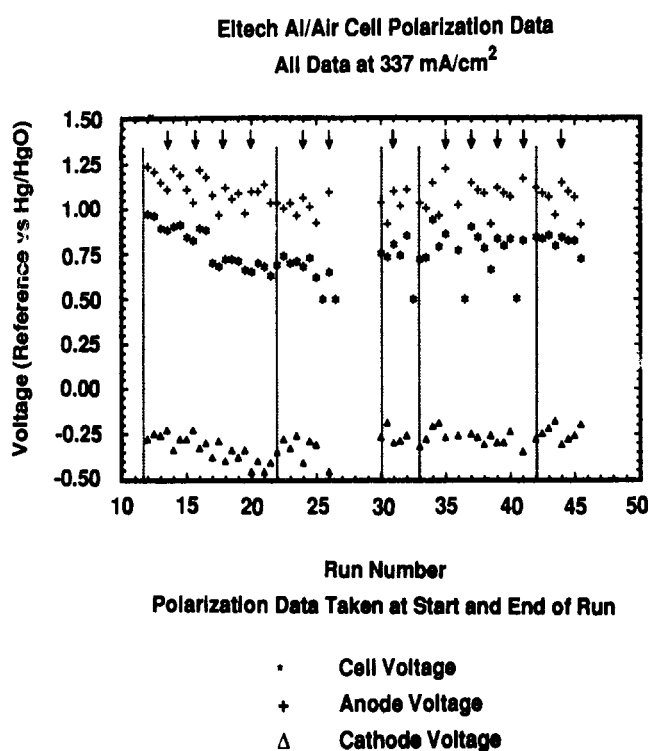


Figure 4-9. Cell and Reference Electrode Voltages for Aluminum/Air Cell (October - December 1988). Arrows indicate that a new aluminum electrode was installed. Vertical lines indicate that both a new aluminum electrode and a new air electrode were installed. Reference electrode voltages not IR-corrected.

- Anode refueling mechanism was not optimized and should be simplified.
- Use of nickel foil on the back of anodes presented operational problems (see above) and added cost.
- Several gaskets developed leaks during the experiments and had to be replaced.

- Cathode structure was sensitive to pressure differentials and should be strengthened.
- Cathode mounting arrangement in the cell was complex and considerable time was required to replace a failed cathode.

Eltech has redesigned the B-300 cell to resolve most of these problems. An improved cell will be delivered to SNL in early 1989. The final series of experiments on the present cell will involve a quadratic test matrix.

Sodium/Sulfur Technology

During 1988, SNL tested sodium/sulfur cells and cell strings from the following technologies:

- CSPL - 10 cells and two 4-cell strings
- Ford Aerospace and Communications Company (FACC) - two cells
- Powerplex - six cells
- Ceramatec - two cells.

Table 4-6 provides the following information on each cell and cell string:

- SNL and manufacturer identification numbers
- Cell type, which can be LL (load-leveling), EV (electric vehicle), or PB (standard CSPL cell)
- Total charge/discharge cycles accumulated during standard capacity testing
- Test regimes (capacity, charge rate, discharge rate, constant power, peak power, SFUDS, and parametric)
- Capacity at the end of 1988, which is expressed as a percent of initial capacity and is measured

Table 4-6. Sodium/Sulfur Cells and Cell Strings Tested at SNL in 1988

SNL ID No.	Mfr. ID No.	Type	Capacity (Ah) Rated	Initial	Accumulated Cycles	Test Regimes	Present Capacity (% of initial)
(a) CSPL Cells¹							
437 ²	7503	PB	8.8	8.7	1,564	Cap/SFUDS/Peak Power	40.0
438 ²	7435	PB	8.8	8.8	800	Cap/Par/SFUDS	80.0
464	P1874-1	PB	8.5	8.0	258	Chg Rate/Cap/SFUDS/ Const Power/Peak Power	99.0
465	P1877-8	PB	8.5	8.0	281	Chg Rate/Cap	101.0
469	P1969-9	PB	8.6	8.0	163	Chg, Dischg Rate/Cap	104.0
470	P1970-8	PB	8.58	8.1	170	Chg, Dischg Rate/Cap	96.0
471	P1970-7	PB	8.64	8.0	162	Chg, Dischg Rate/Cap	98.0
472	P1970-4	PB	8.51	7.6	165	Chg, Dischg Rate/Cap	101.0
475	P1970-3	PB	8.61	8.0	100	Chg Rate/Cap ³	99.0
476	P1969-6	PB	8.61	7.9	49	Cap ⁴	99.0
(b) CSPL 4-Cell Strings⁵							
473	1179	PB	8.77	8.1	104	Chg Rate/Cap	98.0
474	1181	PB	8.72	8.1	74	Chg Rate/Cap	99.0
(c) FACC Cells⁶							
3902	LL972	LL	155.0	157	967	Cap	69.0 ⁷
4072	VBO07	EV	55.0	60	520	Cap/Const Power	85.0 ⁷
4102	VBO03	EV	55.0	60	423	Cap	104.0 ⁷
(d) Powerplex Cells⁸							
4522	P-091-040	EV	38.0	38/35.4	95	Cap/Par	45.0
4532	P-090-015	EV	38.0	37/33.4	93	Cap/Par	80.0
4572	P-090-001	EV	38.0	33/31.3	372	Cap/Par	101.0 ⁷
4602	P-090-018	EV	38.0	36.1/33.2	381	Cap	99.0 ⁷
462	P-111-629	EV	38.5	36.0/31.0	340	Chg Rate	98.0
4632	P-111-656	EV	38.8	35.9/32.5	290	Chg Rate/Cap	97.0 ⁷
(e) Ceramatec Cells⁹							
454 ¹⁰	2582	EV	36.0	36.5	501	Chg, Dischg Rate/Cap/ Const Power	99.0
455 ¹⁰	2536	EV	36.0	35.3	513	Chg, Dischg Rate/Cap/ Const Power	96.0

- 1 CSPL cell rated and initial capacity: C/3 to 1.9 VOC at 350°C (discharge); 2.5 A to 2.4 V (charge).
- 2 Removed from test.
- 3 Deep DOD test performed (1.75 VOC at end of discharge, cycle 73).
- 4 Higher charge voltage test performed (2.6 V for cycles 32 through 36).
- 5 CSPL string rated and initial capacity: C/3 to 7.6 V (discharge); 2 A to 9.6 V (charge).
- 6 FACC rated and initial capacity: C/5 (LL) or C/3 (EV) to 1.9 VOC at 350°C (discharge).
- 7 Capacity prior to failure.
- 8 Powerplex rated capacity: C/8 to 1.8 VOC at 350°C (discharge and charge); Powerplex initial capacity: first value C/8 to 1.8 VOC (discharge and charge); second value C/2.4 to 1.8 VOC at 350°C (discharge).
- 9 Ceramatec rated and initial capacities: C/2 to 1.9 VOC at 350°C (discharge).
- 10 Experienced a F/T cycle.

at the same charge/discharge rate at which the initial capacity was determined.

The 1988 SNL evaluations on the sodium/sulfur technology are summarized in Table 4-7 and discussed below.

Table 4-7. Summary of Sodium/Sulfur Testing at SNL

CSPL Technology

MkIIa Cells

- Cell 437 Sulfur seal failure after 1,564 cycles following SFUDS and peak-power tests.
- Cell 438 Sulfur seal failure at 770 cycles following SFUDS tests.

MkIII Cells and Cell Strings

No cell failures to date on these eight cells and two 4-cell strings; accumulated cycles range from 49 to 281.

Charge-Rate Tests

Low charge acceptance at the standard (C/3.5) charge rate. Characterization testing showed an 18% loss in capacity when the charge current was varied from C/8 to C/3 rate.

Discharge-Rate Tests

Decreasing capacity as discharge rate is increased.

Four-Cell Strings

Two four-cell strings placed on test in late 1988.

FACC Technology

- Cell 390 Removed from test after completing 520 cycles; 69% of initial capacity remaining.
- Cell 407 Corrosion problems with current leads fixed; testing suspended at 520 cycles after constant-power tests did not succeed.
- Cell 410 Removed from test after completing 423 cycles. Could not continue testing because of increased internal cell resistance.

Powerplex Technology

Charging/discharging at standard rates lowered capacity of all Powerplex cells tested by SNL.

- Cells 452 and 453 Cell 452 failed after 95 cycles; polysulfides released near the top of the cell. Cells 452 and 453 returned to Powerplex.
 - Cell 457 Failed after 371 cycles.
 - Cell 460 Failed at 381 cycles after completing an unscheduled F/T cycle.
 - Cells 462 and 463 Cell 462 performing well after 340 cycles completed; charge-rate tests show a 10% loss in capacity when the charge current was varied from the C/8 to C/3 rate. Cell 463 completed 290 cycles before failing. Discharge-rate testing had little effect on the capacity of cell 463, larger effect on the capacity of cell 462.
-
-

Table 4-7. Summary of Sodium/Sulfur Testing at SNL (Continued)

Ceramatec Technology

Cells 454 and 455 show excellent performance: capacity exceeds 96% after accumulating over 500 cycles.

Parametric Tests

Capacity increased with temperature, and charge rate had little effect on cell capacity.

Charge-Rate Tests

Capacity loss of 6% when the charge current was varied from C/8 to C/3 rate.

Discharge-Rate Tests

Drop in capacity at C/1 rate attributed to the high end-of-discharge cutoff voltage and increased temperature caused by higher discharge rate.

Specific Energy vs Specific Power

141 Wh/kg at 9.6 W/kg; 116 Wh/kg at 46.8 W/g.

CSPL Technology

During 1988, SNL evaluated CSPL PB cells with two types of electrode seals

- MkIIa direct metal-to-ceramic bonded seal
- MkIII seal (direct metal-bonded sodium-electrode closure and a sulfur-electrode closure that employs chromized mild steel and an aluminum interstrate).

None of the MkIII cells tested during 1988 featured totally enclosed safety containment of the sodium electrode, which CSPL has recently developed.

MkIIa Cells

SNL completed tests on two CSPL PB cells with the MkIIa seal: cells 437 and 438. As with many of the CSPL cells tested in 1987 (*ETD Annual Report for 1987*, pp. 115-119), SNL identified the electrode seal as the probable cause of failure in cells 437 and 438.

Cell 437. This cell completed 439 charge/discharge cycles during 1988, bringing the total number of cycles on the cell to 1,564. In addition to capacity cycles, the cell also underwent SFUDS and peak-power tests after 1,343 cycles were completed. Before the power tests, the cell's capacity was ≈ 7 Ah, 80% of the

initial capacity of 8.7 Ah. However, the capacity dropped to less than 5 Ah after the SFUDS and peak-power tests. When the cell was removed from test, its capacity had decreased to 3.5 Ah. Upon examination, it appeared that the sulfur seal was starting to fail.

Cell 438. After accumulating 770 charge/discharge cycles and completing several SFUDS tests, this cell self-discharged while on open-circuit. Upon examination, it appeared that the sulfur seal had just started to fail. X-rays did not reveal any electrolyte fractures.

MkIII Cells and Cell Strings

SNL initiated evaluations on eight PB cells and two strings each consisting of four series-connected PB cells: cells 464, 465, 469, 470, 471, 472, 475, and 476; strings 473 and 474. All 14 cells have the MkIII seal, but none feature the recently developed total enclosure of the electrode. By the end of the year, none of the cells had failed. Accumulated cycles ranged from 49 for cell 476 to 281 for cell 464 (Table 4-6).

Testing showed, however, that these cells must be charged at lower rates than previous CSPL cells to attain full capacity. During 1988, SNL thoroughly characterized the discharge-rate performance of these cells and began evaluating the 4-cell strings.

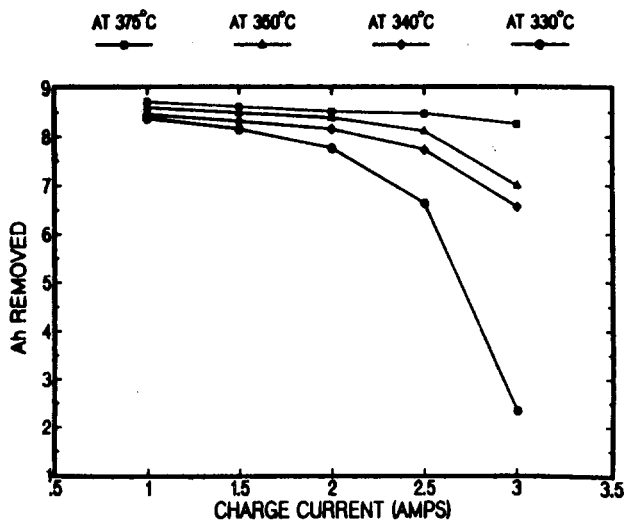


Figure 4-10. CSPL Average Capacity vs Charge Rate and Temperature—Cell 469

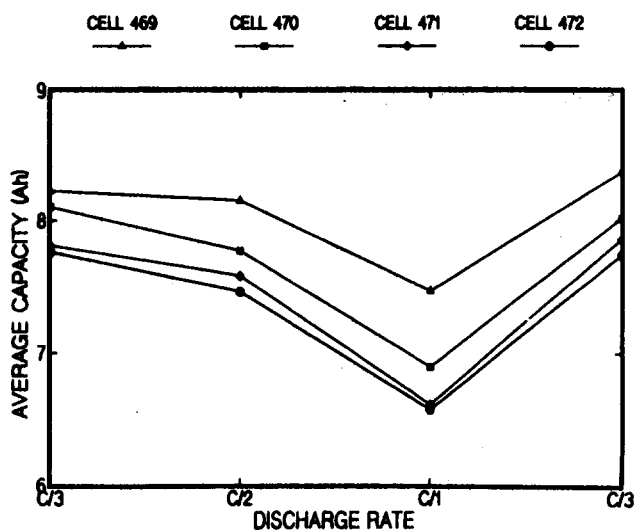


Figure 4-11. CSPL Average Capacity vs Discharge Rate and Temperature—Cells 469, 470, 471, and 472

Charge-Rate Tests. The MkIII cells underwent a series of tests in which the charge current was varied from 1 A (C/8 rate) to 3 A (C/3 rate) in 0.5-A steps, and the cell temperature varied from 330 to 375°C at each charge rate.

The performance of cell 469 represents the charge acceptance phenomenon observed in all the MkIII cells on test at SNL (Figure 4-10). Cell capacity diminished with increasing charge rate, especially at lower temperatures. At 350°C (the standard operating temperature for sodium/sulfur cells), there was an 18% loss in capacity when the charge current varied from 1.0 A to 3.0 A. For

the most part, the greatest capacity losses occurred at charge rates above 2.5 A.

SNL performed a deep depth-of-discharge cycle (discharge to 1.75 V open circuit) on cell 475 to correct its slow charge acceptance. Though SAIC had success with this procedure, the SNL deep discharge did not increase in cell capacity. SNL is planning additional tests in 1989.

Discharge-Rate Tests. Figure 4-11 shows test results on average capacity versus discharge rate for cells 469, 470, 471, and 472. The tests were run at C/3 rate (3 A), C/2 rate (4.5 A), and C/1 rate (9 A) to an end-of-discharge open-circuit voltage of 1.9 V. A final test was run at the C/3 rate to ensure that the capacities returned to their original (C/3-rate) values. The capacity profiles for these cells show that capacity decreased as discharge rate increased. All cells lost ≈1 Ah of capacity at the C/1 rate.

Four-Cell Strings. Break-in cycles were performed on two series-connected 4-cell strings: strings 473 and 474.

The operating values for both strings were

- End-of-discharge cell resistance - ≈ 150 mohms
- End-of-discharge voltage - 9.6 VOC (2.4 V/cell)
- Initial string capacity - 8.1 Ah (below the 8.7-Ah rated capacity).

FACC Technology

During 1988, SNL finished testing three FACC cells: cell 390 (an LL cell with 160-Ah nominal capacity) and cells 407 and 410 (EV cells with 60-Ah nominal capacities). Evaluations, which had been suspended in June 1987 because of a change in testing equipment, resumed in May 1988. Both cells were maintained at operating temperature while testing was suspended.

Cell 390. When this LL cell was placed back on test, it appeared to be operating well. However, capacity decreased gradually after the cell experienced an unscheduled F/T cycle. After completing 967 cycles, capacity had decreased to 69% of initial capacity and the cell was removed from test.

Cell 407. This EV cell experienced problems when testing resumed and had to be cooled to room temperature. The cell was removed from the furnace and examined. Corrosion in the connections to the current leads was discovered and repaired. The cell was reheated and testing continued. In addition, cell 407

underwent an unscheduled F/T cycle. After completing 498 cycles, capacity had declined to 85% of initial capacity. Testing was suspended after constant-power tests did not succeed. The cell experienced a total of 520 cycles.

Cell 410. This EV cell was at temperature for several months before attempts were made to continue testing. SNL, however, was unable to discharge this cell at the proper discharge current, and the cell was removed from testing. The cell had completed a total of 423 cycles.

Powerplex Technology

In late 1987, SNL began testing Powerplex sodium/sulfur EV cells. Although this work is not performed as part of the DOE/OESD-funded ETD Project, these evaluations are included in this report for completeness. (The Powerplex evaluations are conducted by the SNL Electric Vehicle Advanced Battery Systems (EV-ABS) Project, which is sponsored by the DOE Electric Hybrid Propulsion (EHP) Division of OTS.)

SNL has agreed to test Powerplex cells in the same manner as it tests other manufacturers' sodium/sulfur cells. Upon completion of the tests or occurrence of a failure, the cells are returned to Powerplex, and no posttest analysis is conducted by SNL. During 1988, six 38-Ah Powerplex EV cells were evaluated: cells 452, 453, 457, 460, 462, and 463.

Charge/Discharge Regime. SNL began characterizing Powerplex cells in November 1987. Initial capacity was determined at a 5-A (C/8) discharge rate to an open-circuit voltage of 1.8 V and a 5-A charge rate to end-of-charge voltage of 2.4 V. This regime yielded initial capacity values close to the rated capacity; however, the Powerplex charge/discharge regime was slower than the CSPL, FACC, and Ceramtec regimes (Table 4-6). Therefore, capacity was also determined at the C/2.4 discharge rate to an end-of-discharge voltage of 1.8 V and at an 8-A charge rate to 2.4 V. As shown in Table 4-6, charging and discharging at the higher rate lowered the capacity of all Powerplex cells tested in 1988.

Cells 452 and 453. Cell 452 failed after completing 95 cycles. After it was on open-circuit stand for 10 days, only a few ampere-hours could be removed before the end-of-discharge voltage was reached. The end-of-discharge resistance at this point also increased significantly from 8 mohms to over 54 mohms. Several cycles that followed were run at a discharge/charge rate of 5 A. This cycle rate restored the cell capacity to 33 Ah and reduced the cell resistance to 12 mohms.

The discharge/charge rate was then increased to 16 A/8 A, but this lowered the capacity to approximately 22 Ah. The cell was again placed on open-circuit stand for a week and then cycled. The results were identical to those of the previous test, with only 1.3 Ah removed before the end-of-discharge voltage was reached. It appears the cell self-discharged during this open-circuit stand. The coulombic efficiency of the subsequent cycles showed a gradual decline.

Tests on this cell were terminated, and after cool-down the cell was removed from the furnace and examined. The cell apparently failed at or near its top, releasing polysulfides. This cell and cell 453 were returned to Powerplex.

Cells 457 and 460. After cell 457 completed 371 cycles, its capacity suddenly dropped to less than 3 Ah. Attempts were made to revive the cell with little or no success. The cell was therefore removed from the furnace and returned to Powerplex for posttest analysis.

Cell 460 cycled 381 times before it failed. This cell experienced an unscheduled F/T cycle. The cell was reheated to 350°C, and several capacity cycles were run. The capacity of the cell was ≈32 Ah before and after the cooldown, and there was no indication the cell had been damaged. Several additional capacity cycles were performed, and on cycle 380, the cell capacity decreased to less than 7 Ah. The cell was removed from test and returned to Powerplex for posttest analysis.

Cells 462 and 463. These cells were designed to have a lower end-of-discharge cell resistance. By the end of 1988, cell 462 had completed 340 cycles and was performing well, and cell 463 completed 290 cycles before failing. In addition to electrical cycling, the cells' charge and discharge performance was characterized.

Figure 4-12 plots the charge-acceptance performance for cell 462. When the charge current for Powerplex cell 462 was varied from a C/8 charge rate to a C/3 rate at 350°C, the capacity decreased ≈10%.

Figure 4-13 plots the average capacity versus discharge rate for cells 462 and 463. From this plot, it appears that the discharge rate had little effect on the capacity of cell 463 and a larger effect on the capacity of cell 462.

After cell 463 completed the charge-acceptance tests at 375°C, one baseline capacity test was performed. Cell capacity was 31.54 Ah, and everything seemed normal. However, on the following cycle, the capacity dropped to 1.4 Ah. After unsuccessful attempts to revive the cell, it was removed from test. Close examination indicated a breach, and the cell

was returned to Powerplex for posttest analysis. In addition, the data from all the cycles performed on Powerplex cells were sent to the developer. Powerplex plans to send a new set of cells to SNL for future testing in 1989. In addition, Powerplex will formulate a test plan to be used on the new set of cells.

Ceramtec Technology

Two sodium/sulfur cells from Ceramtec were placed on test at SNL in February 1988: cells 454 and 455. These cells had a rated capacity of 36 Ah at a discharge rate of 18 A (C/2 rate) to an open-circuit

voltage of 1.8 V. The charge current was 7 A to an end-of-charge voltage of 2.3 V.

Both Ceramtec cells underwent an unscheduled F/T cycle without any noticeable performance degradation. By the end of 1988, the cells had accumulated over 500 charge/discharge cycles and retained over 96% of their initial capacity.

In addition to charge/discharge testing, parametric tests and the following characterizations were performed:

- capacity vs charge rate
- capacity vs discharge rate
- specific energy vs specific power.

Parametric Tests. As with the FACC and CSPL parametric tests SNL conducted in 1987, the parametric tests on the Ceramtec cells were based on a Box-Behnken quadratic test matrix (*ETD Annual Report for 1987*, page 120). For the Ceramtec cells, the temperature was varied between 330°C and 360°C, with a center-point temperature of 345°C. The discharge currents ranged from 8 to 28 A, with a center-point current of 18 A. The end-of-discharge open-circuit voltage was 1.8 V. The charge current was varied from 6 to 14 A, with a center-point current of 10 A. The charge was always a two-step charge with the finishing current of 5 A to an end-of-charge voltage of 2.3 V. These results were used to derive a prediction equation, and plots were generated. Figure 4-14 is an example of these results. The plot indicates that the capacity increases with temperature and that the charge rate had little effect on the cell capacity.

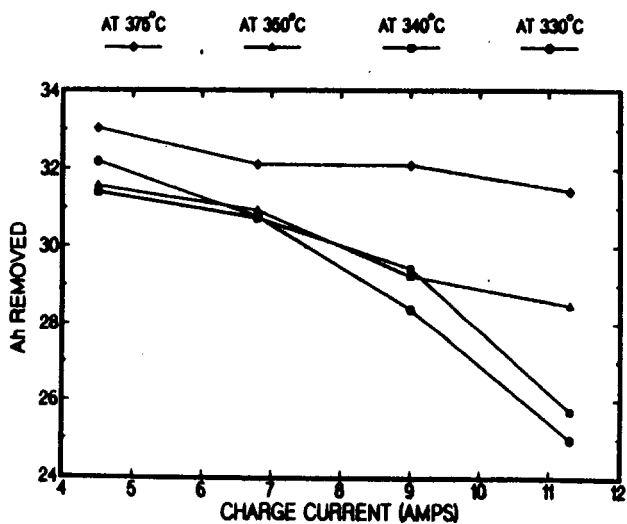


Figure 4-12. Powerplex Average Capacity vs Charge Rate and Cell Temperature—Cell 462

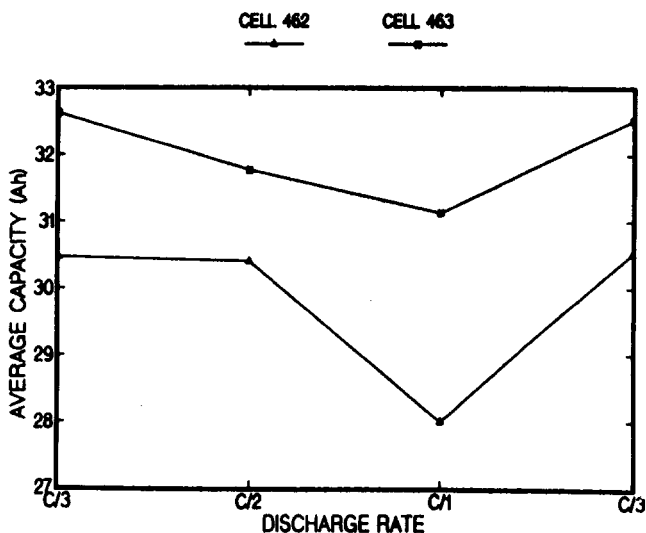


Figure 4-13. Average Capacity vs Discharge Rate—Powerplex Cells 462 and 463

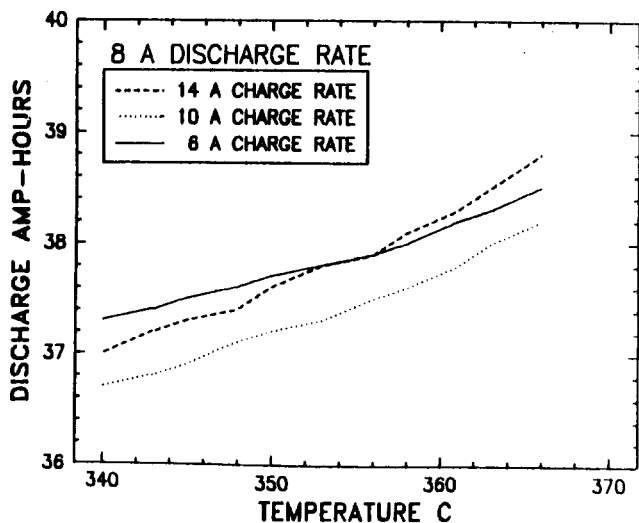


Figure 4-14. Predicted Capacity of Ceramtec Sodium/Sulfur Cell 454 vs Temperature and Charge Rate (8-A Discharge Rate)

Capacity vs Charge-Rate. Figure 4-15 plots average capacity versus charge current at 350°C for cell 454. At this operating temperature, the cell experienced a capacity loss of only 6% over the range of charge rates (C/8 to C/3). Cell 455 experienced similar losses. Further charge-rate tests at different temperatures will be performed on both cells in early 1989.

Capacity vs Discharge Rate. Figure 4-16 shows how the capacity of the Ceramtec cells decreased when the discharge rate was increased. The capacity at C/1 was lowest for both cells. This degradation was caused in part by the higher end-of-discharge open-circuit voltage value (>1.8 V). Another contributing factor to the loss in capacity could be cell heat-up during the high discharge rate. However, for either cell, the maximum loss in capacity was less than 6%.

Specific Energy vs Specific Power. A Ragone plot (Figure 4-17) was generated from constant-power tests on cell 454. The cell weighed 0.534 kg. When the cell was operated at a specific power of 9.6 W/kg, the cell's specific energy was 141 Wh/kg. However, when the specific power was increased to 46.8 W/kg, the specific energy dropped to 116 Wh/kg.

Nickel/Hydrogen Testing at SNL

A nickel/hydrogen battery is being developed for remote stand-alone applications in which the battery is interfaced with a photovoltaic array and/or a wind generator. The emphasis continues to be reduction of battery cost to the point where it would be cost competitive with the lead-acid battery on a life-cycle cost basis without unduly compromising performance. This development work is being conducted by JCI. The latest battery design consists of individual prismatic cells in a common pressure vessel.

Typically batteries evaluated at SNL represent state-of-the-art technology or contain experimental components modified to reduce cost or improve performance. Six nickel/hydrogen cells and three batteries were tested during 1988. Table 4-8 lists the cell configuration and test conditions. Both cycle and solar tests were conducted, with data gathering and switching functions controlled from a desktop computer.

Cycle Tests

The standard cycle test consists of a constant current discharge to 1.0 V/cell, followed by a charge until the pressure slope drops to one-half of the linear value. This is a severe test with a 100% depth-of-discharge on each cycle and continuous cycling without rest periods.

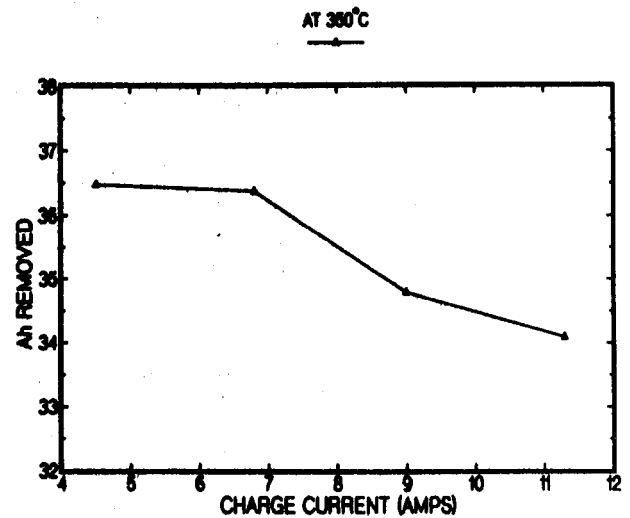


Figure 4-15. Ceramtec Average Capacity vs Charge Rate—Cell 454

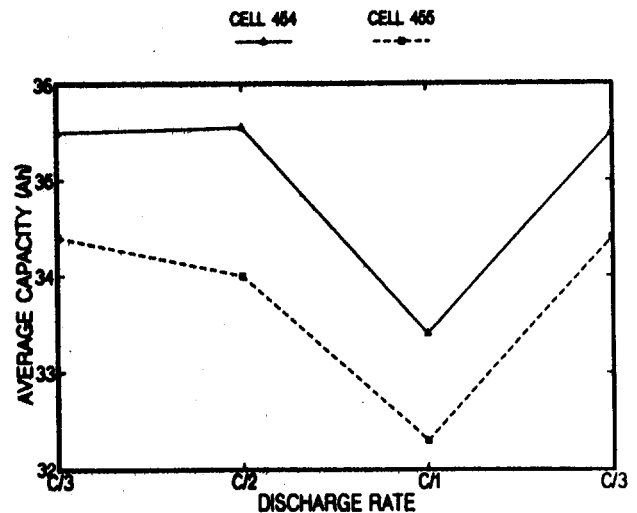


Figure 4-16. Ceramtec Average Capacity vs Discharge Rate—Cells 454 and 455

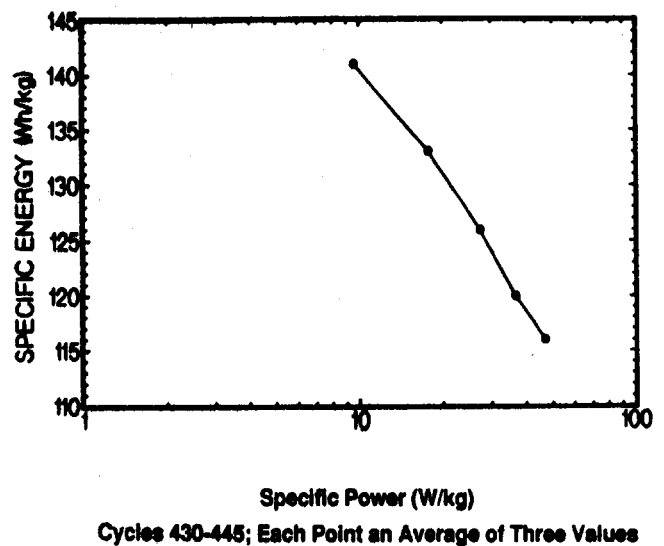


Figure 4-17. Ragone Plot for Ceramtec Cell 454. Results are based on an unencumbered cell weight (0.535 kg)

Table 4-9 summarizes the cycle test results. The column headings are self-explanatory except for the delta pressure, which is the difference between the end-of-charge and end-of-discharge pressures. Performance of the individual cells and batteries is discussed in detail below. Results are listed in chronological order rather than as listed in Tables 4-8 and 4-9.

Cell 12. This cell was removed from test in November 1988 after completing 2,350 deep cycles since November 1984. Cell 12 represented early technology, and capacity was declining.

Battery 2. This battery has six cells in a monoblock case—the same design as cell 12. Battery 2 had been on

Table 4-8. Configuration and Test Conditions

<u>Serial Number</u>	<u>Cell Modules</u>	<u>Positive Thick. (in)</u>	<u>Li Additive</u>	<u>Goretex on Neg.</u>	<u>KOH (%)</u>	<u>Coolant (°C)</u>	<u>Current Chrg/ Disch.(A)</u>
Cell							
12	10.5	.030	No	Yes	40	10	20/25
18	7	.070	Yes	Yes	38	10	25/25
19	7	.070	No	Yes	38	10	25/25
23	7	.070	Yes	Yes	33	10	25/25
144	9	.070	Yes	Yes	24	None	25/25
161	7	.090	Yes	Yes	24	None	25/25
Battery							
02	10.5	.030	No	Yes	40	10	20/20
04	7	.070	Yes	Yes	33	10	20/20
212	9	.070	Yes	Yes	24	None	30/30

Table 4-9. Summary of Cycle Test Results (December 23, 1988)

<u>Serial Number</u>	<u>Cycles</u>	<u>Capacity (Ah)</u>		<u>Effic. (%)</u>		<u>Mid-Point Discharge (V/C)</u>	<u>Delta Pressure (psig)</u>
		<u>Nominal</u>	<u>Latest</u>	<u>Ah</u>	<u>Wh</u>		
Cell							
12 ¹	2,350	80	76.1	87.4	69.2	1.201	174
18 ²	1,325	120	109.1	85.6	69.5	1.221	161
19 ²	1,257	120	102.1	88.0	69.7	1.207	141
23	1,439	120	132.5	91.6	74.9	1.233	182
144	920	150	194.9	89.8	71.9	1.231	241
161	553	160	142.6	84.9	69.5	1.242	220
Battery							
02 ³	1,519	80	73.2	89.0	74.2	1.223	51
04 ⁴	679	120	142.1	92.5	73.9	1.221	169
212	354	600	658.9	88.7	78.7	1.301	212

- 1 Removed from test November 1988
- 2 Removed from test August 1988
- 3 Testing suspended March 1988
- 4 Testing suspended July 1988

solar test a little over a year when testing was suspended in March to make room for Battery 4.

Cell 18. Cell 18 has 70-mil positive electrodes in place of the earlier 30-mil electrodes. This design increased theoretical capacity for the same size case from 80 Ah to 120 Ah. Cell 18 performed well and had accumulated 1,325 cycles when it was removed from test in August for posttest analysis.

Cell 19. This cell is configured the same as cell 18 except there is no lithium additive in the electrolyte. (The lithium additive has proven beneficial to cell performance and has been used in all recent cells.) Cell 19 was also removed from test in August and returned to JCI.

Cell 23. Cell 23, which represents 1986 technology, is still performing well. Its configuration is the same as cell 18 except that the KOH concentration in the electrolyte was reduced. The latest capacity of 132.5 Ah is down 17 Ah from that reported a year ago but is still higher than its nominal rating of 120 Ah after 1,439 cycles.

Battery 4. This battery has five individual cells in a common pressure vessel—the cell design is the same as cell 23. Solar tests were performed on battery 4 until July, when testing was suspended and the solar testing effort transferred to the 7-kWh battery.

Cell 144. Cell 144 is performing particularly well with a capacity of 195 Ah after 920 cycles. This capacity represents the theoretical capacity of the cell, and cycling of this severity would not be recommended for field use. The configuration of cell 144 represents the present baseline design and is the same configuration used in cells for the 7-kWh battery. Design changes from cell 23 include nine-cell modules rather than seven-cell modules per cell, reduced KOH concentration, and an improved electrolyte management system. Cell 144 was designed to operate passively at ambient temperatures to 30°C, and all testing at SNL has been done without active cooling.

Cell 161. This cell shows a declining capacity trend; the latest capacity of 143 Ah is 29 Ah less than reported last year. Cell 161 was the first cell to use the thicker 90-mil positive electrodes. The thicker electrodes may be a factor in the declining capacity because the distribution of active material in the thicker plaques is not uniform. This potential problem is being addressed as part of the development contract.

Battery 212. Battery 212 consists of four 12-V battery modules, each containing ten 150-Ah cells, the same as cell 144, in a reusable pressure vessel. With the modules wired in a series/parallel configuration, the

nominal rating of the battery is 300 Ah at 24 V, or 7 kWh. Additional details concerning the design of the cells and battery are given in SAND88-7100 (see Appendix).

Initial cycle testing of battery 212 was conducted to obtain baseline performance of the 7-kWh battery after receipt at SNL. Battery 212 was configured for a nominal 24-V, 300-Ah output. The battery was discharged to 20.0 V (1.0 V/cell), and the charge input was varied from 320 to 340 Ah in increments of 10 Ah. The charge and discharge currents were both 20 A. The tests were conducted at room ambient temperature without active cooling. The results are shown in Table 4-10.

The coulombic efficiencies are quite high, even with a charge input of 340 Ah. This finding, along with the fact that the pressure slope during charging was still linear, indicates that the battery is capable of additional capacity with more charge input.

For a subsequent test, the charge and discharge currents for battery 212 were increased. The 7-kWh battery was cycled by charging it with a constant 340 Ah at 30 A and discharging to 1.0 V/cell at 27 A. A complete cycle took about 24 h. Figure 4-18a is a plot of voltage vs time for the first module in each of the two strings; the curves are virtually identical until the very end of discharge. Figure 4-18b is a plot of string current using the same time base; here, too, the load is shared equally with a slight divergence at the end of discharge. Output for this cycle was 328.9 Ah and 8.623 kWh, resulting in a coulombic efficiency of 96.7% and an energy efficiency of 85.6%.

Solar Tests

Battery 212, a 7-kWh battery, has been evaluated using a flat plate photovoltaic array and an electrical load. No controller was used between the three elements, since the gases generated on battery overcharge

Table 4-10. Initial Cycle Test Results for Battery 212

Charge (Ah)	Discharge (Ah)	Ah Efficiency (%)	Mid-point VN
320	311	97.2	1.327
330	321	97.1	1.327
340	333	97.9	1.317

are recombined internally. However, since a significant temperature rise can occur at high rates, the array was disconnected if the battery reached 35°C and reconnected when the temperature dropped to 30°C.

A portion of an existing fixed, flat-plate photovoltaic array in the Photovoltaic Advanced Systems Test Facility (PASTF) at SNL was used for the solar test. Each of the Solarex panels had a nominal rating of 5 V, 60 W. For the initial tests, two panels in parallel and eight panels in series were used. A current-voltage (I-V) curve made on a clear day in March 1988 gave a short-circuit current of 28.2 A and an open-circuit voltage of 48 V. The peak power was 695 W, with 22.2 A and 31.3 V at the peak. Charging voltage required for a 24-V nickel/hydrogen battery is about 30 V (1.5 V/cell); therefore, eight panels in series appear to be a good match. For subsequent tests, the number of panels in parallel was increased to three panels and then to four panels. Table 4-11 summarizes the array output for the three array configurations.

With the array in the 4 x 8 configuration, tests were run with two different load regimes. Both load regimes resulted in 200 Ah/day. One regime was a continuous 8.3 A while the other regime was 12.5 A turned on at 1600 and turned off at 0800 to simulate night lighting. With the continuous load, the array generally supplied the load during the day. This finding is reflected in the SOC vs time plots in Figure 4-19. The night load (Figure 4-19a) results in a deeper depth-of-discharge than the continuous load (Figure 4-19b).

For a subsequent test, the electronic load was replaced with two resistive loads that could be disconnected independently. The A load was a constant 5 ohms, while the B load was an 8-ohm resistor in parallel with a 24-V fluorescent light. The B load was programmed to be disconnected (shed) when the SOC dropped to 50% and was reconnected when the SOC reached 55%. While the load shedding at SNL was accomplished using a computer, JCI has demonstrated that it can be accomplished with a simple pressure switch.

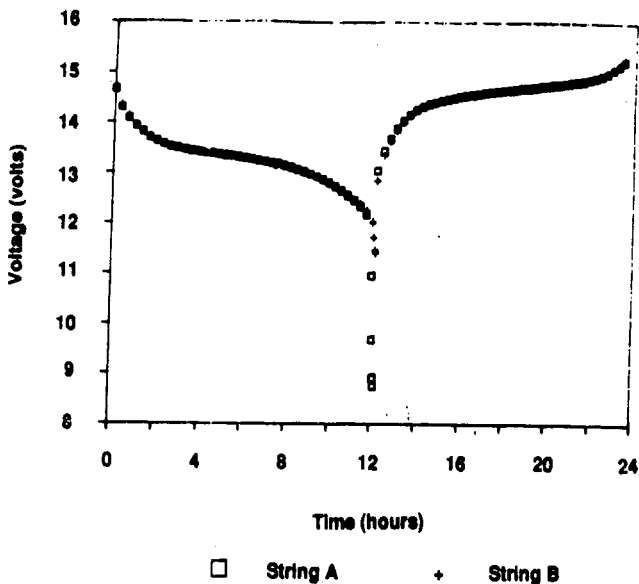


Figure 4-18a. Voltage vs Time, 7-kWh Battery (Cycle 251)

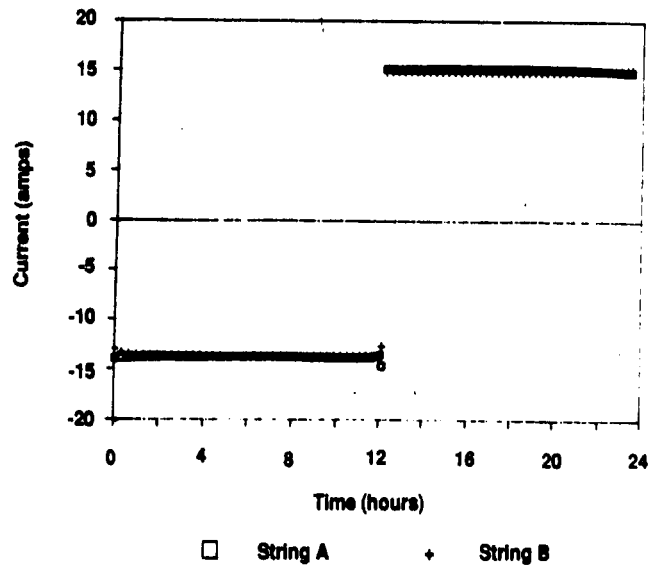


Figure 4-18b. Current vs Time, 7-kWh Battery (Cycle 251)

Table 4-11. Array Output for Battery 212

Array Configuration	Month	No. of Days	Array Output (Ah)		
			Avg.	Max.	Min.
2 x 8	May	20	153	190	77
3 x 8	Aug	28	199	240	124
4 x 8	Sep	24	236	306	65

Figure 4-20a shows SOC plotted vs time for a 4-day period starting at midnight. Both the array and load currents are plotted in Figure 4-20b for the same time period. The B load disconnects for several hours in the early morning, dropping the load current from about 10 A to 5 A. On the fourth day, the array current shows considerable fluctuations because of intermittent sunshine; on that day the array output was only 188 Ah, while the loads consumed 239 Ah.

The 7-kWh battery was then reconfigured from a nominal 24-V, 300-Ah unit to a 12-V, 600-Ah unit. This change was accomplished by putting the four battery modules in parallel. The array was changed to a 4 x 4 configuration to match the voltage of the battery, and a refrigerator and fluorescent lights were used as loads. The refrigerator is a Norcold Tek II dual-voltage (120 Vac, 12 Vdc) model DE-400D designed for recreational vehicle use. The refrigerator was used in the 12-Vdc

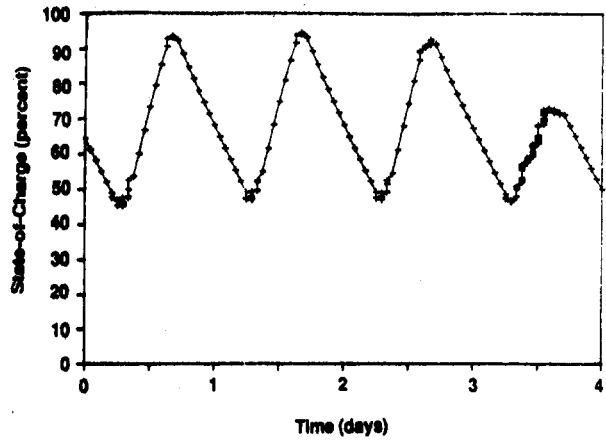
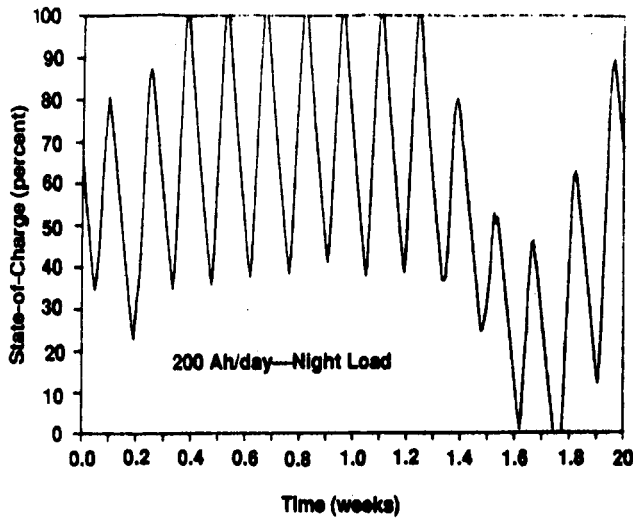


Figure 4-19a. State-of-Charge vs Time, 7-kWh Battery (September 2 - 15, 1988)

Figure 4-20a. State-of-Charge vs Time, 7-kWh Battery (October 26 - 30, 1988)

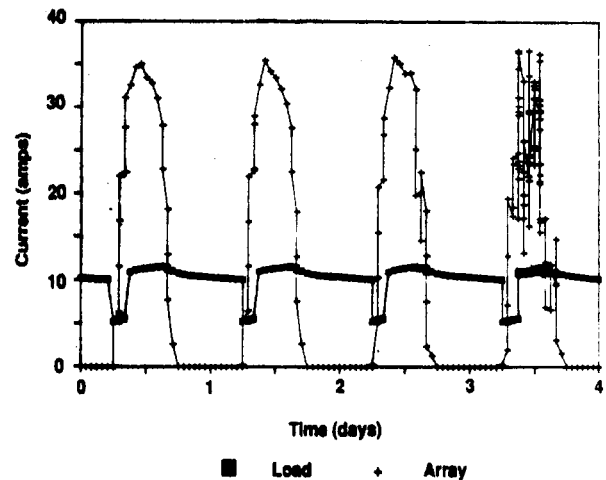
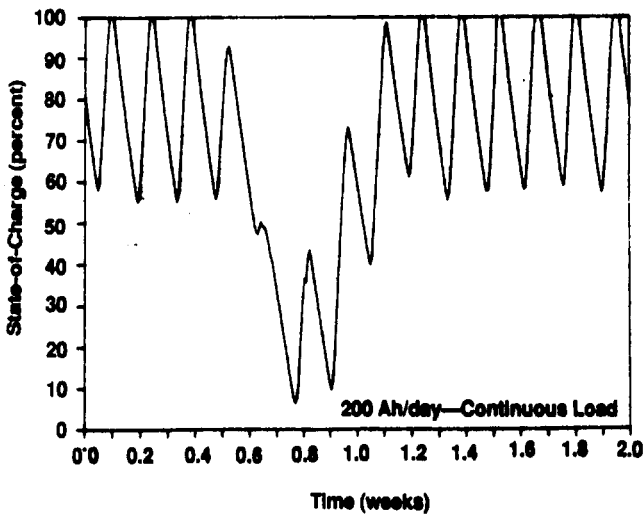


Figure 4-19b. State-of-Charge vs Time, 7-kWh Battery (September 17 - October 2, 1988)

Figure 4-20b. Array and Load Current vs Time, 7-kWh Battery (October 26 - 30, 1988)

mode. Overall dimensions of the refrigerator are about 30 x 20 x 20 in. The refrigerator is free standing and includes a freezer compartment. The remainder of the load consisted of four 30-W, 12-Vdc, Thin-lite model 116 fluorescent lights with individual switches.

For the initial test, the refrigerator was connected to Aux. load A, and the lights were conducted to Aux. load B. The refrigerator was connected continuously but was cycled on and off by its thermostat, which was set to 4 (range 1-5). The four lights in parallel were programmed to disconnect when the SOC dropped to 80% and were reconnected when the SOC rose to 85%, thus reducing the likelihood of overcharging the battery.

SOC and load current vs time are plotted in Figure 4-21a and 4-21b, respectively, for an 8-day period

just before the holiday shutdown. The effect of the lights can be seen in the slope of the SOC curve; the battery never did go into an overcharge condition. The program was initially set to record data every time the refrigerator came on or went off. However, it was not anticipated that the unit would cycle so frequently, about every 14 minutes. The recording scheme was changed during the second day so that data were stored only when the change in current exceeded 5 A rather than 3 A.

The refrigerator drew about 3.8 A, and the lights drew slightly over 2.0 A each. Daily consumption of the refrigerator was about 32 Ah; daily output of the array averaged 139 Ah with a maximum and minimum of 188 Ah and 81 Ah. Testing will continue next year.

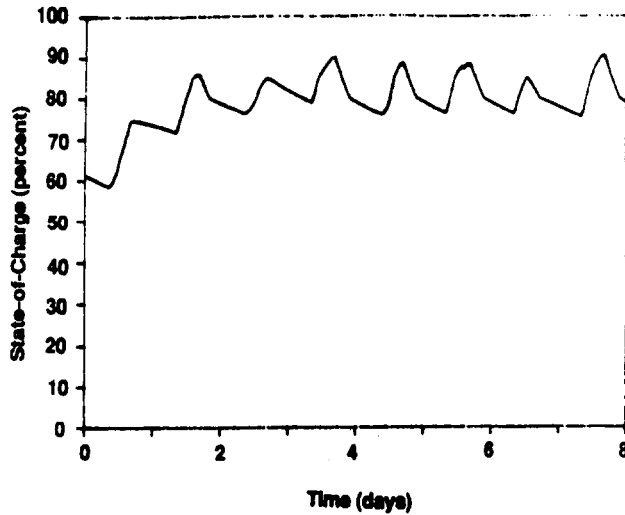


Figure 4-21a. State-of-Charge vs Time, 7-kWh Battery (December 15 - 22, 1988)

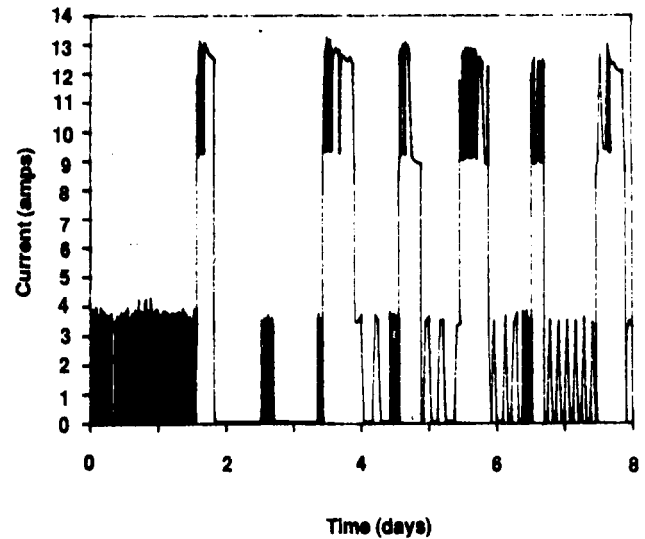


Figure 4-21b. Load Current vs Time, 7-kWh Battery (December 15 - 22, 1988)

Chapter 5. Battery Technology Improvement

The SNL Technology Improvement element investigates and solves specific problems in the development of advanced secondary batteries. The following criteria are used in the selection and continuation of the tasks in this element:

- The final product must be an important contribution to the near-term development of the technology
- The task can be more efficiently performed at SNL than at the prime contractor
- Adequate resources must be available to allow a timely contribution.

The indirect benefits of this element to the ETD program include (1) a better and more active understanding of the obstacles facing each technology that, in turn, allows more effective program management and (2) a means to utilize the wide range of capabilities and resources at SNL directly in battery development. The number and size of the tasks are limited to ensure proper perspective with respect to the primary objective (technology development) of the ETD program. Finally, nonessential overlap with TBR activities is minimized because of a close relationship with the industrial partner.

This element was established as part of the ETD program in 1985. During 1988, the element had four active tasks: two each supporting the zinc/bromine and the sodium/sulfur technologies. The progress during 1988 is summarized separately in the remainder of this chapter. Each task continues an effort started in 1987, although the scope of all four has changed. The status of a fifth task, sodium/sulfur electrolyte failure analysis, is also reported. However, progress was limited during the past year to redefining new objectives that are more consistent with the advancing status of the CSPL technology.

Advanced Membrane Development for Zinc/Bromine Batteries

Zinc/bromine batteries are being developed for both stationary and vehicular applications. The separators currently used in the developing zinc/bromine battery

technologies are silica-filled sheets of microporous polyethylene. Separators of this type are generally quite inexpensive and have low ionic resistance in the electrolytes. The concentration of free bromine in the electrolyte is reduced by addition of quaternary ammonium bromide salts to allow the use of these microporous separators rather than the more expensive ionic membranes that are permselective. One serious disadvantage of these separators is that bromine and negatively charged bromine moieties can permeate these materials and react with the zinc deposit. This reaction results in partial self-discharge of the battery and low coulombic efficiencies. Because the reaction of bromine with zinc is exothermic, additional external cooling may also be required. The energy needed for thermal management reduces the net energy efficiency.

The purpose of this task is to improve separator performance by impregnating and/or coating the microporous material with small quantities of a cationic polyelectrolyte. This approach should reduce the rate of unwanted bromine transport by two mechanisms:

- Donnan exclusion of negatively charged bromine complexes by the fixed negatively charged groups in the polyelectrolyte
- Physical closure of some fraction of the pores.

If the ion exchange capacity of the impregnating agent is sufficiently high, energy losses because of higher separator resistance should be minimal. The ideal polyelectrolyte would be stable and insoluble in the electrolyte and soluble in a solvent that does not attack the microporous separator. Sulfonated polysulfone (SPS) resins, developed earlier for use in the zinc/ferricyanide battery, were found to satisfy these general requirements. The current status of this composite membrane development effort is summarized in Table 5-1.

Membrane Preparation

The microporous separator in this study was Daramic, a 0.64-mm-thick sheet of silica-filled microporous polyethylene made by the W. R. Grace Company. Impregnation of this microporous product was achieved by two procedures. In the first procedure, Daramic was simply immersed in a 20% solution of the acid form of SPS in dimethyl formamide (DMF) for

several minutes and dried at 60°C for 1 h. This procedure was repeated twice to ensure maximum uptake of SPS. In the second procedure, Daramic was immersed in a hot (90°C) solution of SPS, which was then placed in a vacuum oven at 106 mm Hg for 15 min or until the air bubbles ceased. The concentration of SPS in DMF was varied from 10% to 30%. Using the second procedure, membranes were made from both acid (H⁺) and sodium (Na⁺) forms of SPS.

Additionally, dense films containing only SPS were made by coatings from 20% solutions in DMF onto clean glass plates using a 15-mil doctor blade and then drying at 110°C for 1 h.

Table 5-1. Status of Membrane Development Task

- Uniform impregnation of microporous separators achieved
- Extensive range of separator performance demonstrated
- Mathematical model of cell performance developed to guide optimization
- Cell testing in progress to verify separator performance

Membrane Characterization

The area resistivity of both separators and membranes was determined using an RAI Research Corporation, Model 2401, impedance meter. Before the actual measurement, the samples were soaked in anolyte for 24 h. The anolyte was a proprietary electrolyte formulated for zinc/bromine batteries. All measurements were made at 1,000 Hz.

The rate of bromine transport was determined using a two-cell diffusion apparatus. The membrane or separator was clamped between these cells, one of which contained the catholyte. The other cell contained the anolyte. The catholyte was vigorously stirred with a mechanical stirrer to ensure adequate contact of the bromine complex with the membrane, thereby simulating the flow of electrolyte during battery operation. The amount of bromine diffused through the separator or membrane after 4 h was determined titrimetrically with 0.1-M sodium thiosulfate after the addition of sodium iodide.

The distribution of SPS across the thickness dimension of the membrane was determined by monitoring the sulfur concentration as a function of depth using a Cameca Model MBX electron microprobe.

Results and Discussion

A summary of the performance of the various separators is shown in Table 5-2. The first entry in Table 5-2 is for the SPS-only membrane. As expected,

Table 5-2. Performance Parameters of Various Zinc/Bromine Battery Separators

Separator	SPS Conc. (%)	Weight Gain (%)	Resistivity (ohm-cm ²)	Br ₂ Transport (mol/cm ² x 10 ⁹)
SPS Cast Membrane/0.07 mm	100	—	99.3	<0.05
Daramic/No Treatment	—	—	1.1	5.2
Daramic/Immersion Three Times at Ambient	20	66.8	5.0	0.05
Daramic/Vacuum Immersion at 90°C (H ⁺ Form)	10	17.3	1.6	1.7
	20	39.1	2.8	0.4
	30	97.7	41.9	<0.05
Daramic/Vacuum Immersion at 90°C (Na ⁺ Form)	10	16.9	1.4	2.4
	20	15.8	4.1	0.4
	30	159.0	28.3	<0.05

the bromine permeation is very low for this true ion-exchange material. However, its resistance is much too high to be of any practical use as a separator in the zinc/bromine battery. Presumably, the resistivity could be reduced by preparing a thinner membrane, but its mechanical strength would be unacceptable. The second and third entries in Table 5-2 show the performance of Daramic alone and of Daramic that was dipped three times in a 20% solution of SPS at room temperature. Thus, SPS, when dispersed as an additive in a microporous matrix, provides much lower area resistivities than do cast SPS membranes.

Figure 5-1 shows the sulfur profiles across the thickness dimension of membranes impregnated at room temperature and at 90°C. Sulfur content scales with the concentration of SPS because no sulfur is present in the untreated separator. The concentration of SPS in the multiply immersed (room temperature) membrane was considerably higher at or near the surface. This non-uniform distribution was detrimental for two reasons. First, this membrane must be analyzed as a composite membrane consisting of three layers. The outer two layers are similar to a cast membrane, while the inner layer is an SPS-impregnated Daramic membrane. The complex nature of the membrane could possibly mask the beneficial nature of SPS impregnation. Second, the composite nature of the membrane means that there are probably no simple relationships between membrane thickness and performance parameters such as resistivity and permeation.

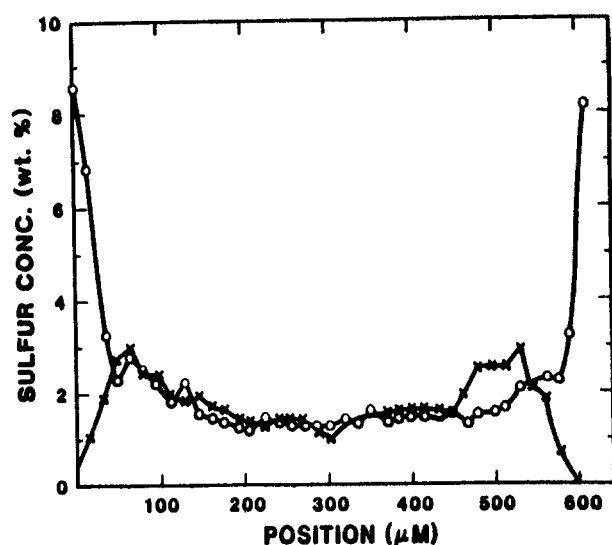


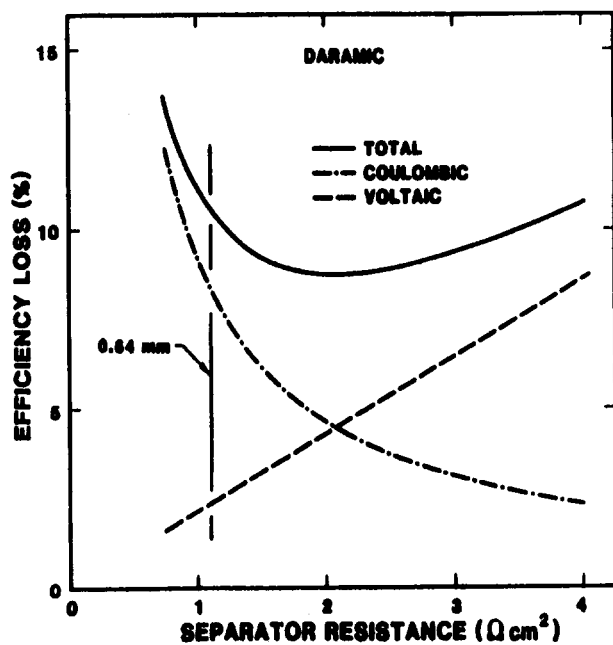
Figure 5-1. Sulfur Content as a Function of Depth Across the Thickness Dimension of Two Membranes: Impregnated with SPS at Room Temperature Three Times (O); Impregnated with SPS at 90°C Under Vacuum (X)

To simplify the analysis of membrane performance, several procedures were investigated for preparation of uniformly impregnated membranes. The best method was a vacuum immersion of Daramic in various concentrations of SPS solutions at 90°C. The sulfur profile of such a membrane is also shown in Figure 5-1. The internal concentration of SPS is the same for this membrane as for the membrane dipped three times at ambient, but no buildup of SPS at the Daramic surface is observed. Substantial changes can be introduced in the properties of such a membrane by varying the SPS solution concentration. The results of preparing a membrane with 10%, 20%, and 30% SPS solutions are shown in Table 5-2. Membrane performance appears to correlate with the degree of weight gain of SPS. The performance of the membrane can be further modified by changing the thickness of the Daramic substrate. Because the SPS concentration across the membrane thickness is uniform, presumably the resistance would be a simple function of the Daramic thickness.

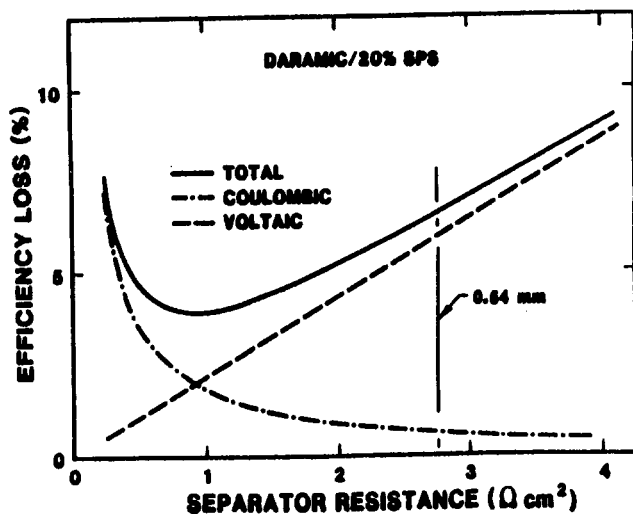
Similar changes in membrane performance were observed (Table 5-2) when the separators were impregnated with solutions of SPS in the sodium salt form. Differences between the performance of membranes impregnated with different forms of SPS may be attributable to differences in the wettability of the substrate by these two materials. In general, better wetting was observed with the salt form of SPS. This fact may account for the higher weight gains observed when Daramic was impregnated with the Na⁺ form of SPS.

The impregnation of Daramic involves trade-offs between resistivity and bromine permeation. To relate these trade-offs to the energy efficiency of a battery containing such a membrane, the voltaic, coulombic, and energy losses attributed to the separator were calculated by a very simple model. This model is based on a 5-h charge cycle to 90 mAh/cm² and a 2.5-h discharge cycle. The internal resistance of the battery without a separator was set equal to 6.1 ohms-cm².

The resulting efficiency losses for a Daramic separator are shown in Figure 5-2a. The performance of a 0.64-mm Daramic separator is indicated by the vertical line, while the complete curves show the performance as a function of separator thickness. The curves assume that resistance is proportional and that bromine permeation is inversely proportional to the separator thickness. Figure 5-2b shows the corresponding performance curves for the Daramic composite treated with vacuum immersion in a 20% SPS solution at 90°C. The performance of the impregnated 0.64-mm Daramic separator is again indicated. The curves assume that the resistance and bromine permeation are inversely proportional to each other. Presumably, the position on a curve



a. Daramic Separator



b. Daramic Separator Vacuum Immersed in 20% SPS Solution at 90°C

Figure 5-2. Voltaic, Coulombic, and Energy Efficiencies Calculated with a Cell Performance Model

can be changed by varying the thickness of the separator. This assumption appears reasonable for a separator that contains a uniform distribution of SPS. These curves demonstrate that although the membranes that have been prepared should show some reduction in separator efficiency loss (from 10.6% to 6.6%), further improvements could be attained by reducing the thickness of the SPS-treated separator.

In-cell testing is mandatory to verify these concepts. The actual long-term performance of these composite separators in single zinc/bromine cells is being determined in a separate study at SNL.

Durability of Zinc/Bromine Materials

The flow frames in zinc/bromine batteries need to be stable in bromine-containing electrolytes. Flow frames for the zinc/bromine battery are being developed by ERC. The frames are fabricated from PVC for two reasons: (1) PVC is more stable toward bromine than polyolefin material such as polypropylene or polyethylene and (2) PVC is relatively inexpensive and easy to fabricate into complex parts. The flow frame used in ERC's battery is indeed a complex part. One disadvantage of PVC is that it is intrinsically unstable during high temperature fabrication if certain chemical additives are absent. Accelerated aging studies performed jointly at SNL and ERC demonstrated that these additives are either leached out or chemically attacked by the electrolyte. The combination of chemical attack and leaching results in the formation of porosity and the loss of mechanical properties.

During the past year, efforts were focused on the following durability-related issues: (1) the chemical nature of the additives that are attached or leached by the electrolyte, (2) the extent of degradation of flow frames under nonaccelerated conditions (that prevail in an operating battery), (3) the stability of "pure" PVC in bromine-containing electrolytes, (4) the existence of alternative thermoplastics that do not require additives that are stable in bromine-containing electrolytes, and (5) the effect of the combination of stress and corrosion brought on by exposure to the electrolyte and mechanical stress. The current status of this task is summarized in Table 5-3, and specific results are discussed below.

Generic Structure of PVC Additives

The different types of carbon that are present in PVC formulations that contain organic or organometallic additives can be detected by ^{13}C Nuclear Magnetic Resonance (NMR) spectroscopy. A ^{13}C NMR spectrum of PVC-1 is shown in Figure 5-3a. The two large peaks at chemical shifts of 47.7 and 57.9 ppm are attributable to chain backbone carbons of PVC itself. The smaller peak at 33.7 indicates the presence of an additive that contains a series of CH_2 groups. Two likely compounds that could give rise to this peak would be lead octoate or calcium stearate. These compounds are commonly used

Table 5-3. Program Status of PVC Durability Task

- Both aliphatic and aromatic additives were detected in PVC-1 by ^{13}C NMR. The concentration of these additives was reduced by about 90% after exposure to electrolyte at 60°C for 18 weeks.
- Surface degradation in the flow channels and adjacent regions was observed in a PVC-1 flow frame that had been in use for one year.
- Pure PVC is more stable to bromine-containing electrolytes than PVC that contains additives. Pure PVC is too brittle, however, for use as flow frame material.
- Tefzel, a DuPont thermoplastic, has been identified as a possible alternate material. The primary advantage of Tefzel is the absence of leachable additives. Initial stability tests are promising.
- Aging studies of PVC materials were initiated to evaluate the combined effect of stress and environmental exposure to the electrolyte in material durability.

as thermal stabilizers. The small peak at 133 ppm is characteristic of aromatic carbons. In this case, one likely candidate is tetraphenyl lead, another thermal stabilizer. These stabilizers scavenge hydrogen chloride that evolves when PVC is heated. It is well known that hydrogen chloride catalyzes the degradation of PVC. From Figure 5-3b, the concentration of these additives was apparently greatly decreased after aging in the electrolyte at 60°C for 18 weeks. The loss of these organic salts may at least partially account for the development of porosity in PVC alluded to above.

Surface Degradation of PVC Flow Frames

In an operating battery, the electrolyte is circulated through channels in the flow frame. It was of interest to determine whether degradation of PVC in the flow channels was more extensive than at other nearby locations on the flow frame. Variations in the extent of degradation can be conveniently monitored as a function of location by using a technique known as modulus

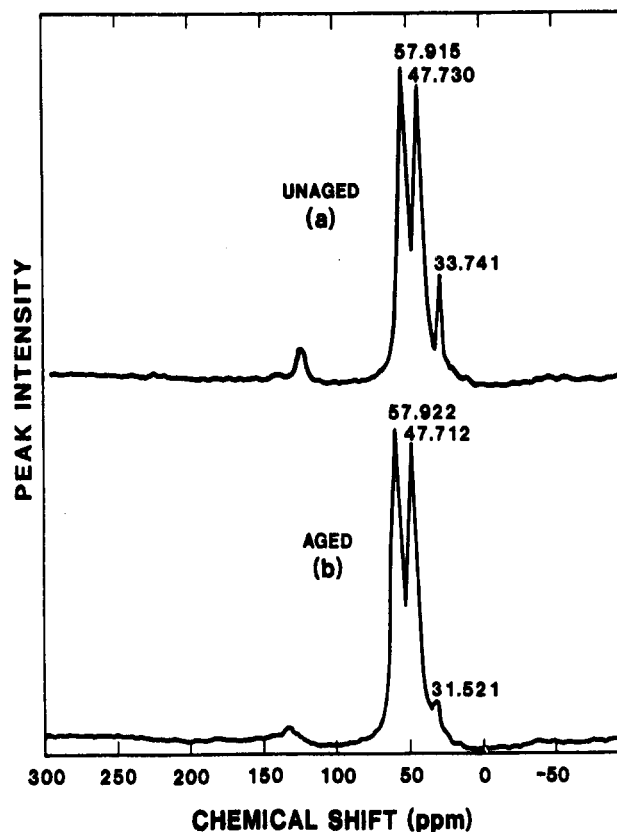


Figure 5-3. ^{13}C NMR Spectra of (a) Unaged and (b) Aged PVC-1 (solid). Aging Conditions: 60°C for 18 Weeks in a Bromine-Containing Electrolyte

profiling (described in the *ETD Annual Report for 1987*). In this technique, the depth of penetration of a weighted probe can be used as a measure of the material's tensile modulus. The change in modulus that occurs as a result of environmental exposure is a sensitive measure of degradation. The modulus profile taken across the surface of a flow frame that included the groove of a flow channel is shown in Figure 5-4. It is clear from these data that degradation was most extensive in the flow channel. It is interesting to note, however, that considerable degradation occurred on the shelf surfaces adjacent to the flow channel. This is probably because of seepage in the seams that are created when the flow frames are assembled into a battery stack. Beyond a distance of about 1 mm, degradation appears to be minimal. These results confirmed our expectation based on accelerated aging tests that degradation would occur under operating conditions. It should be noted here that these modulus measurements were made only on the surface of the flow frame.

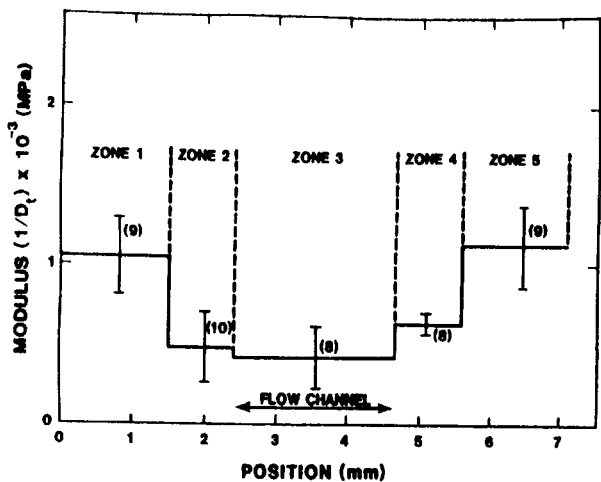


Figure 5-4. Tensile Modulus as a Function of Location on Surface of PVC-1 Flow Frame Used in an Operational Battery for About 1 Year

Further work is required to determine the depth of degradation into the bulk.

Comparative Stability Tests

Comparative stability studies of commercial formulations of PVC considered by ERC (PVC-1, PVC-4, PVC-6), along with "pure" PVC and Tefzel, a copolymer of ethylene and tetrafluoroethylene made by DuPont, were performed by determining the effect of electrolyte exposure on the shear modulus of these materials. The motivation for this study was twofold: (1) to identify possible substitutes for PVC and (2) to determine the mechanical effect of additives on the stability of PVC in aqueous bromine-containing electrolytes. Identification of backup or replacement materials for PVC is justified for the following reasons: early exposure tests indicate that some degradation of PVC did occur and that additives were chemically attached and leached out by the electrolyte. Some of these leached additives or their decomposition products may have harmful catalytic effects on the electrochemical processes that occur during charge (e.g., hydrogen evolution).

The results obtained after two-week exposures are summarized in Figure 5-5. While relatively small decreases in the shear modulus were observed for PVC-1 and PVC-4, PVC-6 suffered a rather significant loss of modulus (30%). In contrast, no change in modulus was observed for "pure" PVC. This PVC sample was specially made by B. F. Goodrich and

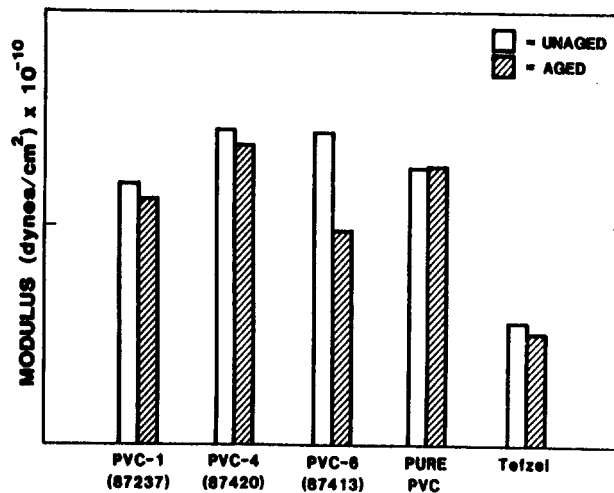


Figure 5-5. Effect of Aging on the Shear Modulus of Various Thermoplastics. Aging conditions: 70°C for 2 weeks in a bromine-containing electrolyte

contained only a very small amount of a proprietary thermal stabilizer, just enough to prevent degradation during the molding process. Unfortunately, this material is quite brittle and would not be practical for fabrication into a flow frame. Tefzel is a chemically stable thermoplastic without additives or fillers. Although the initial modulus of Tefzel is lower than that of PVC, it is more ductile than PVC, and it was fairly stable in the electrolyte. The modulus loss was only about 10%, possibly because of plasticization rather than degradation. It should be noted that Tefzel is denser than PVC and, as a consequence, it was partially immersed in the oily phase of the electrolyte. Whether this would enhance or retard degradation is not known. The chief advantage of Tefzel, should it prove sufficiently stable, is the lack of leachable additives.

Stress-Rupture Studies of PVC Materials

In the ERC technology, flow frames and gasket materials are bolted together, resulting in some degree of component stress. In the current aging studies at both SNL and ERC, the effect of stress is not taken into account. A stress-rupture study has been initiated to determine if stress-assisted failure is possible. Pre-cracked compact tension specimens have been immersed in bromine-containing electrolyte and are being subjected to various static loads. The time to failure is being measured. Control tests are being carried out in air. To date, static fracture toughness tests have been completed.

Failure Analysis of the Beta"-Alumina Electrolyte

The overall objective of this continuing task is to identify mechanisms that cause beta"-alumina electrolyte failures in sodium/sulfur cells. During 1987, two subtasks were pursued: (1) fractographic analysis of failed electrolytes from actual cells and (2) experimental evaluation of the electromechanical degradation of beta"-alumina. Early in 1988, an additional evaluation was made of the 1987 results and the status of the CSPL cell technology. In the latter area, the general failure of a CSPL-PB cell can now be traced to identifiable outside factors, such as contamination or a problem during production of a particular component. The conclusion was reached that only limited useful new information would be gained from further detailed analyses of electrolytes taken from failed cells. Given this situation, the decision was to suspend activity on the two subtasks and investigate other specific mechanisms of electrolyte degradation.

The new study concerns an aspect of electrolytic degradation that recently became more apparent. In some of the CSPL cells that failed during testing at SNL, cracks were found in the electrolytes even though the cell currents were low enough to have theoretically prevented electrolytic degradation. Additionally, the character of the cracks was much like that of cracks generated by electrolytic-driven failure at high current densities. Careful examination of the crack surfaces showed a thin layer of the inner wall that was compressed while the cracks were growing.

The implication is that the compressive stress layer enhanced cracking by closing the mouths of the cracks, raising the sodium pressure in the cracks and greatly increasing their rate of growth. Such a failure process is supported by the experimental and mathematical modeling results obtained during previous analyses of electromechanical degradation. From a practical viewpoint, this observation could be very important because of its impact on the logic behind using transformation-toughened beta"-alumina and the need to keep the electrolyte completely free of residual stresses.

To determine the viability of stress-assisted electrolytic degradation of beta"-alumina electrolytes, three specific subtasks are now being pursued: (1) the identification of possible mechanisms—occurring during processing of the ceramic, cell assembly, or cell operation—that can result in thin compressive layers in the electrolyte surface, (2) the measurement of the growth rate of cracks within thin compressive layers, and (3) an evaluation of the potential for subcritical

crack growth within the electrolyte. Significant delays have been experienced in obtaining appropriate, high-quality beta"-alumina samples. The actual experimental investigations will begin in early 1989.

Component Stress During F/T Cycling of Sodium/Sulfur Cells

Sodium/sulfur batteries in both motive power and utility applications will be subjected to numerous F/T cycles during their lifetime. These thermal cycles must be expected and cannot result in significant cell failures. The F/T durability of cells being produced today is much better than that typically attained several years ago. However, most developers, including CSPL, feel that further improvement will be needed when and if cost issues force larger cell sizes to be considered again.

The overall goal of this continuing task is to provide developers with an analytical tool and the necessary knowledge to improve the long-term F/T durability of cells. Based on the results obtained in 1987, discussions at the Beta-Battery VII workshop, and the observation that this task is the only phenomenological-type F/T study being performed worldwide, the specific objectives of this task were reconsidered. The conclusion was that the general approach below is still viable, but that activities for FY89 should concentrate on understanding the stress-producing processes and validating a thermomechanical model for a normally operating cell (as opposed to a cell with known problems such as leaking seals).

The above objective was chosen because it yields a very useful and timely product: a methodology that can immediately be employed in cell redesign and in the analysis of potential failure mechanisms. These efforts are realistically constrained to normal cells because detailed information on actual F/T failures is not and probably will not be available for at least several years, possibly never. The intent of this task is to develop a capability that is applicable to many cell designs. A close tie is being maintained, however, with CSPL because of their prime contract with SNL for the development of the sodium/sulfur technology.

To accomplish the task objectives, three integrated activities are currently being performed:

- Physical property measurement - determine as a function of temperature, the coefficient of thermal expansion, the tensile strength, and the elastic modulus for sulfur and sodium tetrasulfide (sodium tetrasulfide)/graphite composites

- Cell behavior - experimentally measure the strain and thermal response of both CSPL and SNL lab cells to determine cell-to-cell strain variability, and the effects of cycle life and state-of-charge
- Mathematical modeling - using the information from the property measurement and cell behavior subtasks, refine the materials-behavior models to allow the thermomechanical code to predict quantitatively all observed experimental results.

The approach that has been and is now being followed in this multiyear task consists of the following steps:

1. Develop an initial thermomechanical model and numerically simulate known, yet simple, electrolyte-failure mechanisms to determine the feasibility, status, and basic requirements of such a modeling effort (completed 1987).
2. Numerically evaluate the sensitivity of component stress to changes in cell operating and physical property parameters (completed 1987). This study allowed the types of conditions and cell behavior that could lead to high component stress to be identified, thus establishing detailed information needs (physical property data and cell characteristics).
3. Measure and/or empirically determine the detailed information needs identified in step 2 (initiated 1987).
4. Measure and model expected cell behavior to refine and validate the materials models contained in the thermomechanical code (initiated 1987).
5. Model and perform in-cell testing of proposed failure mechanisms to determine their viability and applicability to various cell designs (initiated 1988).

During 1988, the effort centered on steps 3 and 4. A summary of the important results from each subtask is presented in the following sections.

Physical Properties of Positive-Electrode Materials

To provide the mathematical modeling effort with accurate values for the important physical properties of the positive-electrode materials, a complementary experimental study is being performed. Specific

thermomechanical properties (elastic modulus, Poisson's ratio, compressive strength, and thermal expansion coefficients) for sulfur, the single-phase sodium polysulfides and the sulfur/graphite and sodium tetrasulfide/graphite composites are being measured as a function of temperature to near their respective melting points. The properties of sulfur and sulfur/graphite composites were described in the *ETD Annual Report for 1987*.

Along with relatively unknown sodium tetrasulfide properties, the results from a recently completed mathematical sensitivity study showed the importance of accurately characterizing the properties of the beta"-alumina electrolyte and the container material. During 1988, activity concentrated on measuring the most important of these properties, the coefficient of thermal expansion (CTE), for all three components.

Sample preparation and handling of the toxic, brittle, and very hygroscopic sodium tetrasulfide material presented many problems. A new inert environment sample preparation box was constructed. After many trials, the decision was made that the composite samples must be vacuum cast to ensure good integrity. A fairly elaborate apparatus for accomplishing this was designed and fabricated. The samples are needed to allow accurate measurement techniques (Dynamic Mechanical Analysis and ultrasonic testing) to be used. Measurements of the composite samples will be completed in 1989. In the meantime, samples of pure sodium tetrasulfide were cast into graphite molds. The CTE for this material was measured with Thermal Mechanical Analysis (TMA) across all three directions of grain alignment. The degree of recrystallization of the material had a small effect on the results with an observed range of values of 31-36 microstrain/°C.

Stress-strain compression testing of pure sodium tetrasulfide yielded an average elastic modulus of 88 + 40 MPa, whereas ultrasonic attenuation gave a value of 8.5 GPa. The ultrasonic shear modulus was 3.8 GPa and the Poisson's ratio was 0.11. Similar to the case for sulfur, the ultrasonic measurements give intrinsic properties (i.e., do not take flaws into account). All of these values (CTE and moduli) are consistent with our previous expectations, and none appear to have a large temperature coefficient.

Many beta"-alumina samples in different orientations were fabricated from electrolytes used in the SNL lab cell. Figure 5-6 shows a compilation of the obtained results. The primary conclusions from these data are that the CTE is lower and more temperature dependent than assumed.

Cell Behavior

Other than stresses generated solely by rapid temperature changes, thermomechanical processes in the positive electrode are believed to be responsible for F/T-induced cell failures. Given this situation, the experimental part of this task consists of measuring strain on the cell case, a component that tracks the mechanical behavior of the positive electrode. The 1988 measurements mainly involved the SNL laboratory cell because these data are the primary information used to validate the thermomechanical model under development.

As reported in the *ETD Annual Report for 1987*, not all aspects of the general strain behavior of the CSPL and the SNL lab cells are similar. Because of drastically different designs and fabrication procedures, this result was not surprising. However, the disconcerting observation about the strain measurements is the relatively poor reproducibility obtained from one F/T cycle to the next. The intent of the first strain measurements completed this past year was to determine the source of this variability. The approach consisted of (1) mathematically modeling the strain behavior of the SNL lab cell to identify the optimum locations of the strain gauges, (2) instrumenting a new lab cell and performing a series of F/T cycles, (3) disassembling the cell, fabricating a new cell using the same instrumented container, and repeating the series of F/T cycles.

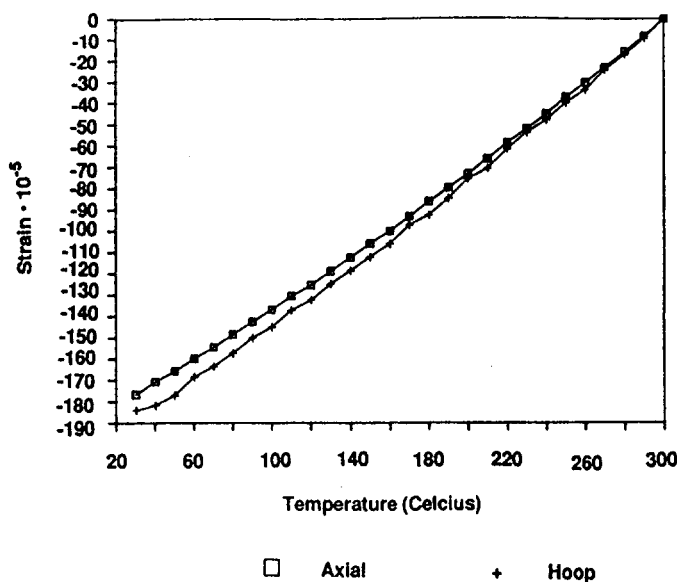


Figure 5-6. Effect of Temperature on the Strain Observed in Ceramtec Beta[®]-Alumina for Numerous Samples Taken in Various Orientations from Actual SNL Cell Electrolytes. The CTE is the change in strain per °C.

The strain responses obtained during freezing of these two lab cells fabricated using the same instrumented container are qualitatively similar. This observation is shown in Figures 5-7 and 5-8. Figure 5-7 is for the first cell and Figure 5-8 for the second cell. Given this similarity, the variability from F/T cycle to cycle is probably real (i.e., not representative of an instrumentation problem) and is caused by changes in the behavior of the positive electrode materials. By considering the results from a series of F/T cycles on the second cell (e.g., Figures 5-8 and 5-9), the quantitative variability is evident. When studying these results, remember that the strain data are mechanical strain; that is the strain produced on the container due to the presence of the positive electrode and electrolyte. These data do not include thermal strain.

Based on the observed size of the exotherms, the quantity of amorphous sodium polysulfides was increasing in each subsequent F/T cycle. The volumetric change associated with the different phases probably produced the differences in strain behavior. Two consequences of the variability are that effects on strain due to time, electrical cycling, and rate of heat-up/cool-down cannot be statistically identified and is probably why a failure during a freeze or thaw is not an expected event. R. Knodler, from BBC, stated in recent discussions that they had also observed quite variable behavior in their characterization of sodium polysulfides and that the above conclusions are quite reasonable.

The majority of the strain measurements have been made on three different lab cells, each with a relatively small number of electrical cycles (<25). During 1988, the first strain measurements were completed on a lab

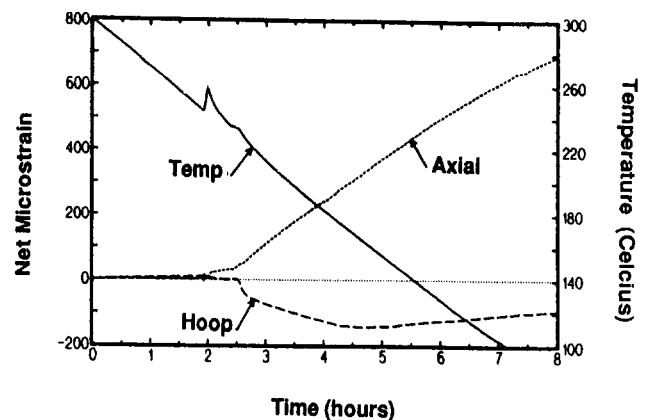


Figure 5-7. Average Mechanical Strain Measured During the Freezing of a Discharged SNL Cell, OCV = 1.9 V; Cell 1, Freeze Cycle 16

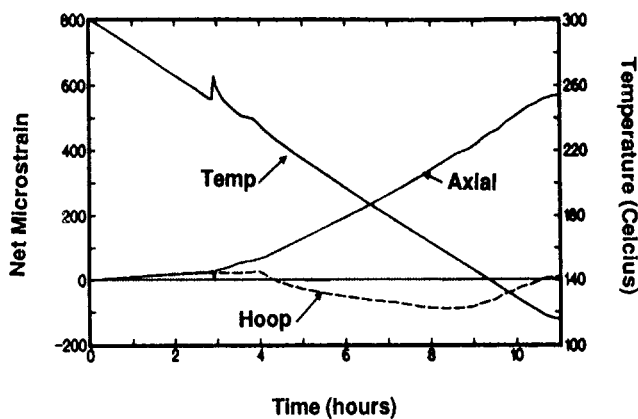


Figure 5-8. Average Mechanical Strain Measured During the Freezing of a Discharged SNL Cell, OCV = 1.9 V; Cell 2, Freeze Cycle 4

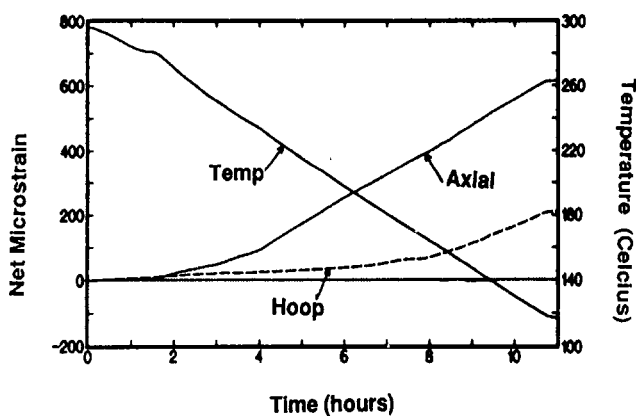


Figure 5-9. Average Mechanical Strain Measured During the Freezing of a Discharged SNL Cell, OCV = 1.9 V; Cell 2, Freeze Cycle 6

cell that had been subjected to numerous full electrical cycles (>75). The strain response for this well-conditioned cell was much more stable and reproducible than that observed previously for the relatively uncycled cells. Several new conclusions can be drawn from the collected data:

- The maximum compressive hoop strain in the container occurs during the freeze cycle at a temperature between 160 to 170°C for a cell with an open-circuit voltage (OCV) = 1.9 V, and at 145 to 150°C for a cell with an OCV = 1.77 V. As mathematical modeling shows, the strain goes through this maximum because of the complex interaction of the various cell

components, each having different temperature-dependent physical properties. The value of the maximum strain appears to be greatest for a freeze cycle performed immediately following electrical discharge rather than performed after another F/T cycle. This difference probably results because the porosity inherent in the positive electrode allows some degree of plastic stress relaxation.

- Axial strain appears greatest in cells with a discharged OCV = 1.9 V, whereas hoop strain is greatest in cells with a discharged OCV = 1.77 V. In terms of resultant stress, modeling has shown that these small strain differences are probably not significant.
- Undercooling of the sodium polysulfides is greater ($\approx 50^\circ\text{C}$) at an OCV = 1.9 V than at an OCV = 1.77 V ($\approx 10^\circ\text{C}$). Regardless of the discharged OCV, both the axial and the hoop strain return to near zero upon thawing at around 240°C.

Modeling of Cell Behavior

Two general conclusions were gained from the sensitivity studies completed in 1987: (1) volumetric changes in the positive electrode can cause electrolyte stresses to develop during a freeze cycle and (2) discontinuities in the positive electrode (gap, amorphous/crystalline, multiple phases with differing coefficients of thermal expansion) may lead to electrolyte failure. The stresses generated by volumetric changes and discontinuities can qualitatively explain many characteristics of actual F/T failures, including the effects of cooling rate and state-of-charge, the necessity to cool slowly around the melting point, and finally the infrequency or uncertainty of electrolyte failures.

The modeling efforts completed before this year centered on examining resultant electrolyte stress. The primary goal of the current modeling activity is to refine the material models such that accurate correlations of the strain state on the external surface of the cell to the state of stress within the cell can be made. This effort, started in 1987, concentrated on quantitatively explaining why the hoop strain during a freeze cycle in both the lab and CSPL cells can be consistently compressive and begin relaxing at about 160°C.

To aid in the analysis, an activity was undertaken to develop an analytical (nonnumerical) solution to the governing stress and strain equations. Prior modeling studies showed that a one-dimensional, radial approach

can be utilized if the region of interest is distant from the ends of the container. This condition applies to the SNL lab cell in the region where the strain gauges are located.

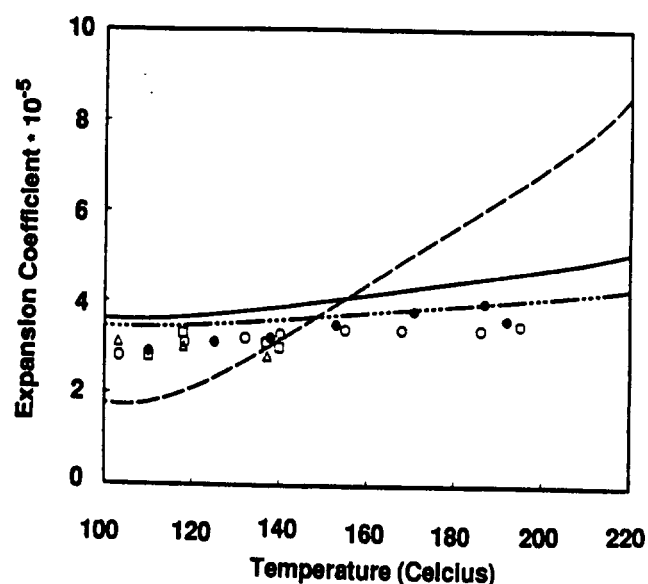
One-dimensional strain equations were written for the three components of interest (electrolyte, positive electrode, container). The principal variables were the temperature-dependent elastic modulus and CTE for the sodium tetrasulfide/graphite composite. These equations were reduced into a single, very large (~6 page) algebraic expression using symbolic manipulator software on one of the SNL VAX computers (MACSYMA). Once this expression was programmed, hoop and axial strain could be input and CTE or elastic modulus calculated as a function of temperature. Alternately, the physical properties could be input and mechanical strain calculated.

The results from one particular simulation are shown in Figure 5-10. The strain data (both axial and hoop) from a freeze experiment (similar to those shown in Figure 5-8) were fit to two polynomial equations and input with the elastic modulus and CTE values for the container and electrolyte. The required CTE for the positive electrode was calculated with the elastic modulus as a parameter. For reference, measured CTE data from BBC for a variety of pure sodium polysulfides are also included in the figure. As can be seen, the derived CTE values are in reasonable agreement with those obtained by BBC, except when the elastic modulus is very low (70,000 psi or 0.5 GPa), in which case a very high CTE must exist to result in the observed container strain.

The results above demonstrate that the model has been refined to the point that accurate correlations are now possible. During 1989, an effort will be made to quantify the strain variability using this analytical model, to complete the validation of the actual numerical code, and to begin the consideration of thaw cycle response.

The progress in this task has yielded sufficient confidence in the status of the model that at a minimum, semi-quantitative analyses of actual cell performance can be made. Two F/T simulations relative to CSPL-PB cells were completed that involved analyzing the potential effect of a gap in the positive electrode on electrolyte stress and of a seal-design change.

An early application of the first version of the thermomechanical model consisted of verifying the proposed detrimental effect of the presence of an axial gap in an FACC cell design. In 1987, voids were also observed in the positive electrode of some earlier CSPL-PB cells. X-radiographs showed that the gaps appeared to extend around the entire circumference of the electrolyte with a general shape as indicated in Figure



Legend

E = 7.86

E = 7.84

E = 7.88

△ NA283

● NA284

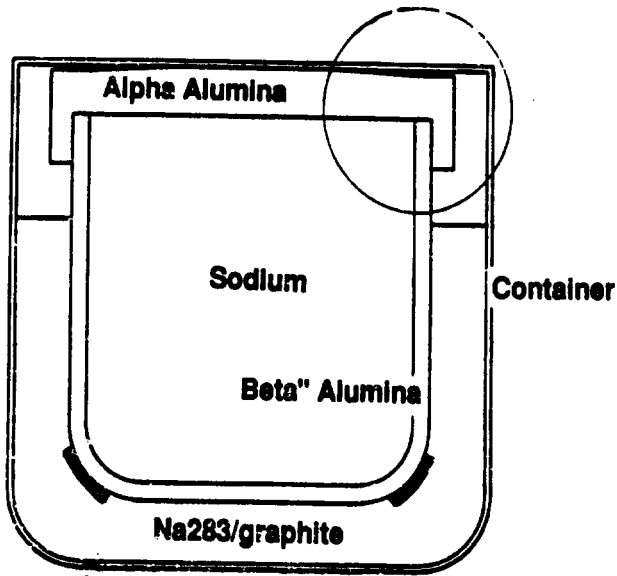
○ NA285

□ NA2810

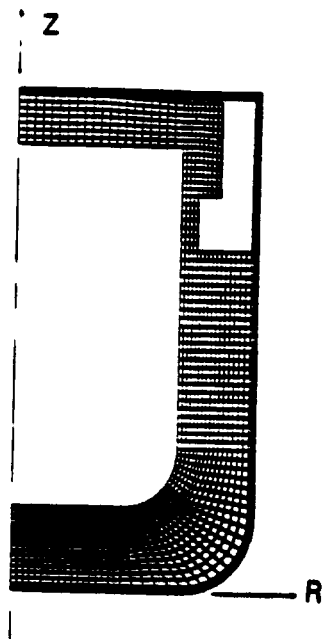
Figure 5-10. Calculated Coefficient of Thermal Expansion for Sodium Tetrasulfide/Graphite Composite as a Function of Temperature. Calculation based on container strain data taken during a freeze cycle performed on the SNL cell. The Elastic Modulus Parameter (E) is in psi. The symbols represent data taken by BBC for pure sodium polysulfides.

5-11a. A two-dimensional, axisymmetric finite-element model of the CSPL-PB cell containing the gap was then constructed (Figure 5-11b) and a F/T simulation performed.

Several simplifying assumptions were used in the analysis. Although the positive electrode of actual cells contains several different sodium polysulfides, only a homogeneous sodium polysulfide, sodium tetrasulfide, was considered. Freezing was assumed to occur slowly, so the effects of temperature gradients could be neglected. Both of the latter assumptions are supported by the strain and temperature measurements described in previous reports. Because the sodium remains liquid over a predominate portion of the range in temperature drop, it was not included in the model. The material



a. General Shapes of Observed Voids (Indicated by Shaded Regions)



b. Finite-Element Mesh of an Axisymmetric Cell Section

Figure 5-11. Schematic Diagrams of a CSPL-PB Cell Used in the Mathematical Analyses of the Effect of Voids in the Positive Electrode on Electrolyte Stress

properties used in the analyses are similar to those discussed in the previous subsection.

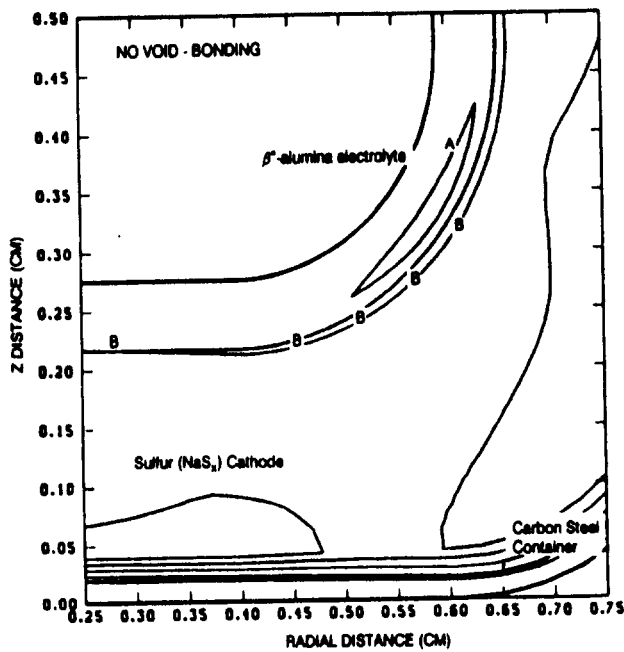
The analysis used the finite-element code ABAQUS. Because the integrity of the electrolyte was the major issue, the results given here are for the maximum principal stresses. Maximum stress contours in the region of the cell where the gap exists are shown in Figure 5-12. The convention in this figure is that tensile stresses are positive and the units of the stress are pounds per square inch. Figure 5-12a indicates that, without a gap, cell freezing results in maximum stresses in the electrolyte that are all compressive. Similar to the FACC analyses, a gap results in tensile stresses in the region of the discontinuity in the PB cell design, as shown in Figures 5-12b. However, the levels of stress were much lower than the approximate failure stress of the beta"-alumina (20,000 to 40,000 psi).

The second simulation was motivated by the concern that a switch at CSPL from a flexible seal design to a relatively stiff seal might reduce the excellent F/T durability of the PB cell. This situation would result because, with the stiff design, the container could be more rigidly fixed to the seal and the electrolyte. Thus, the potential could be increased for the F/T processes in the positive electrode to cause higher stresses in the electrolyte and ceramic-metal seals.

The two-dimensional axisymmetric model of the CSPL-PB cell, the material properties, and the assumptions used in the first simulation were again employed. Calculated constant stress contours for the region of the glass seal, where "cantilever-type" failures are often observed, are shown in Figure 5-13. The contours represent the difference in stress state that would result when a cell at 350°C is cooled to room temperature. Comparison of these figures shows that no significant differences in the stresses generated during a freeze cycle should be produced by the change to the rigid seal design. A similar observation can be made about the stress state predicted in the metal-ceramic seal region. Here, the stresses are high in both seal configurations because of a large mismatch in thermal expansion coefficients of the two materials.

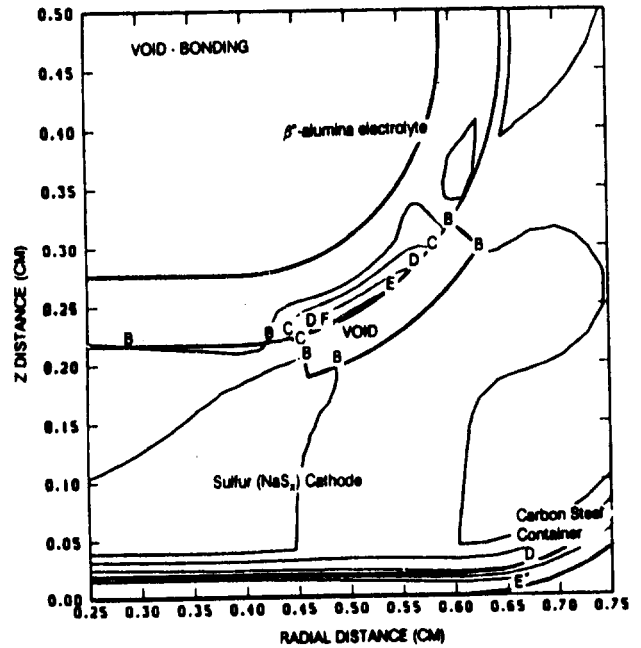
Improved Chromium Plating of Sodium/Sulfur Cell Containers

A major unsolved materials problem in the development of the sodium/sulfur technology is the identification of a suitable sulfur-container material. The



Principle Stress (psi)

- A = -2000
- B = 400
- C = 2800
- D = 5200
- E = 7600
- F = 10000



Principle Stress (psi)

- A = -2000
- B = 400
- C = 2800
- D = 5200
- E = 7600
- F = 10000

a. Cell without Void in Positive Electrode

b. Cell with Void

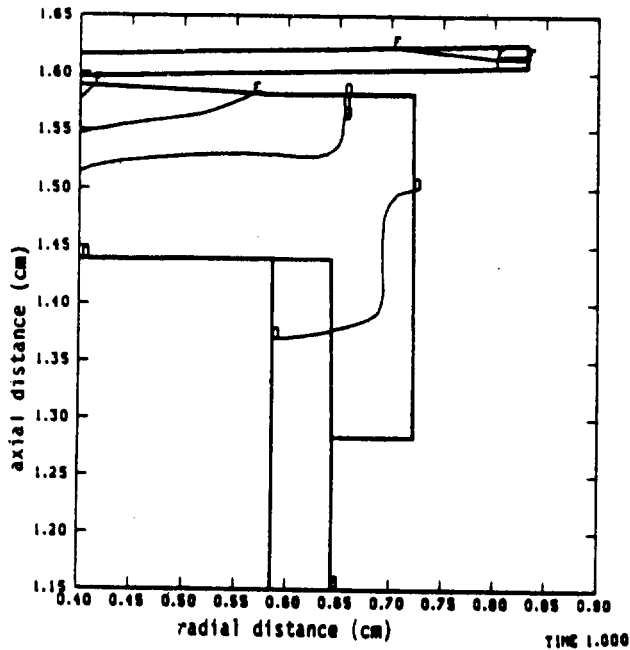
Figure 5-12. Stress Contours Calculated for the CSPL-PB Cell That Result from a Freeze Cycle to 25°C

solution is difficult because the container must be very corrosion resistant, have good electrical conductivity and mechanical properties, and yet be light and inexpensive. Corrosion is important not only because of its adverse effect on cell lifetime, but also because corrosion products are known to affect long-term cell performance. These diverse and demanding requirements have forced developers to select and use composite materials: usually an inexpensive substrate (e.g., aluminum, carbon steel, or stainless steel) that has been coated, plated, or sheathed with at least one corrosion-resistant material. If the substrate is a material that readily corrodes (e.g., steel), one must ensure that the corrosion-resistant layer is defect free, thus preventing undermining, substrate attack, and spalling.

Both major sodium/sulfur development programs supported by the DOE, previously at FACC and currently at CSPL, have selected a chromium-containing layer as the primary corrosion barrier. One of the

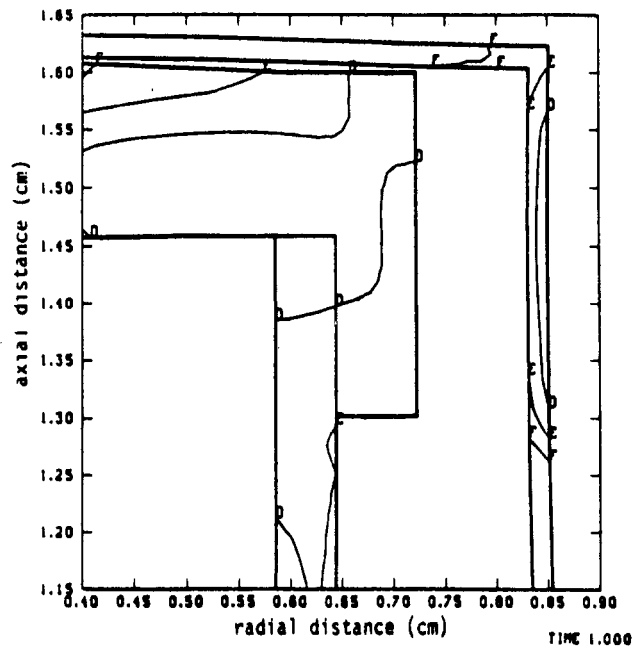
preferred methods for applying chromium onto sodium/sulfur containers is by electroplating. This process can be cost effective and theoretically can produce deposits with good chemical, physical, and mechanical properties. In practice, however, electroplated chromium is typically a hard, brittle, highly stressed deposit.

Although many sodium/sulfur developers have studied and used chromium electroplating, techniques have not yet been identified for reliable and effective platings. CSPL is actively pursuing a number of options to improve its current corrosion prevention scheme (thermally chromized steel). Because of this lack of a suitable technique and CSPL's immediate needs, this study was initiated. Its goal is to develop new techniques that improve the quality and efficiency of chromium electroplating when applied to sodium/sulfur containers. Both CSPL and SNL agree that a high-quality electroplated chromium layer could, by itself,



Stress (psi)
 A = -6.000 E + 3
 B = -3.000 E + 3
 C = -1.200 E + 3
 D = 1.200 E + 3
 E = 3.600 E + 3
 F = 6.000 E + 3

a. Flexible Seal



Stress (psi)
 A = -6.000 E + 3
 B = -3.000 E + 3
 C = -1.200 E + 3
 D = 1.200 E + 3
 E = 3.600 E + 3
 F = 6.000 E + 3

b. Rigid Seal

Figure 5-13. Stress Contours Calculated for Two Seal Designs in CSPL-PB Cells due to a Freeze Cycle to 25°C. Region shown is indicated by circle in Figure 5-11a.

improve durability and cost (compared to chromizing), but also could be an effective base layer for a subsequent post-processing step (e.g., thermal diffusion treatment, carburizing).

The specific objectives of this continuing activity are to develop improved techniques to electroplate chromium onto carbon and stainless steels and to identify methods to use these techniques to plate effectively containers used in the fabrication of the two cell designs being considered by CSPL. The initial laboratory investigations were completed this past year, and a summary is presented in the remainder of this section. Although some progress has been made, the deposit quality is still not adequate for a long service life. A ductile, stress-free, or compressively stressed deposit remains the goal because better longevity for the container should be attained.

Program Plan

This task is divided into four separate activities, the first three involving the optimization of different plating techniques and the fourth concerned with the evaluation of the platings.

Crack-Free

The modification of a commercial electrolyte that produces crack-free deposits (CF-500) by adding vanadium pentoxide (V₂O₅): this chemical additive will reduce stress, improve ductility, and increase plating efficiency. An improvement in efficiency is important because it will allow thicker deposits to be produced in less time, thus reducing cost.

Pulse-Plating

Development of pulse and pulse-reverse plating techniques as a method to reduce deposit stress: published information has established that crack-free chromium is possible using either on- and off-times of ≈ 1 ms or pulsed reversed current plating with short anodic periods and very low frequencies (< 1 Hz). These should have a significant reduction in hardness and an increase in deposit quality over conventional plating methods.

Highly Cracked

Investigation of the potential for producing and utilizing a highly cracked deposit: this type of deposit may be desirable because the thermal expansion coefficients of the steel and the chromium are better matched. Corrosion protection could be enhanced by using a diffusion layer formed during a post-plating step. As such, the presence of a cracked surface may not be detrimental.

Evaluation

The characterization of the quality and performance of the platings using a variety of techniques: (1) scanning electron and optical microscopy to evaluate surface morphology and deposit integrity; (2) deposit stress and hydrogen gas content to identify whether reductions in hydriding were produced; and (3) corrosion tests to determine the performance of the platings. These latter tests are being performed both at SNL and CSPL. The CSPL studies involve predominantly in-cell exposures. The evaluations at SNL are being conducted mainly to screen the effectiveness of the potential plating processes. To accomplish the in-cell testing, end plates for the SNL lab cell along with the inside of PB containers are being plated. The performance of the platings at both SNL and CSPL will be determined using post-mortem analyses.

Results

The initial screening of potential plating techniques has been completed. This involved studying the effect of four different electrolytes on deposit quality and performance.

Crack-Free

Plating was performed with M&T Unichrome CF-500, a proprietary, chemical self-regulating, electrolyte, using optimized parameters previously developed and listed in the *ETD Annual Report for 1987*. Flat steel

samples were plated and their performance evaluated by exposing the deposit to sodium tetrasulfide for two weeks at 400°C . The container in this test was constructed from 304SS. The unprotected container was severely attacked, whereas the uncracked chromium layer was virtually unaffected. The attack on the stainless steel demonstrates that these test conditions are indeed extremely corrosive.

Based on the above positive result, a special conforming anode was designed, fabricated, and used to plate 25 CSPL-PB containers. As expected, problems occurred when plating the closed-end CSPL-PB containers. With the PB container, the ratio of plating anode area to the cathode area was less than 1:1, resulting in poor plating uniformity and efficiency, and a thin deposit especially in the lower rounded corner. These containers were shipped to CSPL for post-processing and in-cell evaluation.

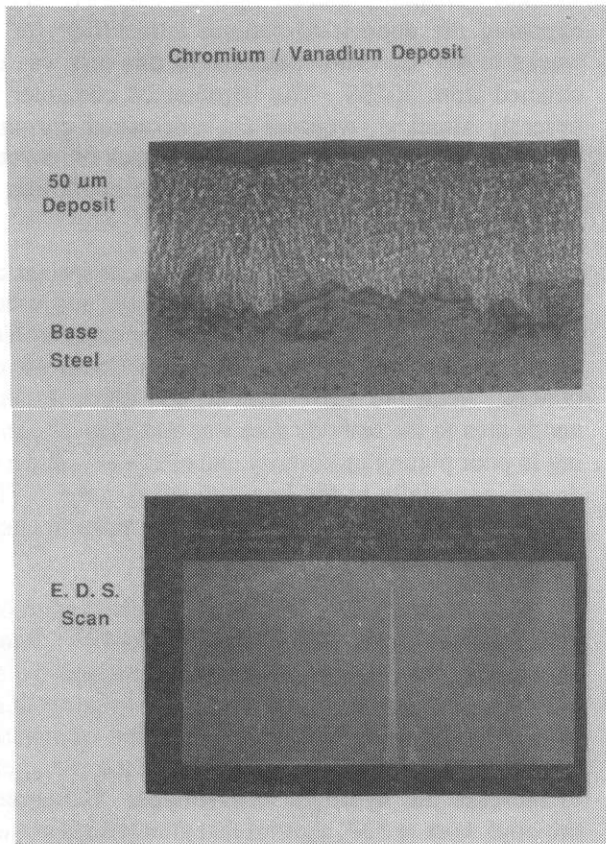
Next the M&T CF-500 was used with an addition of vanadium pentoxide. By adding 10 g/l of V_2O_5 to the electrolyte, the plating rate can be increased from 25 mm/h to 100 mm/h. Analysis of the plating quality showed no cracking and no codeposition of vanadium (Figure 5-14). The primary function of the vanadium is to increase the hydrogen overvoltage. Furthermore, previous work at SNL showed that after the solution was electrolyzed to 300 Ah/l, the stress in the deposit was reduced to 300 psi compressive, compared with a 23,000 psi tensile stress when the vanadium was not present.

Highly Cracked

Another self-regulating electrolyte, M&T CR-110, was used to produce a compressively stressed deposit with approximately 1,200 cracks/cm. This procedure yielded a deposit that should be very suitable for the thermal-treatment process being developed at CSPL. Twenty PB cell containers were then plated and subjected to this proprietary thermal treatment. A few were utilized in their effort to optimize the time and temperature parameters of this treatment, and some were subsequently used in cell fabrication. One container was returned to SNL for analysis to identify the effect of the treatment on deposit quality. The ultimate performance of the deposit is being determined at CSPL by holding discharged cells at the 350°C operating temperature. Based on all the results to date, this procedure has yielded the most attractive platings.

Pulse-Plating

A conventional chromium-plating solution with a 100:1 ratio of chromium to sulfuric acid will be used to evaluate pulse and pulse reverse-plating techniques.



The required rectifier has been received and actual plating tests have started. To evaluate the many different parameters of pulse plating, a new gauge was developed at SNL that allows in situ measurements of stress as plating proceeds, thus providing an immediate feedback on plating results.

Figure 5-14. Optical Micrograph (Upper), and X-Ray Dispersive Chemical Analysis (Lower) of Chromium Deposit Produced with the M&T Unichrome CF-500 Electrolyte Modified with the Addition of 10 g/l of Vanadium Pentoxide. Note the lack of a vanadium peak.

Appendix

Presentations and Publications, 1988

- Atherton, G., S. N. Heavens, M. McHamee, A. J. Rich, "Electrolyte Fabrication, Strength and Microstructure," presented at the Beta (sodium/sulfur) Battery Workshop VII. Published in Conference Proceedings, DOE/EPRI, EPRI Report AP-6012-SR, paper No. 19, Toronto, Canada, May 31 - June 3, 1988.
- Auxer, W., "Maintenance Considerations for a Sodium Sulphur Load Leveling Battery," presented at the 172nd Meeting of The Electrochemical Society, Honolulu, HI, October 1987.
- Auxer, W., and D. Riley, "Sodium Sulphur Load Leveling Battery Design," presented at the Beta (sodium/sulfur) Battery Workshop VII. Published in Conference Proceedings, DOE/EPRI, EPRI Report AP-6012-SR, paper No. 50, Toronto, Canada, May 31 - June 3, 1988.
- Beauchamp, R., and J. Sindorf (Johnson Controls, Inc.), "Nickel Hydrogen Battery Development," SAND88-7100 (Albuquerque: Sandia National Laboratories) August 1988.
- Bindin, P. J., "Small Battery Performance," presented at the Beta (sodium sulfur) Battery Workshop VII. Published in Conference Proceedings, DOE/EPRI, EPRI Report AP-6012-SR, paper No. 43, Toronto, Canada, May 31 - June 3, 1988.
- Bindin, P. J., "Vehicle Batteries," presented at the Beta (sodium/sulfur) Battery Workshop VII. Published in Conference Proceedings, DOE/EPRI, EPRI Report AP-6012-SR, paper No. 49, Toronto, Canada, May 31 - June 3, 1988.
- Bindin, P. J., A. Gibson, S. N. Heavens, S. Jackson, and F. M. Stackpool, "Theoretical and Experimental Investigations of Factors Affecting the Performance and Reliability of Sodium Sulphur Cells and Batteries," Research Project 128-13, Final Report, CSPL, Principal Investigators: Prepared for EPRI, 3412 94304, EPRI Project Manager R. D. Weaver. To be published.
- Bolstad, J. J., "Effects of Conductivity Additives in the Zinc/Bromine Flowing Electrolyte Battery," presented at the 174th Electrochemical Society Meeting, Chicago, IL, October 1988.
- Bolstad, J. J., W. Delaney, M. Eskra, R. Vidas, and J. Zagrodnik, "Computer Modeling Studies for Zinc/Bromine Battery Application Design," presented at the Third Annual Battery Conference on Applications and Advances, Long Beach, CA, January 1988.
- Bolstad, J. J., R. A. Vidas, and J. P. Zagrodnik, "Zinc/Bromine Computer Model for Battery Application Design," presented at the Ninth Electric Vehicle Symposium, Toronto, Canada, November 1988.
- Braithwaite, J. W., et al., "Component Stress During Freeze/Thaw Cycling," presented at the Beta (sodium/sulfur) Battery Workshop VII. Published in Conference Proceedings, DOE/EPRI, EPRI Report AP-6012-SR, paper No. 37, Toronto, Canada, May 31 - June 3, 1988.
- Braithwaite, J. W., F. M. Stackpool, et al., "Effect of Thermal Cycling on CSPL Sodium Sulphur Cells," presented at the Beta (sodium sulfur) Battery Workshop VII. Published in Conference Proceedings DOE/EPRI, EPRI Report AP-6012-SR, paper No. 38, Toronto, Canada, May 31 - June 3, 1988.
- Bush, D. M., "Evaluation of Terrestrial Nickel/Hydrogen Cells and Batteries," (Albuquerque: Sandia National Laboratories) May 1988.
- Eskra, M. D., and J. P. Zagrodnik, "Zinc/Bromine EV Battery Development at Johnson Controls," presented at the Ninth Electric Vehicle Symposium, Toronto, Canada, November 1988.

- Featherby, M., "Real Time Radiography of a Sodium Sulphur Cell," presented at the Beta (sodium/sulfur) Battery Workshop VII. Published in Conference Proceedings, DOE/EPRI, EPRI Report AP-6012-SR, paper No. 28, Toronto, Canada, May 31 - June 3, 1988.
- Gentry, W., and W. Segall. "A Storage System for Autonomous Photovoltaics," presented at the Third Annual Battery Conference on Applications and Advances, Long Beach, CA, January 1988.
- Jones, I. W., "Overview of Sodium Sulfur Battery Development at CSPL," presented at the Beta (sodium/sulfur) Battery Workshop VII. Published in Conference Proceedings, DOE/EPRI, EPRI Report AP-6012-SR, paper No. 13, Toronto, Canada, May 31 - June 3, 1988.
- Koenig, A. A., "Analysis of Sodium Sulfur Cell Testing: Polarization and Capacity Degradation," presented at the Beta (sodium/sulfur) Battery Workshop VII. Published in Conference Proceedings, DOE/EPRI, EPRI Report AP-6012-SR, paper No. 30, Toronto, Canada, May 31 - June 3, 1988.
- Koenig, A. A., "Na/S Cell Design Considerations for Power Applications," presented at the 33rd Power Sources Symposium, Cherry Hill, NJ, June 1988.
- Koenig, A. A., et al., "Considerations of Latent-Heat-Storage Salts for Secondary Thermal Battery Applications," presented at the Beta (sodium/sulfur) Battery Workshop VII. Published in Conference Proceedings, DOE/EPRI, EPRI Report AP-6012-SR, paper No. 44, Toronto, Canada, May 31 - June 3, 1988.
- Leo, A., "Zinc Bromine Battery Testing at Energy Research Corporation," presented at the 33rd International Power Sources Conference, Cherry Hill, NJ, June 13 -16, 1988.
- MacLachlan, S., and F. M. Stackpool, "Corrosion Resistant Materials for Sodium Sulphur Cells," presented at the International Power Sources Symposium, Bournemouth, England, September 1988.
- MacLachlan, S., and F. M. Stackpool, "Corrosion Resistant Materials for Sodium Sulfur Cells," presented at the Beta (sodium/sulfur) Battery Workshop VII. Published in Conference Proceedings, DOE/EPRI, EPRI Report AP-6012-SR, paper No. 24, Toronto, Canada, May 31 - June 3, 1988.
- Mangan, M. F., "Sodium Sulphur Batteries for Electric Road Vehicles," presented at the Electric Vehicle Symposium IX, November 1988.
- Marr, J. J., and A. J. Smaga, "Post-Test Observations on CSPL Cells," presented at the Beta (sodium/sulfur) Battery Workshop VII. Published in Conference Proceedings, DOE/EPRI, EPRI Report AP-6012-SR, paper No. 39, Toronto, Canada, May 31 - June 3, 1988.
- McGreavey, G., and D. J. Riley, "Manufacturing Approaches for Demonstrations and for the Future," presented at the Beta (sodium/sulfur) Battery Workshop VII. Published in Conference Proceedings, DOE/EPRI, EPRI Report AP-6012-SR, paper No. 42, Toronto, Canada, May 31 - June 3, 1988.
- Rudd, E. J., "Aluminum-Air Battery Program," presented at the Air Systems Review Meeting, Cleveland, OH, April 1988.
- Rudd, E. J., "The Development of Aluminum-Air Batteries for Electric Vehicles," presented at the 33rd International Power Sources Symposium at Cherry Hill, NJ, June 1988.
- Rudd, E. J., "The Development of Aluminum-Air Batteries for Electric Vehicles," presented at the Ninth International Electric Vehicle Symposium in Toronto, Canada, November 1988.
- Stackpool, F. M., "Cell Development - A Focus on Safety," presented at the Beta (sodium/sulfur) Battery Workshop VII. Published in Conference Proceedings, DOE/EPRI, EPRI Report AP-6012-SR, paper No. 34, Toronto, Canada, May 31 - June 3, 1988.

Distribution

Argonne National Laboratory (8)
9700 South Cass Avenue
Argonne, IL 60439
Attn: C. Christianson
W. DeLuca (3)
J. Marr
K. Myles
P. Nelson
J. Smaga

Asea Brown Boveri AG
Eppelheimer Str. 82
D-6900 Heidelberg 1
Federal Republic of Germany
Attn: H. Birnbreier

Beta Research & Development, Ltd.
50 Goodsmoor Road
Sinfim
Derby DE29GN
United Kingdom
Attn: R. Galloway

Battelle (7)
Pacific Northwest Laboratories
2030 M Street, NW
Washington, DC 20036
Attn: C. Imhoff
L. Fassbender (5)

California State Air Resources Board
Research Division
PO Box 2815
Sacramento, CA 95812
Attn: J. Holmes

Ceramatec, Inc.
163 West 1700 South
Salt Lake City, UT 84115
Attn: D. Richerson
A. Virkar

Chloride Silent Power, Ltd.
Suite 1804
West Valley Road
Wayne, PA 19087
Attn: W. Auxer (5)

Dr. Robert Meredith
PO Box 164
Corvallis, OR 97339

EG&G Idaho, Inc.
Idaho National Engineering Lab
PO Box 1625
Idaho Falls, ID 83415
Attn: G. Hunt

Electric Power Research Institute (7)
PO Box 10412
Palo Alto, CA 94303
Attn: R. Schainker
R. Weaver (5)
G. Cook

Electrotek Concepts, Inc.
Electric Vehicle Operations
4605 Amnicola Hwy
PO Box 16548
Chattanooga, TN 37416
Attn: H. Barnett

Eltech Systems Corporation (3)
Research and Development Center
625 East Street
Fairport Harbor, OH 44077
Attn: E. Rudd (3)
R. Fenn
T. Gilligan

Energetics (3)
9210 Route 108
Columbia, MD 21044
Attn: J. Hurwitch
H. Lowitt

Energy Research Corporation (4)
Three Great Pasture Road
Danbury, CT 06810
Attn: A. Leo
M. Klein
J. Brown

Johnson Controls, Inc. (4)
PO Box 591
Milwaukee, WI 53201
Attn: R. Beauchamp
M. Eskra
J. Zagrodnik
V. Halsall

Lawrence Berkeley Laboratory (7)
University of California
No 1 Cyclotron Road
Berkeley, CA 94720
Attn: E. Cairns
K. Kinoshita
F. McLarnon (5)

Martin Marietta Energy Systems, Inc.
PO Box X
Oak Ridge, TN 37831
Attn: J. Stovall

R. K. Sen & Associates
3808 Veazey St., NW
Washington, DC 20016
Attn: R. Sen

Science Applications International Corporation
10401 Roselle Street
San Diego, CA 92121
Attn: R. Davenport

Electrochemical Engineering Consultants, Inc.
795 Mendocino Way
Morgan Hill, CA 95037
Attn: P. Symons

Wright Patterson AFB
AirForce Wright Aeronautical Labs
AFWAL/POOC-1
Wright Patterson AFB, OH 45433
Attn: W. Bishop
S. Vakson

U.S. Department of Energy (34)
Office of Energy Storage and Distribution
CE-32
FORSTL
Washington, DC 20585
Attn: R. Eaton
K. Klein
A. Landgrebe (30)
J. Quinn

U.S. Department of Energy (4)
Office of Transportation Systems
CE-152
FORSTL
Washington, DC 20585
Attn: K. Barber
P. Brown
P. Patil

U.S. Department of Energy (5)
Albuquerque Operations Office
Energy Technologies Division
Albuquerque, NM 87115
Attn: D. Krenz (2)
K. Smith
R. Holten
D. Christensen

U.S. Department of Energy
Sandia Area Office
PO Box 5800
Albuquerque, NM 87115
Attn: A. Sneddon, Jr.

20 O. Jones
140 W. Hollis
143 R. Thorp
400 A. Blackwell
1521 C. Stone
1811 C. Arnold, Jr.
1811 R. Clough
1812 R. Assink
1812 J. Zeigler
1820 J. Woodard
1840 R. Loehman
1842 W. Hammett
1845 E. Beauchamp
2000 G. Cheney
2500 R. Schwoebel
2520 N. Magnani
2522 R. Clark
2523 J. Searcy
2525 R. Diegle (75)
3141 S. Landenberger (5)
3151 W. Garner (3)
3141-1 C. Ward (8) for DOE/OSTI
3710 L. Welchel
Attn: A. McConnell, 3714
6200 V. Dugan
6220 D. Schueler
6221 E. Boes
6223 G. Jones
8316 W. Bonivert
8316 R. Stoltz
8524 J. Wackerly



8232-2/070067



00000001 -



8232-2/070067



00000001 -



8232-2/070067



00000001 -

